Effect of SHARP1 Knockdown and PLEKHA7 Re-expression on the Growth and Behavior of Acute Myeloid Leukemia Cells induced by Functional Lipid Nanoparticles

Department of Micro-Nano Mechanical Science and Engineering

Nagoya University

Sameh Abdelmoneem Mohammed Ali

List of abbreviations

AML	Acute myeloid leukemia
MLL	Mixed-lineage leukemia
MLL-FP	Mixed-lineage leukemia-fusion protein
MEN1	Multiple Endocrine Neoplasia syndrome type 1 or MENIN
LEDGF	Lens Epithelium-Derived Growth Factor
AF4	Fusion protein 4
MLLr	MLL-rearranged
MLL-AF6	Mixed-lineage leukemia-fusion protein 6
EAP	Elongation-assisting protein
DOT-1L	distributor of telomeric silencing 1-like
PLEKHA7	Pleckstrin homology domain-containing protein family A
AJs	Adherens junctions
ZA	Zonula adherens
E-cadherin	Endothelial cadherin
EGFR	Epidermal growth factor receptor
DDS	Drug delivery system
EPR	Enhanced permeability and retention
ELPs	Elastin-like polypeptides
SLPs	Silk-like polypeptides
PC	Phosphatidylcholine
RES	Reticuloendothelial system
siRNA	Small interfering Ribonucleic acid
PEG	Polyethylene glycol

TR	Transferrin receptor
cRGD	Cyclic arginine-glycine-aspartate
BTZ	Bortezomib
NF-κB	Nuclear Factor-κB
Mcl-1	Myeloid cell leukemia 1 protein
JNK	Jun N-terminal kinase
HER-2	Human epidermal receptor-2
FR	Folate receptor
TR	Transferrin receptor
PBS	Phosphate buffer saline
TEM	Transmission electron microscopy
SEM	Scanning electron microscopy
FITC	Fluorescein isothiocyanate
DAPI	4,6-Diamidino-2-phenylindole
RIPA	Radioimmunoprecipitation
HRP	Horseradish peroxidase
PDI	Polydispersity index
RISC	RNA-induced silencing complex

Chapter 1. Introduction

1.1 Acute myeloid leukemia

Acute myeloid leukemia (AML) is a heterogeneous clonal disorder characterized by an excessive accumulation of immature leukemic cells known as blasts, which lose their ability to differentiate. Blast cells accumulate in the bone marrow, blood, and organs leading to hematopoietic insufficiency. AML can progress rapidly and if left untreated can be fatal in weeks or months hereby, AML becomes one of the massive emerging challenges worldwide. AML incidence is age dependent, rising markedly in patients aged 60 years. Ageing of the European population may therefore contribute to the reported increase in AML incidence in Europe from 3.48 in 1976 to 5.06 patients per 100,000 people in 2013. Across all age groups, the incidence of AML is higher in males than in females. The median age at diagnosis is ~70 years. This could explain that AML survival rates are poor in elderly and pediatric patients with multiple mutations, and patients generally experience high relapse rates [1,2] Hematopoietic homeostasis is maintained via adult normal hematopoiesis, which takes place within the bone marrow microenvironment. The regulation of hematopoietic progenitor differentiation and proliferation in the bone marrow microenvironment could produce an interaction balance between hematopoietic progenitor cells and bone marrow stromal cells [3,4]. Some molecules can manage stromal cells, such as cell adhesion molecules [5].

For decades, the standard therapy of intensive induction chemotherapy has been the backbone for younger and fit patients. This therapy involves a combination of

continuous infusion of cytarabine and anthracycline combinatory treatment. Despite a complete remission rate of 60%–80% in younger patients and 40%–60% in older patients, the rate of overall survival (OS) is lower, approximating 40% as well as the patient relapse and serious toxicity possibilities are still challenged issues.

1.1.1 SHARP1 in AML

MLL (mixed-lineage leukemia; chromosome 11q23) rearrangements are common chromosomal aberrations correlated with AML. *MLL* translocation results in Mixed-lineage leukemia-fusion protein (MLL-FP) complex production, wherein the genomic portion encoding the amino-terminus of *MLL* fuses to the carboxyl-terminal of a group of fusion partner proteins, leading to distinctive leukemogenic transcriptional machinery [6]. Multiple Endocrine Neoplasia syndrome type 1 (*MEN1)*, Lens Epithelium-Derived Growth Factor (*LEDGF)*, *AF4*, and over 70 partner genes of MLL have been characterized in MLL-rearranged (MLLr) AML [7]. MLL-AF6 is the most common leukemogenic MLL fusion protein, recruiting both elongation-assisting protein (EAP) and distributor of telomeric silencing 1-like (DOT-1L) complexes [8].

Identifying therapeutic mechanisms for molecular targeting and effective targeted delivery are crucial for developing a much-needed AML cure. It is known that *SHARP1* is a circadian clock transcription factor implicated in the regulation of several cancer types such as breast, colon, and thyroid carcinomas [9-11]. However, information regarding AML regulation is limited. Recently, a study has demonstrated the crucial function of SHARP1 in MLL-AF6 AML survival, which is significantly regulated by MLL-AF6/DOT1L activity [12]. However, the oncogenic role of *SHARP1* in MLL-AF6 AML growth and maintenance is still unclear.

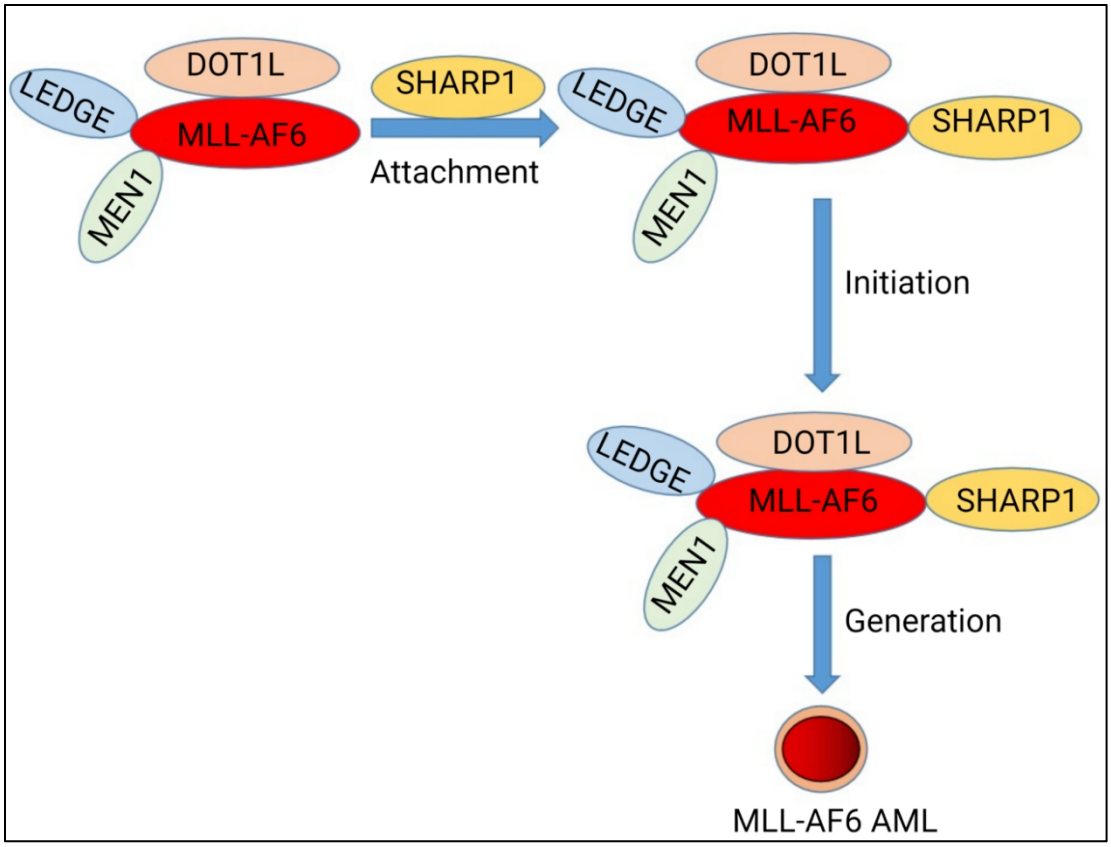

Figure 1.1 Oncogenic role of SHARP1 in MLL-AF6 AML leukemic stem cells.

1.1.2 PLEKHA7 in AML

PLEKHA7, belonging to the pleckstrin homology domain-containing protein family A, is a protein of adherens junctions (AJs), accommodating to the apical zonula adherens (ZA) in epithelial cells and engaging in a structural complex for junction morphogenesis and stabilization [13]. While E-cadherin-based cell-cell contacts are created across lateral membranes among adjacent cells, mature AJs manifest in well-differentiated epithelial cells and particularly centralize at the apical areas of cell-cell contact, whereby they combine with actin filaments to generate ZA [14,15]. PLEKHA7 exhibits outstanding mediation of cell-cell adhesion through specific interactions at the AJs of cells. PLEKHA7 plays a fundamental role in

epithelial integrity whereby they combine to associate with actin filaments in the cytoskeleton [16,17]. Consequently, several studies have discussed the dual oncogenic and tumor suppression activities of PLEKHA7 according to cancer type, such as breast cancer [18,19]. Tumorigenesis has been generated from PLEKHA7 loss, which interferes with the E-cadherin/EGFR signaling pathway, promoting cancer cell growth and progression [20,21]. Recent studies have reported structural variations between apical AJs and the basolateral areas of cell-cell contact. For instance, the PLEKHA7-binding p120 is mainly located at the apical AJs of well-differentiated epithelial cells, but this PLEKHA7-binding p120 composite is not found in the lateral areas of cell-cell contact [22-24]. Additional reports revealed that basolateral cell-cell complexes without PLEKHA7 could enhance tumorigenesis, while the apical AJs could result in tumor suppression via PLEKHA7 [20,22,25]. Furthermore, E-cadherin is widely expressed in areas of cell-cell contact in kidney and breast cancers, whereas PLEKHA7 is still widely downregulated or mislocalized [18,22] at the apical AJs. In leukemogenesis, adhesion abnormalities can readily induce an imbalance between hematopoietic progenitor cells and bone marrow stromal cells, altering the normal hematopoietic bone marrow microenvironment into a leukemic microenvironment, enhancing leukemic growth and prohibiting leukemic cell apoptosis [26-28].

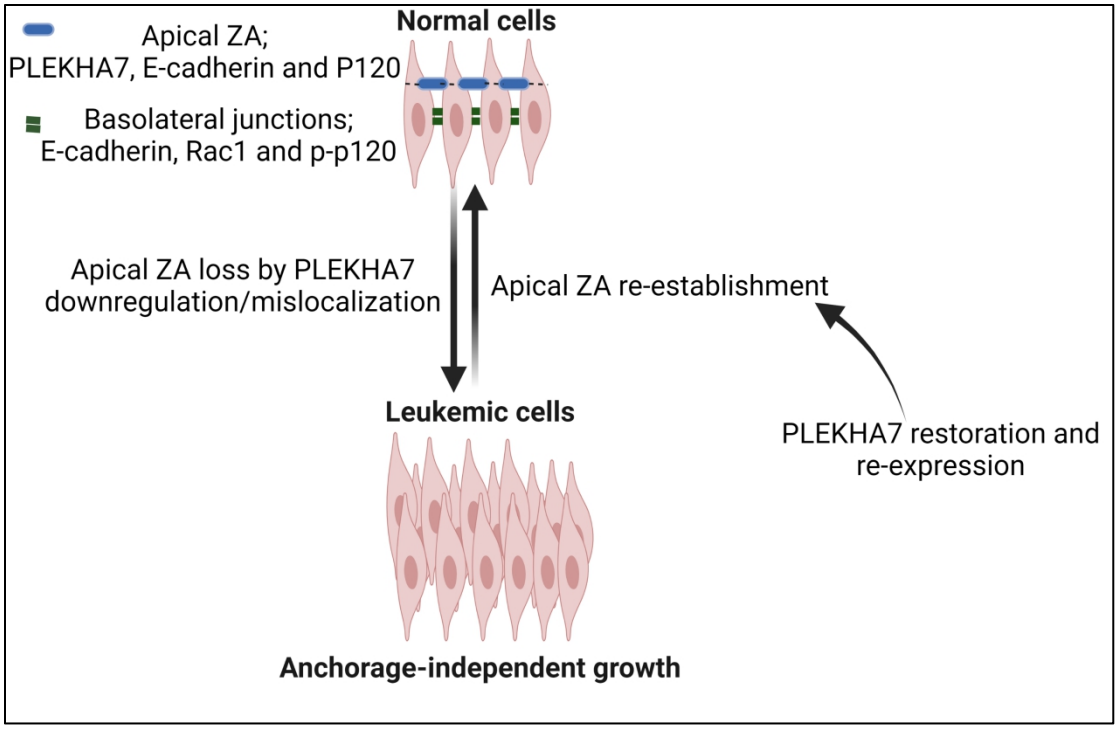

Figure 1.2 Role of PLEKHA7 in establishment of Zonula Adherens (ZA) structure and organizing junctions at the cell-cell interface in normal and cancer cells.

1.2 Nano-based drug delivery for cancer therapy (nanocarriers)

Several therapeutic nanostructures have been fundamentally recruited in the medical aspect with different applications for a subset of cancers and other serious diseases, particularly in recent years. In this specific area, medical researchers and scientists have given full attention and consideration, upgrading traditional methods of drug delivery into a novel revolution and innovation. Stimulating therapeutics' bioavailability and pharmacokinetics has represented the major target of the development of drug nanocarriers generating tremendous effects on clinical applications [29,30]. The drug delivery system (DDS) had obviously started to harness the application of liposomal nanocarriers in the 1960s [31] and polymer-drug conjugates in the 1970s. In the 1990s, the Food and Drug Administration (FDA) has approved AmBisome® as the first applicable DDS, formulated as a liposomal

nanocarrier encapsulating amphotericin B for the treatment of fungal diseases [32]. Otherwise, apart from cancers, antibody-mediated polymeric-drug conjugates have been substantially employed and revolutionized for several human diseases [33]. None of pre-clinical studies has been approved for the clinical application or practice yet, whilst there are several studies highlighting carrier candidates such as PLGA and PVA as examples of fabricated polymers. It has been understood that the efficiency of drug nanocarriers design could play a pivote function in their progress and their potential impact for undergoing clinical application depending on characterizing several necessary factors, encompassing structure or physical properties, toxicity of the used nanocarrier, surface morphologies and encapsulation efficiency. These nanocarriers could deliver therapeutics through firstly active-related targeting utilizing cell-specific targeting ligands as surface-modulated carriers in order to promote the therapeutics accumulation in the intended cells or secondly by the stimulated permeability and retention effect which could induce passive-related targeting [34-36].

1.3 Main categories of drug-delivery systems (DDS)

DDS point out the advanced systems for the effective administration of pharmaceutical products in human in order to fulfill the desired therapeutic impacts. The DDS developments provide a wide variety of advantages: (1) enhanced therapeutic index involving prolonged circulation time, half-life, and volume of distribution in the body, (2) ameliorated drug hydrophilicity or drug protection from enzymatic degradation, (3) cellular and particular uptake with limited off-targeted serious toxicities, (4) controlled and sustained drug release profile. Persistently, extensive efforts were exerted for the development of new DDS for several sorts of

therapeutic agents. Currently, DDS can be primarily divided into two main categories: genetically and chemically engineered carriers.

1.3.1 Genetically engineered carriers

Genetically engineered carriers are fundamental class of DDS and large-scale efforts have been concentrated on this particular area and acquired massive progress for clinical applications. Based on remarkable secondary, tertiary, and quaternary structures of protein, they can be designed to construct into nanostructures for drug and gene delivery [37,38]. Compared to chemically engineered carriers, genetically engineered carriers demonstrate better biocompatibility and higher controlled immunogenicity. The recombinant protein technology is one of widely applied methods for the fabrication of genetically engineered carriers. This molecular cloning method offers good homogeneity where the conjugation of the drug with the nanocarrier taking place at the DNA level. Additionally, the fast cloning procedure provides a great opportunity for large-scale production over the fabrication of chemically synthesized carriers [39,40]. Recently, polymeric or non-polymeric genetically engineered carriers are the main two substantial groups of genetically engineered carriers, depended on the primary sequence of amino acids. Because non-polymeric genetically engineered carriers are deprived of the amino acid sequences repetition, the creation of drug carriers relies on their self-assembled quaternary structures. Elastin-like polypeptides (ELPs) [41,42], silk-like polypeptides (SLPs) [43,44], and silk-elastin-like polypeptides (SELPs) [45] are proficiently-developed examples of polymeric genetically engineered carriers. Viral-based proteins are the popularly utilized non-polymeric genetically engineered carriers [46,47]. Compared to chemically synthesized carriers, proteins can be efficiently engineered by adjusting

the sequences of amino acids at the genetic level, which can alter their secondary structures, and thus drive chemical features to acquire the desired tasks and functions [48,49]. For instance, one residue adjustment from the highly preserved repeats of amino acid sequences of ELPs could modify their water solubility [50]. SLPs synthesized nanocarriers have been mentioned to be utilized for gene-based delivery depending on the addition of polyarginine or cationic polylysine domains for DNA binding on SLPs [51].

1.3.2 Chemically engineered carriers

Liposomes are the most commonest lipid-based nanocarriers consisted of lipid bilayers that have the ability to encapsulate lipophilic compounds in the lipophilic membranes and lipophobic compounds including RNA/DNA in their hydrophilic cores [52,53]. They are basically unilamellar or multilamellar vacuoles that primarily compose of amphipathic phospholipids e.g., phosphatidylcholine (PC). Phospholipids are usually composed of the glycerol backbone, the hydrophilic head moiety, and the extended fatty tail, which could be adjusted for the desired features. For instance, the head moiety can be chemically attached to targeting ligands and functional groups [54]. The addition of polymeric motifs on the head group can enhance the stability of liposomes [55]. The insertion of the PEGylation principle is the first implementation in the nanoformulation aspect [56]. PEGylated liposomes revealed less attraction to be cleared via the reticuloendothelial system (RES) than traditional liposomes, which caused in vivo longer circulating half-life. This approach has been employed in the most types of further liposomal researches [57]. Along with chemotherapeutics, liposomes are utilized to encapsulate oligonucleotide-based compounds for cancer treatment. Although oligonucleotide-based cures demonstrate futuristic outcomes in

cancer therapies, effective delivery into the desired location still continues as a big challenge from several sides, such as enzymatic degradation, successful delivery to targeted cells, endogenous stability, endolysosomal emancipation and renal clearance. The further main kind of chemically engineered carriers is polymer-based delivery system for drug delivery and well considered for its good flexibility and biocompatibility for structure adjustment with intended properties [58,59]. PEG, poly-(lactic acid) (PLA), hyaluronic acid, poly-L-lysine (PLL), poly (cyano acrylates), poly-(ethylenimine) (PEI), poly-(lactic-co-glycolic acid) (PLGA), and chitosan are classical utilized polymers for well nano-based construction [60-62]. PEG, PLA and PLGA based nanocarriers have been most massively studied that were either accepted or in the various phases of clinical trials. PEG is one of bioinert and non-biodegradable hydrophilic polymer. Due to its flexible composition and higher water solubility, it is often utilized to stabilize DDS. A portion of the inherent immune system e.g., RES is the main hindrance to the successful delivery of medicines because of its capability of exogenous compounds engulfment through macrophageal phagocytosis and opsonisation [63]. Several studies have explicit that the surface modification of DDS via mediating hydrophilic PEG could minimize the protein interactions and reduce the opsonin attachments allowing to prolong the systemic half-life and limit the RES clearance [64,65]. As well, PEG as a stealth polymer had been widely harnessed in several present industrial DDS, such as Lipoplatin®, Xyotax®and Dexil®. Nevertheless, PEG is also commonly utilized for polymer-drug complexes in order to maximize the drug stability and solubility such as Oncaspar® which is PEG-attached asparaginase and was approved by FDA as a therapy for leukemia. The clinical trials demonstrated that single dose of this drug usually

replaced 8 doses of asparaginase itself, and more than 17-fold significantly prolong in the systemic circulation time than asparaginase itself [66-68].

1.4 Types of therapeutic drug delivery targeting

The major advantage of DDS used in cancer treatment is its ability to prohibit renal clearance, deliver into specifically targeted destinations with appropriate quantity, drop non-specific interactions and optimize cellular uptake. This important feature could be fulfilled via two fundamental pathways which are namely; passive targeting and active targeting.

1.4.1 Passive targeting

EPR effect is one of the pathophysiological features that is characterized by the accumulation and extravasation of nanoparticles or macromolecules in tumor location [69]. Because the effect of EPR could induce this type of passive drug delivery lonely in the tumor tissue along with minimized penetration into healthy tissues, this explained strategy is named as passive targeting, which mitigates the serious toxicity of chemotherapeutics [70,71]. Because of their smaller size, the aggregation of nanoparticles with each other and also the interaction with blood components could take place [72]. Through polymer coating on the surface of nanoparticles by using PEG, the steric stabilization effect could be created in order to preserve the desired particle size. Furthermore, this effect could limit the RES uptake of nanoparticles and extend their systemic circulation for promoted EPR effect [73]. In addition, the EPR mechanism allowed the nanoconstruct to accumulate in the cancer destination selectively. Polymeric micelles have been reported to be a favorable carrier of hydrophobic drugs as well as liposomes are another category of cancer therapeutic

nanocarrier possessing a self-assembling colloidal composition consisting of lipid bilayers which are biocompatible vesicles, easier to modify their surface, and have high potentiality for selective targeting of cancer cells. Dendrimers nanocarriers can offer good ligand density, controllable bioavailability, and pharmacokinetic profile. The system is adequate to functionalize proficiently and possesses high chemical and structural homogeneity. Although most of the nanostructures substantially focus on ameliorating the drug solubility, drug toxicity, and pharmacokinetic profile, a few nanoparticle-based chemotherapeutics have stimulated curable responses in patients and enhanced the total survival percentage comparatively to the non-formulated standard chemotherapies. For instance, In metastatic breast cancer patients, Abraxane (Albumin-Paclitaxel) nanoformulation significantly triggered the therapeutic response in phase III clinical trial in comparison with the standard Paclitaxel therapy [74-76].

1.4.2 Active targeting

In order to decrease side effects and maximize therapeutic efficacy, the principle of active targeting of nanoparticles to favorable destinations (e.g., cancerous tissues), has been mainly developed. Active targeting was first introduced via recruiting specific antibodies to target cancer cells [77]. Receptor-mediated targeting is one broadly applied approach of active targeting, where the ligands are attached to the surface of nanoparticles to identify particular receptors overexpressed via tumor or tumor microenvironment [78]. Different functional ligands have been estimated for active targeting encompassing proteins, aptamers, antibodies, and peptides [79]. Based on the desired locations, there are two strategies for the receptor-mediated active targeting: (1) target tumor microenvironment/vasculature and (2) target specific receptors on cancer cell surface. The enhancement of cellular uptake of nanoparticles

and thus stimulate the corresponding curable activity could occur by the active targeting of specific receptors overexpressed on the surface of cancer cells. Interestingly, the first antibody-attached liposomal structure was applied for lung cancer in mouse models and since that occasion, antibodies have been applied and evaluated as the targeting ligands for more than three decades [80]. Epidermal growth factor receptor (EGFR), a tyrosine kinase receptor, is widely overexpressed in several cancers including kidney, breast, colorectal and lung cancers, which could be used for active targeting [81]. Human epidermal receptor-2 (HER-2) is broadly overexpressed in breast cancer [82]. Monoclonal antibody-mediated nanoparticles targeting HER-2 or EGFR have been tremendously assessed for cancer treatment [83]. Folate receptor (FR) is typically overexpressed in brain, kidney, breast, lung cancers when compared to its low expression level in normal tissues. Furthermore, folic acid is relatively simple to be attached to nanoparticles and reveals high FR affinity for receptor-mediated endocytosis [84,85]. Transferrin is a serum glycoprotein that is responsible for iron transport within the human body. The expression of transferrin receptor (TR) is approximately 100 times in cancer cells higher than that in normal cells owing to the greater demand of iron for swift proliferation [86]. subsequently, it is a highly fascinating target for particular drug delivery by nanoparticles and several studies have been performed for this goal [87]. αβ-integrins, a type of transmembrane glycoprotein receptors overexpressed in different cancers, could enhance the adhesion of cancer cells to endothelium of blood vessels. Generally, a tripeptide, Arginine-Lycine-Aspartic acid (RGD) having massive integrin affinity, is used to suppress the angiogenesis and adhesion of cancer cells [88]. Actively-targeted nanoparticle based compounds demonstrated tremendous potentiality for cancer therapy through using the stimulated cancer localization and most critically via the selective suppression of

cancer cells limiting the adverse effects in cancer therapy [89]. Basically, the incorporation of actively targeting property with improvement in the design of nanocarrier will facilitate the fabrication of well-functionalized therapeutic nanoplatforms for cancer eradication [90]. Ligands recruited on the surface of actively-targeted nanocarrier promote the accumulation of nanoparticles in the endothelial cells of tumor blood vessels or intravascular cancer cells.

1.5 Research Objective

The current research focuses on the study of the assessment of the potential therapeutic activity of SHARP1 knockdown using multifunctionally targeted delivery system of therapeutic siRNA against MLL-AF6 AML cells. It is gradually being understood that these types of cancer cells are massively resistant to eradication due to high genetic mutations beside also they ultimately cause patient relapse [91]. Cytarabine and Anthracycline combination is still regarded as a standard treatment of AML while the clinical efficacy of this combination is poor and results in the death of millions of patients annually [92]. Consequently, identifying new treatments for AML may contribute substantially towards improving the survival of patients with this type of cancer. However, information regarding AML regulation is limited. Recently, Numata et al have demonstrated the crucial function of SHARP1 in MLL-AF6 AML survival, which is significantly regulated by MLL-AF6/DOT1L activity [93]. Nevertheless, the oncogenic role of *SHARP1* in MLL-AF6 AML growth and maintenance is still unclear. Therefore, *SHARP1* knockdown in ML-2 cells (specifically MLL-AF6 AML cells, which are more sensitive to *SHARP1*) will be investigated to determine *SHARP1* role in stimulating apoptosis and to define *SHARP1*-knockdown therapeutics for MLL-AF6 AML. Furthermore, we will use

bortezomib (BTZ) to augment therapeutic synergy because it can inhibit proteasomal enzymes and interfere with key regulatory signaling pathways such as suppression of nuclear factor-κB (NF-κB) leading to stimulation of apoptosis in different types of cancer, for example, multiple myeloma [94], chronic lymphocytic leukemia [95], and non-small cell lung cancer [96]. BTZ also induces cleavage of myeloid cell leukemia 1 protein (Mcl-1) and stabilization of Bax, p53, and c-Jun *N*-terminal kinase (JNK) overexpression, leading to ER stress-dependent cell death [97,98]. cRGD-mediated PEGylated cationic lipid nanoparticles will be utilized as a biodegradable nanoplatform to co-deliver siRNA/BTZ with targeted *SHARP1* knockdown, demonstrating a potential therapeutic option for MLL-AF6 AML. This approach will open new avenues for applying smart biocompatible re-engineered nanostructures *in vivo* and further clinical translation to produce advanced MLL-AF6 AML-targeting therapeutics.

On the other hands, we will investigate the effect of PLEKHA7 protein on the behavior and growth of AML cells and demonstrate how the existence of PLEKHA7 could alter AML cell characterizations. Since the role of PLEKHA7 in AML has not been studied previously, we attempt to demonstrate the correlation between PLEKHA7 expression and the incidence of AML growth. We further synthesize bioengineered nanoparticles for PLEKHA7 delivery to regulate the induction of AML behavior alteration and growth retardation in order to recruit a potential target for AML modulation.

Furthermore, PLEKHA7 is one of the most important molecules involved in tissue morphogenesis, tissue integrity maintenance, and tumor suppression function [99,100]. Numerous studies have reported a strong correlation between PLEKHA7 loss and the initiation of tumors [101-104]. However, the role of PLEKHA7 in AML had not been

studied previously. To further investigate the significance of PLEKHA7 protein in leukemia, leukemic cells will be transfected with PLEKHA7-loaded cRGD-mediated PEGylated cationic lipid nanoparticles to restore PLEKHA7 expression and PLEKHA7 effects on cellular adhesion and proliferation will be estimated. The restoration of adhesion normality and integrity, which was lost in AML cells, could result in normal homeostasis through regulated induction of AML behavior alteration and growth attenuation. Therefore, the restoration of PLEKHA7 will strengthen apical ZA and restrain AML aggressiveness. This approach will open a different direction for AML cell regulation and reversion.

1.6 Thesis Organization

The dissertation aims to study the potential therapeutic effect of SHARP1 knockdown using multifunctionally targeted delivery system of therapeutic siRNA on MLL-AF6 AML cell survival. Furthermore, we evaluate the effect of PLEKHA7 protein on the behavior and growth of AML cells and also reveal how the existence of PLEKHA7 could alter AML cell characterizations.

Chapter 1 is a general introduction of the research background, such as overview on AML, the vital roles of SHARP1 and PLEKHA7 in AML, as well as a review of the importance, usefulness, and significance of nanotechnology-based therapeutics, drug delivery systems and passive and active targeting for therapeutic drug delivery.

Chapter 2 represents the materials and methods which are utilized in this study.

Chapter 3 describes a comprehensive *in vitro* analysis on new multifunctional bioengineered smart nanoparticles using well-characterized cRGD-conjugated thiolated PEG (NHS-PEG6-maleimide) to effectively co-deliver siRNA/BTZ for targeted *SHARP1* silencing in MLL-AF6 AML cells. This chapter discusses the

effects of *SHARP1* downregulation on DOT1L and MLL-AF6 expression and highlights a new vital oncogenic role of *SHARP1* in MLL-AF6 AML growth and maintenance.

Chapter 4 demonstrates the affect of PLEKHA7, an apical adherens junction protein, using cRGD-mediated PEGylated cationic liposomal nanoparticles as a nanocarrier to investigate the regulated induction of AML behavior alteration and growth retardation. PLEKHA7 re-expression could diminish colony-forming ability and reinforce the incidence of growth retardation without apoptosis in AML cell lines. Furthermore, PLEKHA7 could regulate the restoration of cell surface adhesion and integrity during normal homeostasis.

Chapter 5 is the conclusion of this thesis.

References

1. M. Dorrance, Targeting leukemia stem cells in vivo with antagomiR-126 nanoparticles in acute myeloid leukemia. *Leukemia,* **29**, 2143–2153 (2015).
2. V. Trujillo-Alonso, et al, FDA-approved ferumoxytol displays anti-leukaemia efficacy against cells with low ferroportin levels. *Nat. Nanotechnol..* **14**, 616–622 (2019).
3. J. Zhu, S. G. Emerson, A new bone to pick: osteoblasts and the haematopoietic stem-cell niche. *Bioessays,* **26**, 595–599 (2004).
4. R. S. Taichman, Blood and bone: two tissues whose fates are intertwined to create the hematopoietic stem-cell niche. *Blood,* **105**, 2631–3639 (2005).
5. J. P. Levesque, I. G. Winkler, Cell adhesion molecules in normal and malignant hematopoiesis: from bench to bedside. *Curr. Stem Cell Rep.,* **2**, 356–367 (2016).

6. E. Ballabio, T. A. Milne, Epigenetic control of gene expression in leukemogenesis: cooperation between wild type MLL and M.LL fusion proteins. *Mol. Cell. Oncol*. **1,** e955330 (2014).

7. C. Meyer, et al, The MLL recombinome of acute leukemias in 2013. *Leukemia* **27,** 2165–2176 (2013).

8. K.M. Bernt, et al, MLL-rearranged leukemia is dependent on aberrant H3K79 methylation by DOT1L inhibitor. *Cancer Cell* **20,** 66–78 (2011).

9. M. Montagner, et al, SHARP1 suppresses breast cancer metastasis by promoting degradation of hypoxia-inducible factors. *Nature.* **487,** 380–384 (2012).

10. K. Yamada, K. Miyamoto. Basic helix-loop-helix transcription factors, BHLHB2 and BHLHB3; their gene expressions are regulated by multiple extracellular stimuli. *Front. Biosci*. **10,** 3151–3171 (2005).

11. Z. H. Zhou, et al, Roles of SHARP1 in thyroid cancer. *Mol. Med. Rep.* **13**, 5365–5371 (2016).

12. A. Numata, et al, The basic helix-loop-helix transcription factor SHARP1 is an oncogenic driver in MLL-AF6 acute myelogenous leukemia. *Nat. Commun.* **9,** 1622 (2018).

13. J. Shah, et al, PLEKHA7: Cytoskeletal adaptor protein at center stage in junctional organization and signaling. *Int. J. Biochem. Cell Biol.,* **75**, 112–116 (2016).

14. M. Takeichi, Dynamic contacts: rearranging adherens junctions to drive epithelial remodelling. *Nat. Rev. Mol. Cell Biol.,* **15**, 397–410 (2014).

15. T. J. Harris, U. Tepass, Adherens junctions: from molecules to morphogenesis. *Nat. Rev. Mol. Cell Biol.,* **11**, 502–514 (2010).

16. S. Kurita, T. Yamada, E. Rikitsu, W. Ikeda, Y. Takai, Binding between the junctional proteins afadin and PLEKHA7 and implication in the formation of adherens junction in epithelial cells. *J. Biol. Chem.,* **288**, 29356–29368 (2013).

17. S. Citi, P. Pulimeno, S. Paschoud, Cingulin, paracingulin, and PLEKHA7: signaling and cytoskeletal adaptors at the apical junctional complex. *Ann. N.Y. Acad. Sci.,* **1257**, 125–132 (2012).

18. J. C. Tille, et al, The expression of the zonula adhaerens protein PLEKHA7 is strongly decreased in high grade ductal and lobular breast carcinomas. *PLoS One,* **10**, e0135442 (2015).

19. L. J. Pence, et al, PLEKHA7, an apical adherens junction protein, suppresses inflammatory breast cancer in the context of high E-cadherin and p120-catenin expression. *Int. J. Mol. Sci.,* **22**, 1275 (2021).

20. K. Rea, et al, Simultaneous E-cadherin and PLEKHA7 expression negatively affects E-cadherin/EGFR mediated ovarian cancer cell growth. *J. Exp. Clin. Cancer Res.,* **37**, 146 (2018).

21. A. M. Mendonsa, T. Y. Na, B. M. Gumbiner, E-cadherin in contact inhibition and cancer. *Oncogene,* **37**, 4769–4780 (2018).

22. A. Kourtidis, et al, Distinct E-cadherin-based complexes regulate cell behaviour through miRNA processing or Src and p120 catenin activity. *Nat. Cell Biol.,* **17**, 1145–1157 (2015).

23. W. Meng, Y. Mushika, T. Ichii, M. Takeichi, Anchorage of microtubule minus ends to adherens junctions regulates epithelial cell-cell contacts. *Cell.,* **135**, 948–959 (2008).

24. P. Pulimeno, C. Bauer, J. Stutz, S. Citi, PLEKHA7 is an adherens junction protein with a tissue distribution and subcellular localization distinct from ZO-1 and E-cadherin. *PLoS One,* **5**, e12207 (2010).

25. A. Kourtidis, P. Z. Anastasiadis, PLEKHA7 defines an apical junctional complex with cytoskeletal associations and miRNA-mediated growth implications. *Cell Cycle,* **15**, 498–505 (2016).

26. E. E. Ladikou, H. Sivaloganathan, A. Pepper, T. Chevassut, Acute myeloid leukaemia in its niche: the bone marrow microenvironment in acute myeloid leukaemia. *Curr. Oncol. Rep.,* **22**, 27 (2020).

27. T. Yamaguchi, E. Kawamoto, A. Gaowa, E. J. Park, M. Shimaoka, Remodeling of bone marrow niches and roles of exosomes in leukemia. *Int. J. Mol. Sci.,* **22**, 1881 (2021).

28. N. Asada, Regulation of malignant hematopoiesis by bone marrow microenvironment. *Front. Oncol.,* **8**, 119 (2018).

29. J. K. Patra, et al, Nano based drug delivery systems: recent developments and future prospects. *Journal of nanobiotechnology*, **16**, 71 (2018).

30. M. J. Mitchell, et al, Engineering precision nanoparticles for drug delivery. *Nature reviews. Drug discovery*, **20**, 101–124 (2021).

31. G. Bozzuto, A. Molinari, Liposomes as nanomedical devices. *International journal of nanomedicine*, **10**, 975–999 (2015).

32. C. Faustino, L. Pinheiro, Lipid Systems for the Delivery of Amphotericin B in Antifungal Therapy. *Pharmaceutics*, **12**, 29 (2020).

33. N. Joubert, A. Beck, C. Dumontet, C. Denevault-Sabourin, Antibody-Drug Conjugates: The Last Decade. *Pharmaceuticals*, **13**, 245 (2020).

34. F. U. Din, et al, Effective use of nanocarriers as drug delivery systems for the treatment of selected tumors. *International journal of nanomedicine*, **12**, 7291–7309 (2017).

35. D. Rosenblum, N. Joshi, W. Tao, J. M. Karp, D. Peer, Progress and challenges towards targeted delivery of cancer therapeutics. *Nature communications*, **9**, 1410 (2018).

36. Z. Cheng, M. Li, R. Dey, Y. Chen, Nanomaterials for cancer therapy: current progress and perspectives. *Journal of hematology & oncology*, **14**, 85 (2021).

37. X. Chen, L. Liu, C. Jiang, Charge-reversal nanoparticles: novel targeted drug delivery carriers. *Acta pharmaceutica Sinica. B*, **6**, 261–267 (2016).

38. S. Yadav, A. K. Sharma, P. Kumar, Nanoscale Self-Assembly for Therapeutic Delivery. *Frontiers in bioengineering and biotechnology*, **8**, 127 (2020).

39. S. Kosuri, G. M. Church, Large-scale de novo DNA synthesis: technologies and applications. *Nature methods*, 11, 499–507 (2014).

40. T. Thi Nhu Thao, et al, Rapid reconstruction of SARS-CoV-2 using a synthetic genomics platform. *Nature*, **582**, 561–565 (2020).

41. J. Despanie, J. P. Dhandhukia, S. F. Hamm-Alvarez, J. A. MacKay, Elastin-like polypeptides: Therapeutic applications for an emerging class of nanomedicines. *Journal of controlled release : official journal of the Controlled Release Society*, **240**, 93–108 (2016).

42. M. Tjin, P. Low, E. Fong, Recombinant elastomeric protein biopolymers: progress and prospects. *Polym J,* **46**, 444–451 (2014).

43. W. Huang, A. Rollett, D. L. Kaplan, Silk-elastin-like protein biomaterials for the controlled delivery of therapeutics. *Expert opinion on drug delivery*, **12**, 779–791 (2015).

44. P. Shi, J. A. Gustafson, J. A. MacKay, Genetically engineered nanocarriers for drug delivery. *International journal of nanomedicine*, 9, 1617–1626 (2014).

45. R. N. Parker, W. A. Wu, T. B. McKay, Q. Xu, D. L. Kaplan, Design of Silk-Elastin-Like Protein Nanoparticle Systems with Mucoadhesive Properties. *Journal of functional biomaterials*, **10**, 49 (2019).

46. S. Bhaskar, S. Lim, Engineering protein nanocages as carriers for biomedical applications. *NPG Asia materials*, **9**, e371 (2017).

47. D. Diaz, A. Care, A. Sunna, Bioengineering Strategies for Protein-Based Nanoparticles. *Genes*, **9**, 370 (2018).

48. L. Balabanova, V. Golotin, A. Podvolotskaya, V. Rasskazov, Genetically modified proteins: functional improvement and chimeragenesis. *Bioengineered*, **6**, 262–274 (2015).

49. B. Kuhlman, P. Bradley, Advances in protein structure prediction and design. *Nat Rev Mol Cell Biol,* **20**, 681–697 (2019).

50. Y.Yang, H. B. Jones, T. P. Dao, C. A. Castañeda, Single amino acid substitutions in stickers, but not spacers, substantially alter UBQLN2 phase transitions and dense phase material properties. *The Journal of Physical Chemistry B*, **123**, 3618-3629 (2019).

51. L. Chambre, Z. Martín-Moldes, R. N. Parker, D. L. Kaplan, Bioengineered elastin- and silk-biomaterials for drug and gene delivery. *Advanced drug delivery reviews*, **160**, 186–198 (2020).

52. S. Drescher, P. van Hoogevest, The Phospholipid Research Center: Current Research in Phospholipids and Their Use in Drug Delivery. *Pharmaceutics*, **12**, 1235 (2020).

53. S. Senapati, *et al,* Controlled drug delivery vehicles for cancer treatment and their performance. *Sig Transduct Target Ther,* **3**, 7 (2018).

54. P. Marqués-Gallego, A. I. de Kroon, Ligation strategies for targeting liposomal nanocarriers. *BioMed research international*, **2014**, 129458 (2014).

55. A. G. Kohli, P. H. Kierstead, V. J. Venditto, C. L. Walsh, F. C. Szoka, Designer lipids for drug delivery: from heads to tails. *Journal of controlled release: official journal of the Controlled Release Society*, **190**, 274–287 (2014).

56. A. Puri, et al, Lipid-based nanoparticles as pharmaceutical drug carriers: from concepts to clinic. *Critical reviews in therapeutic drug carrier systems*, **26**, 523–580 (2009).

57. E. Beltrán-Gracia, et al, Nanomedicine review: clinical developments in liposomal applications. *Cancer Nano,* **10,** 11 (2019).

58. E. Caló, V. V. Khutoryanskiy, Biomedical applications of hydrogels: A review of patents and commercial products. *Eur Polym J*, **65**, 252-267 (2015).

59. L. Marsili, M. Dal Bo, F. Berti, G. Toffoli, Chitosan-Based Biocompatible Copolymers for Thermoresponsive Drug Delivery Systems: On the Development of a Standardization System. *Pharmaceutics*, **13**, 1876 (2021).

60. R. Rai, S. Alwani, I. Badea, Polymeric Nanoparticles in Gene Therapy: New Avenues of Design and Optimization for Delivery Applications. *Polymers*, **11**, 745 (2019).

61. N. Avramović, B. Mandić, A. Savić-Radojević, T. Simić, Polymeric nanocarriers of drug delivery systems in cancer therapy. *Pharmaceutics*, **12**, 298 (2020).

62. C. S. Linsley, B. M. Wu, Recent advances in light-responsive on-demand drug-delivery systems. *Therapeutic delivery*, **8**, 89–107 (2017).

63. R. Song, et al, Current development of biodegradable polymeric materials for biomedical applications. *Drug Des Devel Ther*, **12**, 3117–3145 (2018).

64. M. F. Attia, N. Anton, J. Wallyn, Z. Omran, T. F. Vandamme, An overview of active and passive targeting strategies to improve the nanocarriers efficiency to tumour sites. *J Pharm Pharmacol*, **71**, 1185-1198 (2019).

65. T. S. Levchenko, R. Rammohan, A. N. Lukyanov, K. R. Whiteman, V. P. Torchilin, Liposome clearance in mice: the effect of a separate and combined presence of surface charge and polymer coating. *Int J pharm*, **240**, 95-102 (2002).

66. S. S. Banerjee, N. Aher, R. Patil, J. Khandare, Poly(ethylene glycol)-Prodrug Conjugates: Concept, Design, and Applications. *J Drug Deliv*, **2012**, 103973 (2012).

67. I. Ekladious, Y. L. Colson, M. W. Grinstaff, Polymer–drug conjugate therapeutics: advances, insights and prospects. *Nat Rev Drug Discov,* **18,** 273–294 (2019).

68. P. Mishra, B. Nayak, R. K. Dey, PEGylation in anti-cancer therapy: An overview. *Asian J Pharm Sci,* **11**, 337-348 (2016).

69. S. K. Golombek, Tumor targeting via EPR: Strategies to enhance patient responses. *Advanced drug delivery reviews*, **130**, 17–38 (2018).

70. Y. Nakamura, A. Mochida, P. L. Choyke, H. Kobayashi, Nanodrug Delivery: Is the Enhanced Permeability and Retention Effect Sufficient for Curing Cancer?. *Bioconjugate chemistry*, **27**, 2225–2238 (2016).

71. D. Rosenblum, et al, Progress and challenges towards targeted delivery of cancer therapeutics. *Nat Commun,* **9**, 1410 (2018).

72. A. N. Ilinskaya, M. A. Dobrovolskaia, Nanoparticles and the blood coagulation system. Part II: safety concerns. *Nanomedicine*, **8**, 969–981 (2013).

73. J. S. Suk, Q. Xu, N. Kim, J. Hanes, L. M. Ensign, PEGylation as a strategy for improving nanoparticle-based drug and gene delivery. *Advanced drug delivery reviews*, **99**, 28–51 (2016).

74. E. Miele, G. P. Spinelli, E. Miele, F. Tomao, S. Tomao, Albumin-bound formulation of paclitaxel (Abraxane ABI-007) in the treatment of breast cancer. *Int J Nanomedicine,* **4**, 99–105 (2009).

75. P. Vishnu, V. Roy, Safety and Efficacy of nab-Paclitaxel in the Treatment of Patients with Breast Cancer. *Breast cancer : basic and clinical research*, **5**, 53–65 (2011).

76. J. Bhattacharyya, et al, A paclitaxel-loaded recombinant polypeptide nanoparticle outperforms Abraxane in multiple murine cancer models. *Nat Commun,* **6**, 7939 (2015).

77. B. Yu, H. C. Tai, W. Xue, L. J. Lee, R. J. Lee, Receptor-targeted nanocarriers for therapeutic delivery to cancer. *Mol Membr Biol*, **27**, 286–298 (2010).

78. J. Yoo, C. Park, G. Yi, D. Lee, H. Koo, Active Targeting Strategies Using Biological Ligands for Nanoparticle Drug Delivery Systems. *Cancers*, **11**, 640 (2019).

79. A. D. Friedman, S. E. Claypool, R. Liu, The smart targeting of nanoparticles. *Curr Pharm Des*, **19**, 6315–6329 (2013).

80. R. M. Lu, *et al,* Development of therapeutic antibodies for the treatment of diseases. *J Biomed Sci,* **27**, 1 (2020).

81. P. Wee, Z. Wang, Epidermal Growth Factor Receptor Cell Proliferation Signaling Pathways. *Cancers*, **9**, 52 (2017).

82. D. de Melo Gagliato, D. L. Jardim, M. S. Marchesi, G. N. Hortobagyi, Mechanisms of resistance and sensitivity to anti-HER2 therapies in HER2+ breast cancer. *Oncotarget*, **7**, 64431–64446 (2016).

83. A. Juan, et al, Antibody Conjugation of Nanoparticles as Therapeutics for Breast Cancer Treatment. *Int J Mol Sci*, 21, 6018 (2020).

84. P. Kumar, P. Huo, B. Liu, Formulation Strategies for Folate-Targeted Liposomes and Their Biomedical Applications. *Pharmaceutics*, **11**, 381 (2019).

85. B. Frigerio, et al, Folate receptors and transporters: biological role and diagnostic/therapeutic targets in cancer and other diseases. *J Exp Clin Cancer Res,* **38**, 125 (2019).

86. N. M. AlSawaftah, et al, Transferrin-modified liposomes triggered with ultrasound to treat HeLa cells. *Sci Rep*, **11**, 11589 (2021).

87. T. Koneru, et al, Transferrin: Biology and Use in Receptor-Targeted Nanotherapy of Gliomas. *ACS Omega*, **6**, 8727–8733 (2021).

88. J. Zhao, F. Santino, D. Giacomini, L. Gentilucci, Integrin-Targeting Peptides for the Design of Functional Cell-Responsive Biomaterials. *Biomedicines*, **8**, 307 (2020).

89. Y. Yao, et al, Nanoparticle-Based Drug Delivery in Cancer Therapy and Its Role in Overcoming Drug Resistance. *Front Mol Biosci*, **7**, 193 (2020).

90. X. Fu, et al, Precise design strategies of nanomedicine for improving cancer therapeutic efficacy using subcellular targeting. *Sig Transduct Target Ther,* **5**, 262 (2020).

91. H. Minderman, Y. Zhou, K. L. O'Loughlin, M. R. Baer. Bortezomib activity and in vitro interactions with anthracyclines and cytarabine in acute myeloid leukemia

cells are independent of multidrug resistance mechanisms and p53 status. *Cancer Chemother Pharmacol,* **60,** 245-255 (2007).

92. M. Dean, T. Fojo, S. Bates. Tumour stem cells and drug resistance. *Nat Rev Cancer,* **5,** 275-284 (2005).
93. A. Numata, et al, The basic helix-loop-helix transcription factor SHARP1 is an oncogenic driver in MLL-AF6 acute myelogenous leukemia. *Nat Commun,* **9**, 1622 (2018).
94. X. Y. Pei, Y. Dai, S. Grant, Synergistic induction of oxidative injury and apoptosis in human multiple myeloma cells by the proteasome inhibitor bortezomib and histone deacetylase inhibitors. *Clin Cancer Res,***10**,3839–3852 (2004).
95. Y. Dai, et al, Interactions between bortezomib and romidepsin and belinostat in chronic lymphocytic leukemia cells. *Clin Cancer Res,* **14**, 549-558 (2008).
96. D. E. Denlinger, B. K. Rundall, D. R. Jones, Proteasome inhibition sensitizes non-small cell lung cancer to histone deacetylase inhibitor-induced apoptosis through the generation of reactive oxygen species. *J Thorac Cardiovasc Surg,* **128**, 740–748 (2004).
97. M. Boccadoro, G. Morgan, J. Cavenagh, Preclinical evaluation of the proteasome inhibitor bortezomib in cancer therapy. *Cancer Cell Int,* **5**, 18 (2005).
98. Y. Dai, M. Rahmani, S. Grant, Proteasome inhibitors potentiate leukemic cell apoptosis induced by the cyclic-dependent kinase inhibitor flavopiridol through a SAPK/JNK- and NF-kappaB-dependent process. *Oncogene,* **22**, 7108–7122 (2003).

99. S. Citi, D, Guerrera, D. Spadaro, J. Shah, J, Epithelial junctions and Rho family GTPases: the zonular signalosome. *Small GTPases*, **5**, 1–15 (2014).

100. J. Nair-Menon, et al, Predominant Distribution of the RNAi Machinery at Apical Adherens Junctions in Colonic Epithelia Is Disrupted in Cancer. *Int J Mol Sci*, **21**, 2559 (2020).

101. L. J. Pence, et al, PLEKHA7, an Apical Adherens Junction Protein, Suppresses Inflammatory Breast Cancer in the Context of High E-Cadherin and p120-Catenin Expression. *Int J Mol Sci*, **22**, 1275 (2021).

102. K. Rea, et al, Simultaneous E-cadherin and PLEKHA7 expression negatively affects E-cadherin/EGFR mediated ovarian cancer cell growth. *J Exp Clin Cancer Res,* **37,** 146 (2018).

103. A. Kourtidis, et al, Cadherin complexes recruit mRNAs and RISC to regulate epithelial cell signaling. *J Cell Biol*, **216**, 3073–3085 (2017).

104. J. C. Tille, et al, The Expression of the Zonula Adhaerens Protein PLEKHA7 Is Strongly Decreased in High Grade Ductal and Lobular Breast Carcinomas. *PloS one*, **10**, e0135442 (2015).

Chapter 2. Materials and Methods

2.1 Synthesis of nanoparticles

2.1.1 SHARP1 nanoparticles

The siRNA duplex solution was prepared at 200 μM (3 mg/mL) and gently mixed with complexation buffer at 1:1 mol ratio for use as diluted siRNA (naked siRNA) with invivofectamine 3.0/lipofectamine RNAiMAX reagents (Invitrogen, Carlsbad, CA, USA), which were vortex dispersed immediately with 3 mM BTZ (EMD Millipore, St. Louis, MO, USA) diluted in Opti-MEM medium (Gibco, Waltham, MA, USA) just before use. The complex was incubated for 30 min at 50 ºC, sonicated for 1 h, then centrifuged at 500*g* for 5 min at 25 °C, and washed three times with deionized water to collect siRNA/BTZ loaded cationic liposomal nanoparticles (Lipo-siRNA-BTZ). The siRNA/BTZ-loaded cRGD-guided PEGylated cationic liposomal nanoparticles (Lipo-siRNA-BTZ-PEG-cRGD), c(RGDfK) linked with thiolated PEG (NHS-PEG6-maleimide) associated with head-to-tail cyclic modification for cell surface αvβ3 receptor targeting to form the RGD{d-Phe}{Lys(PEG-Mal)} sequence construct, which was purchased from GenScript (peptide-081102 ID: J7777DK130; Piscataway, NJ, USA). This was dissolved in PBS solution (pH 7.4) and stored as a stock. Subsequently, 100 μL of this stock solution was added to previously prepared lipid nanoparticles containing siRNA and BTZ. The resultant mixture was continuously stirred for 24 h at 25 °C in the dark and the nanoparticles were finally recovered by centrifugation at 100g for 10 min at 25 °C and washed three times with deionized water. The siRNA/BTZ

loaded cRGD-mediated PEGylated cationic nanoliposomes (Lipo-BTZ-PEG-cRGD) were formulated using the same protocol without the addition of diluted siRNA solution. Fluorescently labeled Lipo-siRNA-BTZ-PEG-cRGD nanoparticles were also prepared using the same protocol with siRNA conjugated to red fluorescent dye ATTO 550 (Sigma-Aldrich, St. Louis, MO, USA) solution. Briefly, 20 μL siRNA duplex solution was mixed with 60 μL DNase/RNase-free water (Invitrogen), 10 μL binding solution (Thermo Fisher Scientific, Waltham, MA, USA), and 10 μL ATTO 550 solution to obtain 100 μL of final complex.

2.1.2 PLEKHA7 nanoparticles

The PLEKHA7 stock solution was first prepared at 10 μg/mL and gently mixed with complexation buffer at a 1:1 mol ratio for use as diluted PLEKHA7 (50 μL stock diluted in 100 μL Opti-MEM medium (Gibco) just before use) and with Lipofectamine RNAiMAX reagents/invivofectamine 3.0 (Invitrogen). The complex was incubated for 30 min at 50 °C, sonicated for 1 h, centrifuged at 500 g for 5 min at 25 °C, and washed three times with deionized water to collect PLEKHA7-loaded cationic liposomal nanoparticles. For the preparation of PLEKHA7-loaded cRGD-guided PEGylated cationic liposomal nanoparticles (Lipo-PLEKHA7-PEG-cRGD), c(RGDfK) linked with thiolated PEG (NHS-PEG6-maleimide) associated with head to tail cyclic modification for cell surface αvβ3 receptors targeting to form RGD{d-Phe}{Lys(PEG-Mal)} sequence construct, which was purchased from GenScript (peptide-081102 ID: J7777DK130), and was then dissolved in PBS solution with pH 7.4 to be stored as a stock. Subsequently, 100 μL of this stock solution was added to the previously prepared lipid nanoparticle-entrapped PLEKHA7. The resultant mixture was continuously stirred for 24 h at 25–30 ºC in the dark. The nanoparticles

were finally recovered by centrifugation at 100 g for 10 min at 25 °C and washed three times with deionized water. Fluorescently labeled Lipo-PLEKHA7-PEG-cRGD nanoparticles were also prepared by the same protocol through conjugation of PLEKHA7 with the red fluorescent dye ATTO 550 (Sigma-Aldrich) solution. Briefly, 50 μL of PLEKHA7 solution was mixed with 30 μL of biologically free water (Invitrogen), 10 μL of binding solution (Thermo Fisher Scientific), and 10 μL of ATTO 550 solution to obtain 100 μL of the final complex. FITC-labeled Lipo-PLEKHA7-PEG-cRGD nanoparticles were also prepared by the same protocol through conjugation of PLEKHA7 with FITC (Sigma-Aldrich) solution.

2.2 Characterization

The sizes and zeta potentials of SHARP1 and PLEKHA7 nanoparticles were measured by dynamic light scattering using a Malvern Nano ZS90 Zetasizer (Malvern Instruments, Malvern, UK). Transmission electron microscopy (TEM) was performed using a JEOL 1200 EX transmission electron microscope. The morphologies of siRNA/BTZ loaded cRGD-tagged PEGylated cationic nanoliposomes (Lipo-siRNA-BTZ-PEG-cRGD) were studied by scanning electron microscopy (SEM) using a JSM-7200F scanning electron microscope (JEOL Ltd., Akishima, Japan).

2.3 Cell culture

The current study was performed on two different AML cell lines. Firstly, a human ML-2 cell line (ACC 15) was obtained from DSMZ (Braunschweig, Germany). These cells were originated from the peripheral blood of patient with acute myeloid leukemia (AML M4) at diagnosis of AML (following T-non-Hodgkin lymphoma and

T-ALL). These cells were cultured in RPMI-1640 (Gibco) supplemented with 10% heat-inactivated fetal bovine serum (FBS, Gibco). Secondly, a human KG-1a cell line (ECACC 91030101) was obtained from Cell Bank, Riken BRC, Japan). The cells were originated from Human Caucasian bone marrow acute myelogenous leukemia as a lymphoblast cell type. KG-1a cell line was derived from the parental KG-1 cells without responsiveness to colony stimulating factor in soft agar culture or to expression to the la-like antigen. The cells were cultured in IMDM (Gibco) supplemented with 20% heat-inactivated fetal bovine serum (FBS, Gibco). Both types of cells were maintained at 37 °C in a 5% CO_2 atmosphere.

2.4 Delivery study

For SHARP1 nanoparticles, Silencer Select pre-designed siRNA targeting SHARP1 was obtained from Invitrogen (antisense sequence of 5′-UAUACAAAGAGGAAUAGUCCA-3′ and a sense sequence of 5′-GACUAUUCCUCUUUGUAUATT-3′). ML-2 cells were transfected with naked siRNA and the indicated structured nanoparticles and investigated for SHARP1 knockdown efficiency by western blotting and qPCR at 2 d or 3 d post-transfection. For PLEKHA7 nanoparticles, Plekha7 in the pcDNA3.1-C-(K)DYK ORF clone (OHu22298D) was obtained from GenScript. ML-2 cells were transfected with diluted PLEKHA7 and Lipo-PLEKHA7-PEG-cRGD nanoparticles and were investigated to explore PLEKHA7 effectiveness in our experimental design.

2.5 Intracellular uptake and colocalization analysis

For SHARP1 nanoparticles, ML-2 cells were seeded in 35 mm glass-bottom dishes (Corning) (4×10^4 cells per well) 1 d prior to transfection. Lipo-siRNA-BTZ-

PEG-cRGD nanoparticles were prepared with ATTO-550 (Sigma-Aldrich) fluorophore (red, λ_{exc} = 554 nm and λ_{fl} = 576 nm) was used to track intracellular location of nanoparticles. After 4 h incubation at 37 ºC, cells were fixed with 4% paraformaldehyde in PBS (Sigma-Aldrich) for 15 min and directly stained with Hoechst 33342 (Molecular Probes, Eugene, OR, USA) and Concanavalin A-FITC (Sigma-Aldrich) for nuclei (blue, λ_{exc} = 361 nm and λ_{fl} = 461 nm) and cell membrane (green, λ_{exc} = 495 nm and λ_{fl} = 525 nm) labeling, respectively. Visualization of ATTO-labeled Lipo-siRNA-BTZ-PEG-cRGD for colocalization analysis, ML-2 cells was seeded in 35-mm glass-bottom dishes (Corning) at a density of 4×10^4 cells per well 1 d before transfection. ATTO-labeled Lipo-siRNA-BTZ-PEG-cRGD nanoparticles were prepared (red) to track the intracellular location of the nanoparticles. After 12 h of incubation, the cells were fixed with 4% paraformaldehyde in PBS (Sigma-Aldrich) for 20 min and then directly stained with 4,6-Diamidino-2-phenylindole (DAPI; D1306, Invitrogen, blue, λ_{exc} = 405 nm and λ_{fl} = 461 nm) for nuclei labeling.

For PLEKHA7 nanoparticles, KG-1a cells were seeded in 35-mm glass-bottom dishes (Iwaki AGC Techno Glass, Japan) at a density of 4×10^4 cells per well 1 d before transfection. Lipo-PLEKHA7-PEG-cRGD nanoparticles were prepared with ATTO 550 (Sigma-Aldrich) fluorophore (red) to track the intracellular location of the nanoparticles. After 4 h of incubation, cells were fixed with 4% paraformaldehyde in PBS (Sigma-Aldrich) for 15 min and were further stained with Hoechst 33342 (Molecular Probes) and ConcanavalinA-FITC (Sigma-Aldrich) for nuclei (blue) and cell membrane (green) labeling, respectively. Visualization of FITC-labeled Lipo-PLEKHA7-PEG-cRGD for colocalization analysis KG-1a cells was seeded in 35-mm glass-bottom dishes (Corning) at a

density of 4 × 10^4 cells per well 1 d before transfection. FITC-labeled Lipo-PLEKHA7-PEG-cRGD nanoparticles were prepared (green) to track the intracellular location of the nanoparticles. After 12 h of incubation, the cells were fixed with 4% paraformaldehyde in PBS (Sigma-Aldrich) for 20 min and then directly stained with phalloidin (red) for F-actin labeling.

The cells were imaged using a TiE-A1R confocal laser scanning microscope (Nikon). The experimental system was performed by utilizing 405 nm, 488 nm, 562 nm wavelengths of excitation lasers for Hoechst 33342, DAPI, FITC and ATTO-550, respectively. 3D images of the cells were obtained using Z-stack mode measurements. Images were analyzed using Nikon imaging software (NIS-Elements Viewer 4.50). For flow cytometry analysis, KG-1a cells were seeded in 96-well plates and harvested after 4 h for flow cytometry using FACS CantoII (BD Biosciences, Franklin, NJ, USA).

2.6 Cell viability and proliferation

1 × 10^4 cells were seeded in 96-well plates one day prior to transfection, incubated at 37 °C for 2 d, and, on the third day, subjected to CellTiter 96 AQueous Non-Radioactive Cell Proliferation Assay (Promega, Madison, WI, USA) according to the manufacturer's instructions. The absorbance was measured at the wavelength of 490 nm with a microplate reader (Bio-Rad 680, USA).

2.7 Colony formation assay

Colony formation assay was performed by plating 1,000 cells per well on a 6-well plate, transfected, before incubating them for 7 d. The colonies were fixed with

methanol:acetic acid 3:1 (v/v) and stained with 0.5% crystal violet in 20% methanol for 15 min. Number of colonies was counted using an inverted microscope.

2.8 Cell apoptosis and fluorescence

Cell apoptosis was evaluated using an Annexin V-FITC apoptosis detection kit following the manufacturer's protocol (Thermo Fisher Scientific) and analyzed with a FACS CantoII flow cytometer (BD Biosciences) within 1 h post staining as in ref [1]. The stained cells were divided into four populations after identification: Annexin V-FITC(−)/PI(−), Annexin V-FITC(+)/PI(−), Annexin V-FITC(+)/PI(+), and Annexin V-FITC(−)/PI(+), which were considered as living cells, early apoptotic cells, late apoptotic cells, and dead cells, respectively. The percentages of each population and total apoptosis was measured as calculations as below;

$$\text{Population}=N_{pop}/N_{total}\times 100$$

$$\text{Total apoptosis} = \text{Population}_{early} + \text{Population}_{late}$$

where N_{pop} and N_{total} are the number of cells from each individual population and the total population, respectively. $\text{Population}_{early}$ and Population_{late} are the percentages of the populations of the early apoptotic phase and late apoptosis phase, respectively.

For fluorescence imaging, cells were seeded into 35 mm glass-bottom dishes (Corning) and transfected with nanoparticles for 24 h. After two washes with PBS, the cells were stained with 5 μL Annexin V-FITC and PI and incubated at 25 °C in the dark for 15 min. For nuclei staining, stained cells were counterstained with 4,6-Diamidino-2-phenylindole (DAPI; D1306, Invitrogen) and visualized using an inverted fluorescence microscope (Keyence BZ-9000, Osaka, Japan).

2.9 Live-cell imaging and cell growth assay

For phase contrast, ML-2 and KG-1a cells were seeded into 96-well plates (at a density of ~4 × 10^4 cells/well), incubated for 4 h, and then were transfected with Lipo-siRNA-BTZ-PEG-cRGD and Lipo-PLEKHA7-PEG-cRGD nanoparticles. After washing twice with PBS, the cells were suspended in fresh media and monitored using the IncuCyte ZOOM (Essen BioScience, Ann Arbor, MI, USA) acquiring images at 30 min intervals for 48 h to assess the growth rate of cells before and after treatment.

For the fluorescence-based technique, ML-2 and KG-1a cells were seeded into 96-well plates (at a density of ~4 × 10^4 cells/well), incubated for 4 h, and then were transfected with Lipo-siRNA-BTZ-PEG-cRGD and Lipo-PLEKHA7-PEG-cRGD nanoparticles. After two PBS washes, the cells were stained with IncuCyte NucLight Rapid Red Reagent for nuclear labeling (Essen Bioscience) and monitored using the IncuCyte ZOOM (Essen BioScience) acquiring images at 1 h intervals for 48 h.

For cell growth quantification, transfected cells and untreated cells were seeded in 96-well plates (5000 cells/well) using IncuCyte ZOOM (Essen Bioscience) for every 1 h of imaging. The confluence was analyzed using the IncuCyte ZOOM 2016A software.

2.10 Western blot

For SHARP1 nanoparticles, ML-2 cells were treated with naked siRNA, Lipo-siRNA-BTZ, Lipo-BTZ-PEG-cRGD, Lipo-BTZ-siRNA-PEG-cRGD for 3 d, and further cultured for 2 d before lysis. The cells were suspended in a radioimmunoprecipitation (RIPA) lysis buffer (Santa Cruz Biotechnology, Dallas, TX, USA) for whole cell lysis. Proteins were separated by SDS-PAGE and blotted

onto PVD membrane (Millipore). Images were captured and chemiluminescent signals were analyzed using ImageQuant LAS 4010 (GE Healthcare, Chicago, IL, USA). Western blot experiments were performed using the following antibodies: anti-SHARP1 (sc-373763, 1:1000 working dilution, overnight shaking incubation at 4 °C), Cruz Marker molecular weight standards (sc-2035), and β-actin (sc-47778, 1:5000 working dilution, overnight shaking incubation at 4 °C) from Santa Cruz Biotechnology and a secondary horseradish peroxidase (HRP)-conjugated antibody from Abcam (ab205718, 1:2000 working dilution, incubation at 25 °C for 1 h).

For SHARP1 nanoparticles, KG-1a cells were treated with Lipo-PLEKHA7-PEG-cRGD for 3 d, and further cultured for 2 d before lysis. The cells were suspended in a radioimmunoprecipitation (RIPA) lysis buffer (Santa Cruz Biotechnology, Dallas, TX, USA) for whole-cell lysis. Proteins were separated by SDS-PAGE and blotted onto the PVD membrane (Millipore). The same protocol was repeated with untreated KG-1a cells as a control cells to investigate PLEKHA7 expression in the cells before and after the addition of Lipo-PLEKHA7-PEG-cRGD. Images were captured, and chemiluminescent signals were analysed using ImageQuant LAS 4010 (GE Healthcare, Chicago, IL, USA). Western blot experiments were performed using the following antibodies: anti-PLEKHA7 (PA585686, 1:1000 working dilution, overnight shaking incubation at 4 °C), Cruz Marker molecular weight standards (sc-2035), β-actin (sc-47778, 1:5000 working dilution, overnight shaking incubation at 4 °C) from Santa Cruz Biotechnology and secondary horseradish peroxidase (HRP)-conjugated antibody from Abcam (ab205718, 1:2000 working dilution, incubation at 25 °C for 1 h). Image J software was used to quantify PLEKHA7 protein expression in KG-1a cells.

2.11 Quantitative PCR

For SHARP1 nanoparticles, RNA was extracted using an RNeasy kit (QIAGEN, Hilden, Germany) and reverse-transcribed using the QuantiTech Reverse Transcription kit (QIAGEN). PCR was performed using SYBR Green JumpStart Taq Ready Mix (Sigma-Aldrich) and quantitatively assessed on a Mx3000P (Agilent Technologies). For each sample, transcript levels of tested genes were normalized to GAPDH using the $2^{-\Delta\Delta CT}$ method. The highest expression was arbitrarily set to 1 and expressions in the other samples were normalized to this value. All experiments were performed in triplicate. PCR was performed using cDNA and primer sequences listed in Table 2.1.

Table 2.1 RT-PCR primers used in this study

Target gene	Sequence (5′-3′)	
	F	R
SHARP1	TAACCGAGCAACAGCATCAG	TTTGAAATCCCGAGTGGAAC
MLL-AF6	GTCGGGAAGGAACCCGGTAC	GCGTTCCAGTGGTGGATGATGT
DOT1L	CCACCAACTGCAAACATCAC	AGAGGAAATCGCCTCTCTCC
GAPDH	GATGCCCTGGAGGAAGTGCT	AGCAGGCACAACACCACGTT

2.12 Immunofluorescence and image analysis

For SHARP1 nanoparticles, ML-2 cells were treated with Lipo-siRNA-BTZ-PEG-cRGD nanoparticles, fixed with 4% paraformaldehyde for 20 min, and

permeabilized in PBS containing 0.1% Tween 20 (9809S, Cell Signaling Technology, Danvers, MA, USA) for 10 min. For the immune reaction, cancer cells were incubated in a solution containing the primary antibody, anti-SHARP1 (sc-373763, 1:200, Santa Cruz Biotechnology), in staining buffer for overnight at 4 °C. Cells were washed in PBS and then incubated with a goat anti-rabbit IgG secondary antibody conjugated to Alexa Fluor 568 (Thermo Fisher Scientific; A-11036, 4 μg/mL, red, λ_{exc} = 543 nm and λ_{fl} = 603 nm) in staining buffer for 1 h. For nuclei staining, stained cells were counterstained with DAPI (D1306, Invitrogen, blue, λ_{exc} = 405 nm and λ_{fl} = 461 nm) for 1 h before visualization by TiE-A1R confocal laser scanning microscope (Nikon). The experimental system was performed by utilizing 405 nm and 562 nm wavelengths of excitation lasers for DAPI and Alexa Fluor 568, respectively. Image data were analyzed by Nikon imaging software (NIS-Elements Viewer 4.50), and the number of anti-SHARP1-positive cells was counted using MATLAB R2020b software.

2.13 Adhesion-associated proliferation assay

Briefly, 1 × 10^6 KG-1a cells were seeded in 48-well plate and transfected with naked PLEKHA7, Lipo-PLEKHA7, Lipo-PEG-cRGD and Lipo-PLEKHA7-PEG-cRGD nanoparticles for 2 d. After washing, KG-1a cells were resuspended in a Collagen Ⅰ-coated 48-well plate and were incubated at 37 °C for 20 min to allow the cells to adhere with the surface. To washing off the non-adherent cells, 200 μl IMDM were added to each well to wash and repeated 4 times. After complete washing, cells were recovered by adding fresh media and were incubated at 37 °C for 4 h. CellTiter 96 AQueous Non-Radioactive Cell Proliferation Assay (1 mg/ml) was added to each well and cells were continuously incubated at 37 °C for 2 h. The cell count of the

adhered cells was assayed by the measurement of absorbance signals to evaluate the surface adhesion capability of the cells.

For cell surface adhesion investigation, KG-1a cells were seeded into 35 mm glass-bottom dishes (Corning). Untreated cells, naked PLEKHA7 treated cells and Lipo-PEG-cRGD treated cells were used for the comparison with the cells treated with Lipo-PLEKHA7-PEG-cRGD by utilizing the following stains; FITC (green) for cell membrane, ATTO 550 (red) for actin and Hoechst 33342 (blue) for nuclei. KG-1a cells were treated with FITC-labeled Lipo-PLEKHA7-PEG-cRGD nanoparticles for 24 h. After washing twice with PBS, the cells were counterstained with 4,6-Diamidino-2-phenylindole (DAPI; D1306, Invitrogen) for nuclei staining and then visualized using an inverted fluorescence microscope (Keyence BZ-9000, Osaka, Japan).

In order to further confirm cell surface adhesion, cells treated with Lipo-PLEKHA7-PEG-cRGD nanoparticles were compared with untreated cells, for which KG-1a cells were seeded into 96-well plates (at a density of ~4×10^4 cells/well), incubated for 4 h, and then treated with Lipo-PLEKHA7-PEG-cRGD. After washing twice with PBS, the cells were stained with IncuCyte NucLight Rapid Red Reagent for nuclear labeling (Essen Bioscience) and the images were captured at 1 h scan intervals for 24 h.

2.14 Statistical analysis

The statistical significances were analyzed by Student's t-test and ANOVA using JMP Pro 15 software (SAS Institute Inc., Cary, NY, USA), and the data are presented as the mean ± SEM *$p < 0.05$; **$p < 0.01$; ***$p < 0.001$.

References

1. W. Payoungkiattikun, A. Joompang, S. Thongchot, *et al.* Evidence of multi-functional peptide activity: potential role of KT2 and RT2 for anti-inflammatory, anti-oxidative stress, and anti-apoptosis properties. *Appl Biol Chem.* **63,** 5 (2020).

Chapter 3. Effect of multifunctional nanoparticle-mediated *SHARP1* knockdown in MLL-AF6 acute myeloid leukemic cells

3.1 Introduction

Acute myeloid leukemia (AML) is a heterogeneous and aggressive blood cancer resulting from irregular proliferation and differentiation of myeloid blasts initiating in the bone marrow, spleen, and peripheral blood. AML survival rates are significantly low in experienced patients with high relapse rates, elderly and pediatric patients with multiple mutations [1]. *MLL* (mixed-lineage leukemia; chromosome 11q23) rearrangements are popular chromosomal aberrations related to AML. *MLL* translocation induces the production of MLL-FP complex, wherein the genomic portion encoding the amino-terminus of *MLL* attaches to the carboxyl-terminal of a group of fusion partner proteins, leading to marked leukemogenic transcriptional machinery [2]. *MEN1*, *LEDGF*, *AF4*, and over 70 partner genes of MLL have been functionalized in MLL-rearranged (MLLr) AML [3]. MLL-AF6 has been regarded as the most popular leukemogenic MLL fusion protein, employing both distributor of telomeric silencing 1-like (DOT-1L) and elongation-assisting protein (EAP) complexes [4].

Exploring new therapeutic mechanisms for molecular targeting and effective targeted delivery systems are necessary for upgrading a much-needed AML medication. It is known that *SHARP1* is a circadian clock transcription factor involved in the regulation of various types of cancer such as breast, colon, and thyroid

carcinomas [5-7]. However, information regarding *SHARP1* correlation with AML regulation is limited. Recently, a study has demonstrated the crucial function of *SHARP1* in MLL-AF6 AML survival, which is significantly regulated by MLL-AF6/DOT1L activity [8]. Otherwise, the oncogenic role of *SHARP1* in MLL-AF6 AML growth and maintenance is still mysterious. In the current research, *SHARP1* knockdown in ML-2 cells (specifically MLL-AF6 AML cells, which are more sensitive to *SHARP1*) was evaluated to determine *SHARP1* role in stimulating autophagy and apoptosis and to define *SHARP1*-knockdown therapeutics for MLL-AF6 AML. Multifunctional biodegradable lipid nanoparticles engineered to efficiently co-deliver siRNA and bortezomib (BTZ) have improved most emerging challenges of traditional therapeutics [9,10]. Furthermore, BTZ combined with proteasomal enzymes inhibition in order to interfere with key regulatory signaling pathways such as suppression of nuclear factor-κB (NF-κB) leading to stimulation of apoptosis in various types of cancer, for example, multiple myeloma [11], chronic lymphocytic leukaemia [12], and non-small cell lung cancer [13]. BTZ also induced cleavage of myeloid cell leukemia 1 protein (Mcl-1) and stabilization of Bax, p53, and c-Jun *N*-terminal kinase (JNK) overexpression, leading to ER stress-dependent cell death [14,15].

In nanoparticle-mediated drug delivery systems, liposomal nano-based carriers are the most broadly harnessed drug delivery transporters, and this nanoplatform is the only current drug delivery nanoparticle system that has been awarded FDA approval for clinical practice, due to its marvelous physicochemical features and higher biocompatibility [16]. This recent report has focused on bioconjugation approaches that are required for supplying the desired advances in liposomal technologies to ameliorate drug cargo targeting, loading, and potency [16].

Incorporating an inert polymer, polyethylene glycol (PEG), enhances the surface fictionalization of cationic nanoliposome-siRNA complexes (lipoplexes), generating sterically stabilized nanoparticles [17,18]. For selective targeting, surface ligands such as cyclic RGD (arginine-glycine-aspartate), which specifically binds with high affinity to αvβ3 integrin, stimulate cell–nanomaterial interactions and allow targeted cargo penetration [19]. An RGD{d-Phe}{Lys(PEG-Mal)} sequence was synthesized by linking c(RGDfK) to thiolated PEG (NHS-PEG6-maleimide) with head-to-tail cyclic modification, conferring a bioengineered surface that permits optimal nanostructure functionalization.

The purpose of the present study is to investigate the potential therapeutic activity of SHARP1 knockdown using multifunctionally targeted delivery system (Lipo-PEG-cRGD) of therapeutic siRNA against MLL-AF6 AML cells.

3.2 Results

3.2.1 Nanoparticle synthesis and characterization

We exhibit the first preclinical experimental research for *SHARP1*-based AML therapy using therapeutic siRNA nanodelivery (Figure 3.1). We show that *SHARP1* is an MLL-AF6-dependent leukemogenic driver, consistent with multifunctional bioengineered nanoparticle activity in *SHARP1* downregulation, revealing a potential approach for human MLL-AF6 AML treatment. Transmission electron microscopy (TEM) images (Figure 3.2) revealed that the prepared nanoparticles were spherical with regular structure and configuration. Scanning electron microscopy (SEM) also revealed Lipo-siRNA-BTZ-PEG-cRGD uniform spherical shape and narrow size distribution (Figure 3.3). The average hydrodynamic diameters of Lipo-siRNA-BTZ, Lipo-BTZ-PEG-cRGD, and Lipo-siRNA-BTZ-PEG-cRGD were 78.9 ± 13.8 nm,

101.1 ± 15.2 nm, and 138.6 ± 18.5 nm (Figure 3.4), respectively, as estimated by dynamic light scattering. The zeta potentials of the nanoparticles were 26.6 ± 2.1 mV, 13.1 ± 1.1 mV, and 24 ± 1.9 mV, respectively, indicating that the negative charges of siRNA in the nanoformulation are masked (Table 3.1). These results showed that therapeutic siRNA was encapsulated in the nanoparticles without bulky aggregation or degradation.

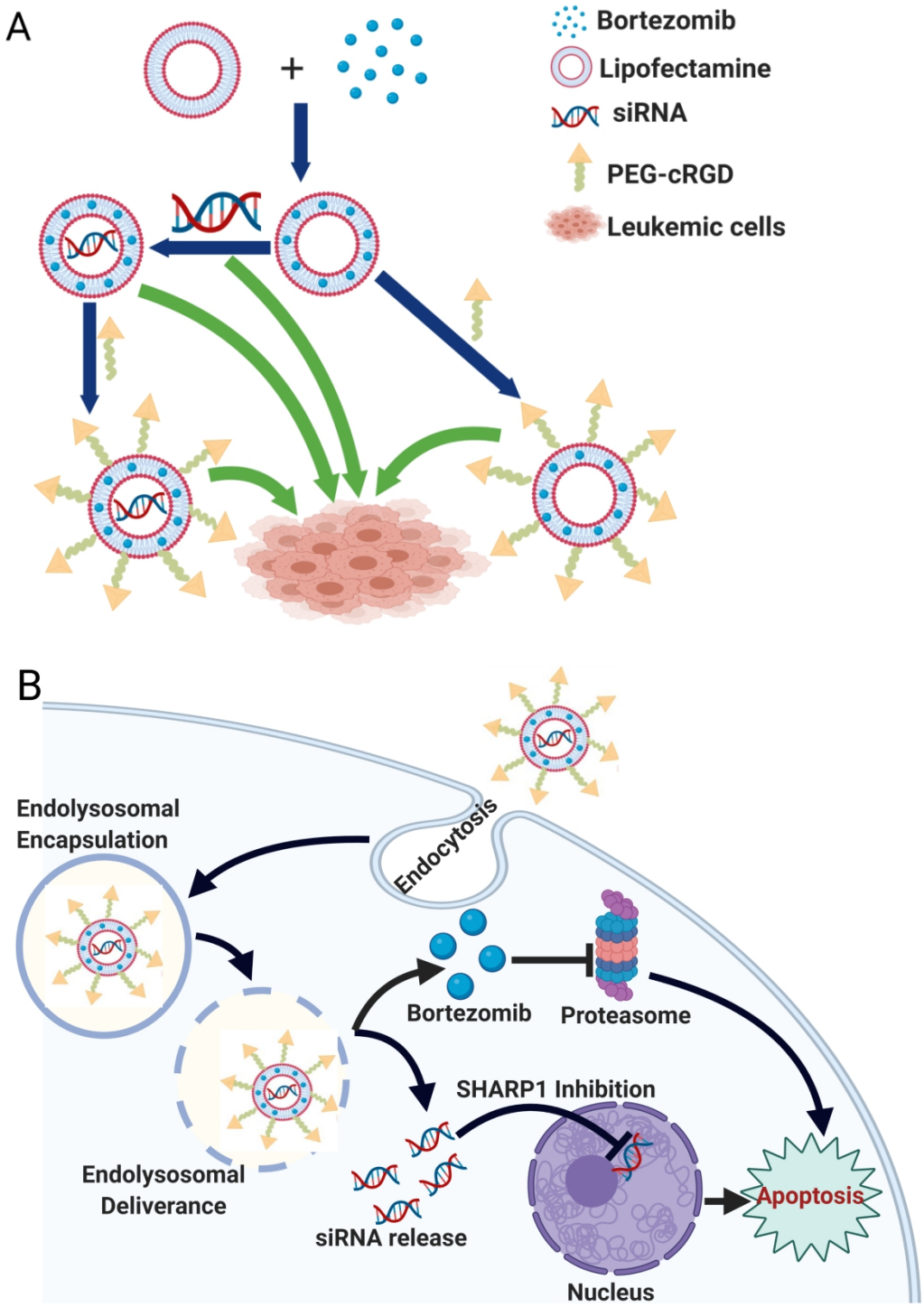

Figure 3.1 (A) A schematic illustration of naked siRNA, Lipo-siRNA-BTZ, Lipo-BTZ-PEG-cRGD and Lipo-siRNA-BTZ-PEG-cRGD for co-delivery of therapeutic siRNA and bortezomib in MLL-AF6 AML cells. (B) Proposed cellular uptake mechanisms of Lipo-siRNA-BTZ-PEG-cRGD and subcellular siRNA and BTZ release to inhibit SHARP1 and proteasomal enzymes, respectively, for inducing cancer cell apoptosis.

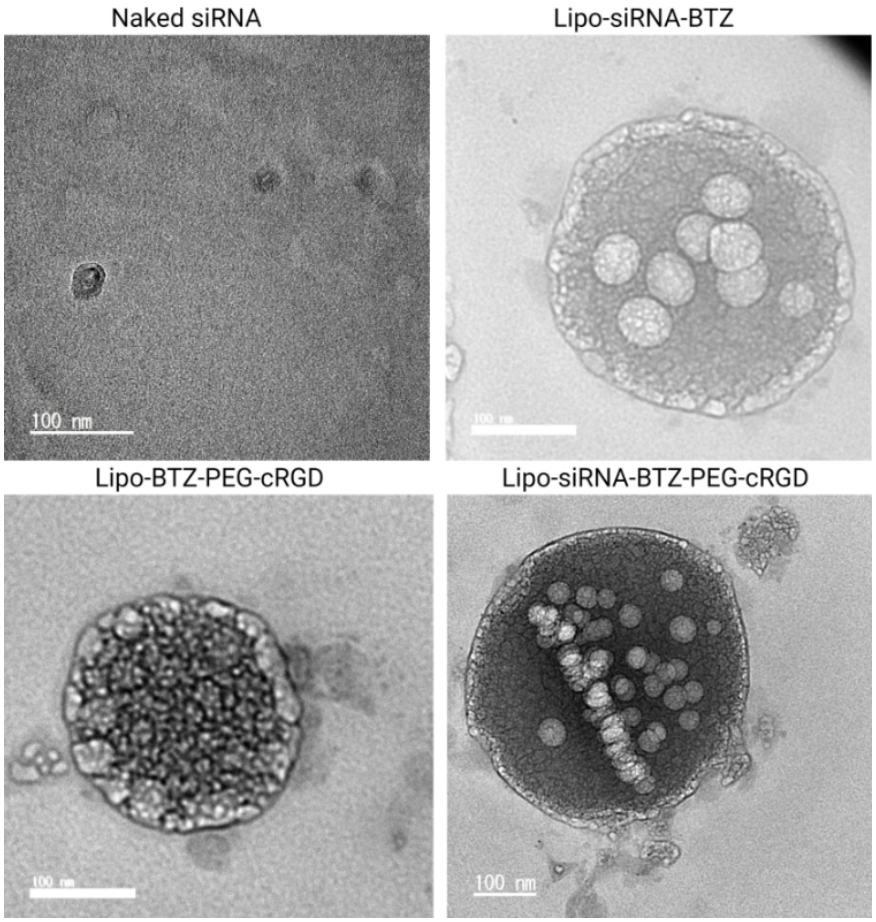

Figure 3.2 Transmission electron microscope (TEM) images of naked siRNA, Lipo-siRNA-BTZ, Lipo-BTZ-PEG-cRGD and Lipo-siRNA-BTZ-PEG-cRGD. Scale bar: 100 nm, n = 3.

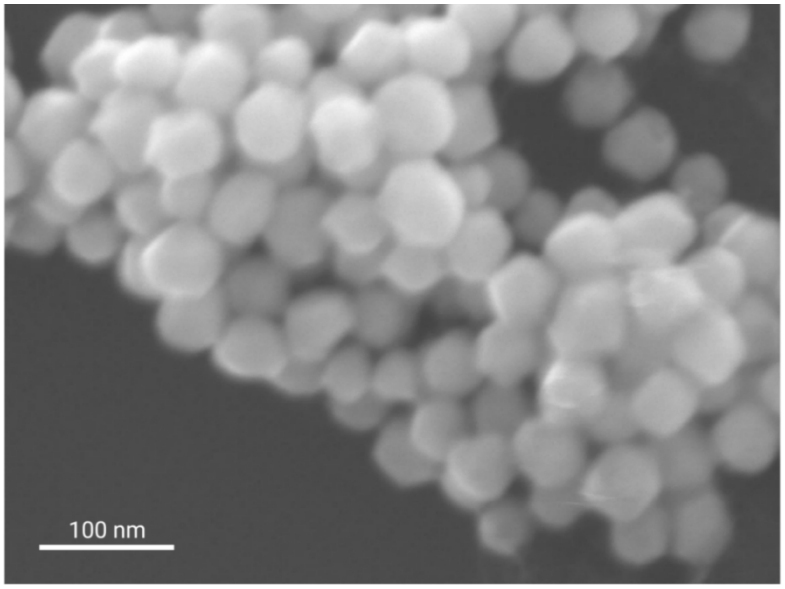

Figure 3.3 Scanning electron microscope (SEM) image of Lipo-siRNA-BTZ-PEG-cRGD. Scale bar: 100 nm, n = 3).

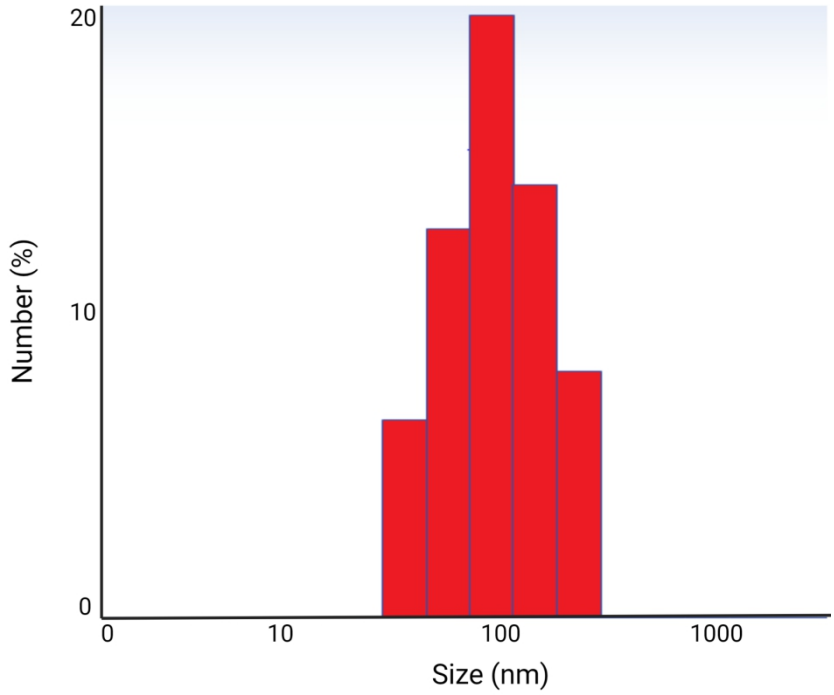

Figure 3.4 Dynamic light scattering plot of Lipo-siRNA-BTZ-PEG-cRGD (n = 3).

Table 3.1 Size and zeta potential characterizations (mean ± SEM) of different treatment groups

Groups	Size (nm)	PDI	Zeta potential (mV)
Lipo-siRNA-BTZ	78.9 ± 13.8	0.473 ± 0.021	26.6 ± 2.1
Lipo-BTZ-PEG-cRGD	101.1 ± 15.2	0.241 ± 0.032	13.1 ± 1.1
Lipo-siRNA-BTZ-PEG-cRGD	138.6 ± 18.5	0.192 ± 0.014	24 ± 1.9

3.2.2 Intracellular uptake and colocalization analysis

We used confocal microscopy to evaluate Lipo-siRNA-BTZ-PEG-cRGD uptake by ML-2 cells (see Figure 3.5). ML-2 cells were transfected with ATTO 550 red-labeled Lipo-siRNA-BTZ-PEG-cRGD, which was observed in the cytoplasm after 4 h of

incubation. A comprehensive cellular uptake study showed aggregated and dense ATTO 550 red-labeled Lipo-siRNA-BTZ-PEG-cRGD surrounding the nucleus. Moreover, 3D images (Figure 3.6) revealed a noteworthy boost of ATTO 550 red-labeled Lipo-siRNA-BTZ-PEG-cRGD. Furthermore, the visible colocalization between cell nuclei (blue) and ATTO 550-labeled Lipo-siRNA-BTZ-PEG-cRGD (red) showed effective nanoparticle transfection in ML-2 cells (Figure 3.7). Flow cytometry with fluorescence intensity quantification further confirmed the intracellular uptake efficiency of Lipo-siRNA-BTZ-PEG-cRGD (Figures 3.8 and 3.9).

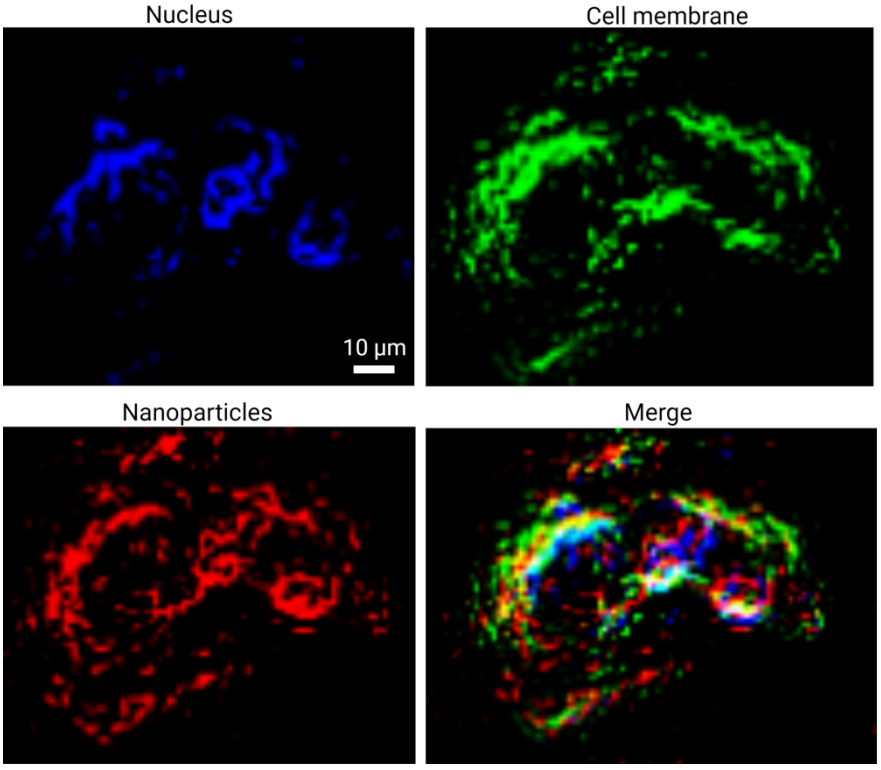

Figure 3.5 Cellular uptake of fluorescently labeled Lipo-siRNA-BTZ-PEG-cRGD into ML-2 cells. Scale bar: 10 µm; blue (Hoechst 33342) represents nuclei, green (Concanavalin A-FITC) the cell membranes, and red (ATTO 550) the Lipo-siRNA-BTZ-PEG-cRGD nanoparticles.

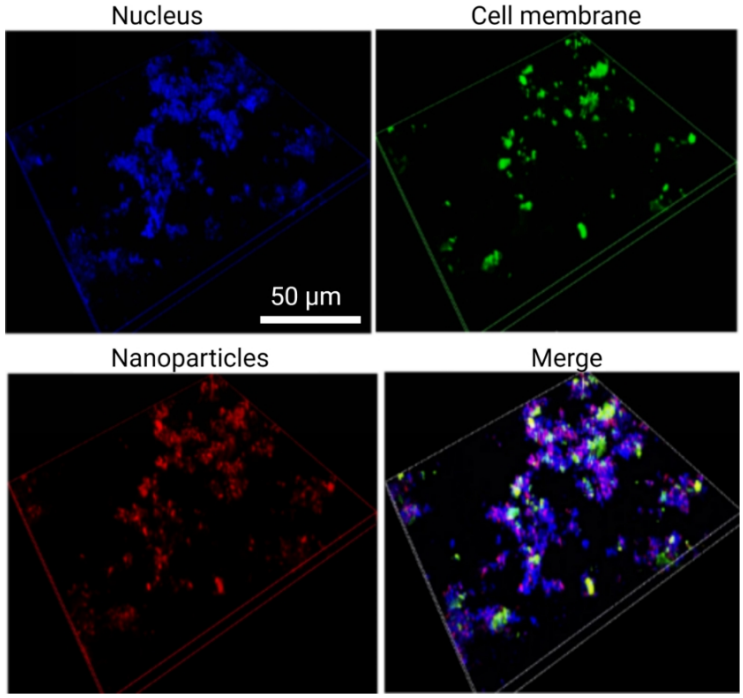

Figure 3.6 3D images of the cellular uptake of fluorescently labeled Lipo-siRNA-BTZ-PEG-cRGD nanoparticles into ML-2 cells. Scale bar: 50 µm; blue (Hoechst 33342) represents nuclei, green (Concanavalin A-FITC) the cell membranes, and red (ATTO 550) the Lipo-siRNA-BTZ-PEG-cRGD nanoparticles.

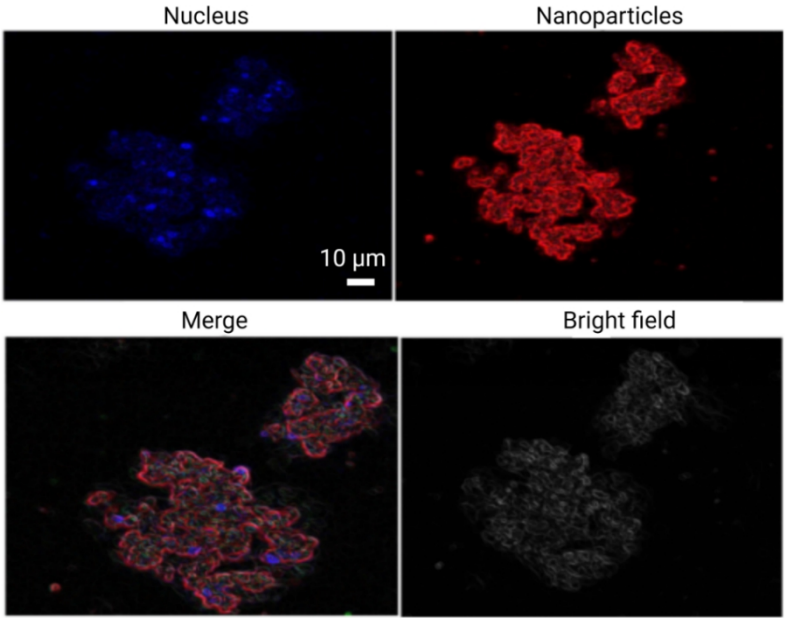

Figure 3.7 Colocalization of fluorescently labeled Lipo-siRNA-BTZ-PEG-cRGD in ML-2 cells. Scale bar: 10 µm; blue (Hoechst 33342) represents nuclei and red (ATTO 550) the Lipo-siRNA-BTZ-PEG-cRGD nanoparticles.

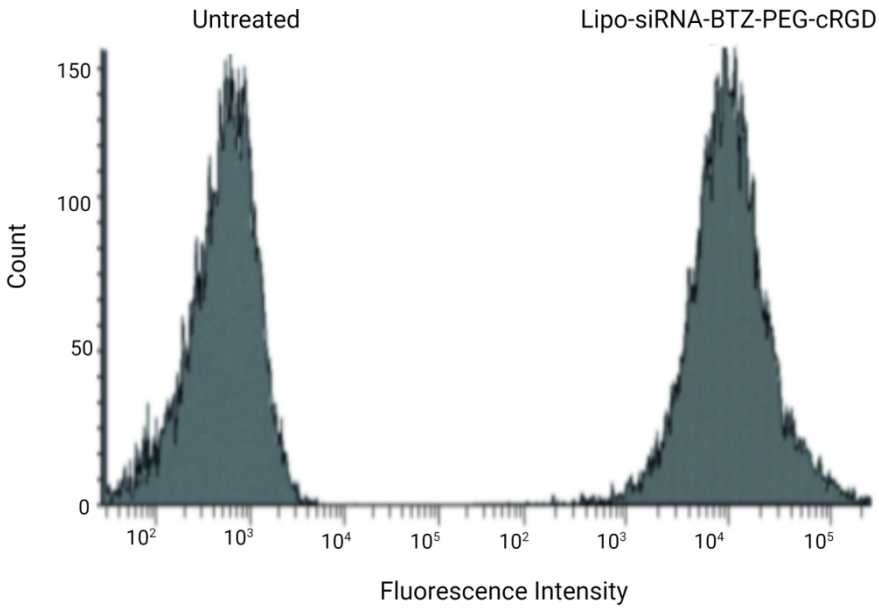

Figure 3.8 Flow cytometry for quantification of the fluorescence intensity of ATTO 550 in ML-2 cells. Experiments were performed in triplicate.

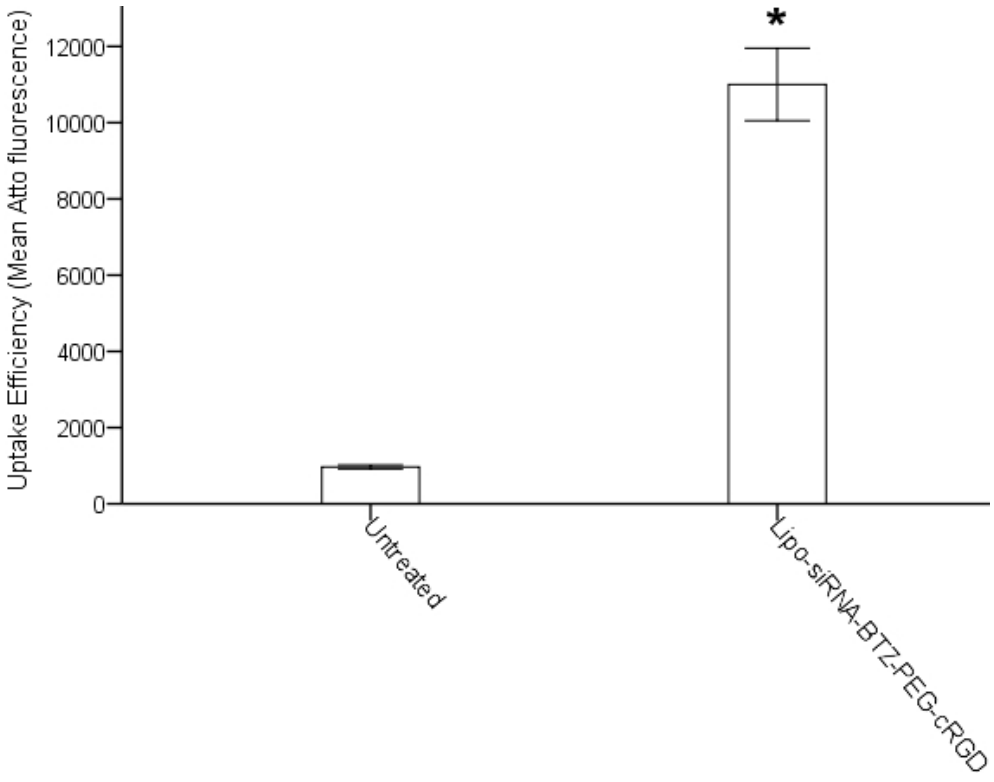

Figure 3.9 Cellular uptake efficiency of Lipo-siRNA-BTZ-PEG-cRGD in ML-2 cells. Data are presented as mean ± SEM (n= 3 biological replicates). Statistical significance was set at $*p < 0.05$.

3.2.3 Nano-mediated siRNA therapy

To elucidate *SHARP1* inhibition in ML-2 cells, naked siRNA and the nanoparticles were compared with control during knockdown experiments. Western blotting, qPCR, and immunofluorescence confirmed knockdown efficiency, displaying that nanoparticle-mediated siRNA delivery significantly reduced *SHARP1* expression. SHARP1 protein expression was significantly downregulated in cells treated with Lipo-siRNA-BTZ and Lipo-siRNA-BTZ-PEG-cRGD (Figures 3.10 and 3.11). We observed 60% and 95% of SHARP1 suppression by Lipo-siRNA-BTZ and Lipo-siRNA-BTZ-PEG-cRGD nanoparticles ($p < 0.05$), respectively. This suppression was further evidenced by our results on mRNA-level *SHARP1* expression in ML-2 cells (Figure 3.12). Lipo-siRNA-BTZ-PEG-cRGD caused the highest *SHARP1* downregulation: approximately 80% lower expression than in other treatments. However, we observed no significant change ($p < 0.05$) in the *SHARP1* expression level in naked siRNA- or Lipo-BTZ-PEG-cRGD-treated cells. We further assessed the antileukemic activity of naked siRNA and nanoparticles with viability and colony formation assays. Immunofluorescence results confirmed successful SHARP1 silencing in Lipo-siRNA-BTZ-PEG-cRGD-treated cells. We observed significant reductions in the number of anti-SHARP1-positive cells (red labeled anti-SHARP1 conjugated to Alexa Fluor 568) upon Lipo-siRNA-BTZ-PEG-cRGD nanoparticle treatment when compared to untreated cells as shown in Figure 3.13. Red labeled anti-SHARP1 conjugated to Alexa Fluor 568 have been counted by MATLAB software in order to show that Lipo-siRNA-BTZ-PEG-cRGD nanoparticles remarkably suppressed the average number of red dots indicating SHARP1 in ML-2 cells to lower than 10 relative to untreated ones as shown in Figure 3.14, suggesting that Lipo-siRNA-BTZ-PEG-cRGD nanoparticle could curb MLL-AF6

leukemogenicity. The cytotoxicity assays revealed that Lipo-siRNA-BTZ, Lipo-BTZ-PEG-cRGD, and Lipo-siRNA-BTZ-PEG-cRGD nanoparticle treatment considerably reduced survival rates of ML-2 cells by 68%, 75%, and 50%, respectively, compared to those of untreated cells ($p < 0.001$) (Figure 3.15). For colony formation assays (Figure 3.16), Lipo-siRNA-BTZ-PEG-cRGD treatment correlated with the lowest average colony numbers: ~70% reduction than that found in the control ($p < 0.001$). The relative number of colonies formed under Lipo-siRNA-BTZ, Lipo-BTZ-PEG-cRGD, and Lipo-siRNA-BTZ-PEG-cRGD were 310 ± 15, 346 ± 13, and 171 ± 15, respectively. Lipo-siRNA-BTZ-PEG-cRGD nanoparticles showed the highest reduction of viable cells and the lowest relative clonogenic growth, promoting the antileukemic effect of *SHARP1* silencing with proteasome inhibition by targeted siRNA/BTZ co-delivery.

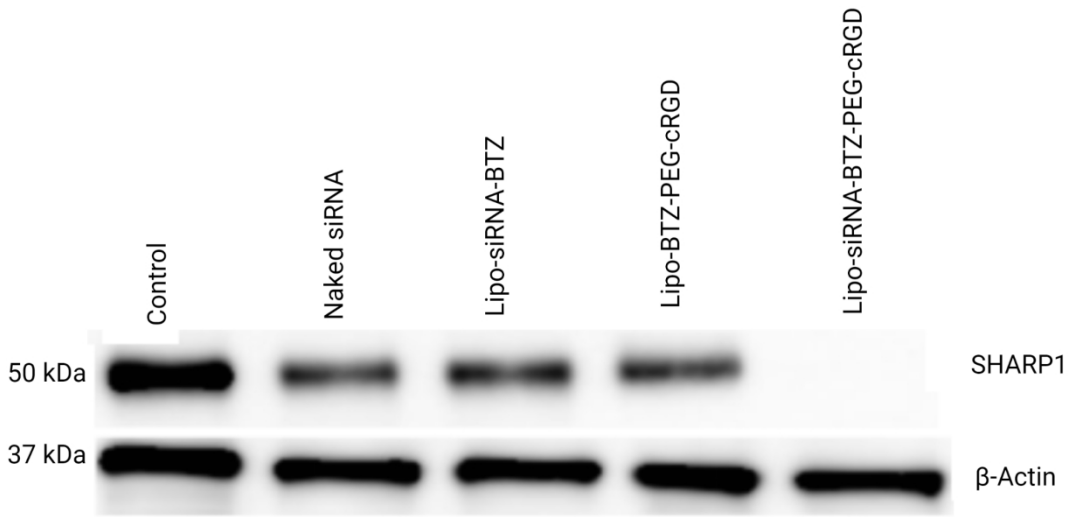

Figure 3.10 Western blots showing SHARP1 protein expression in ML-2 cells transfected with naked siRNA, Lipo-siRNA-BTZ, Lipo-BTZ-PEG-cRGD, and Lipo-siRNA-BTZ-PEG-cRGD compared to untreated cells (n = 3).

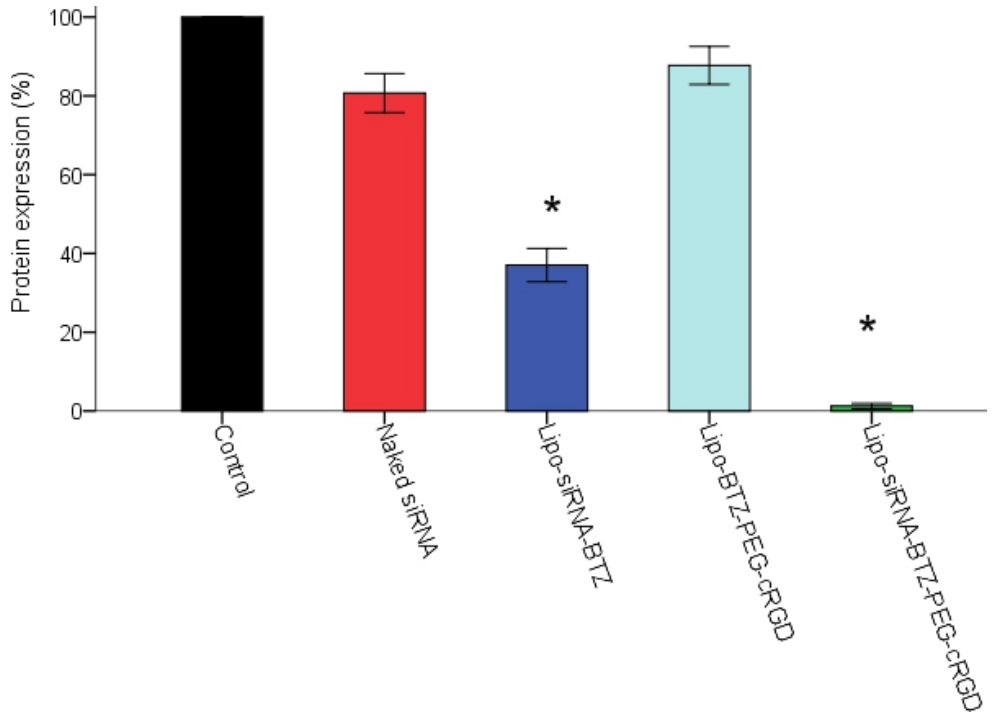

Figure 3.11 Quantification of SHARP1 protein expression in ML-2 cells. Data are presented as mean ± SEM (n = 3 biological replicates); *$p < 0.05$.

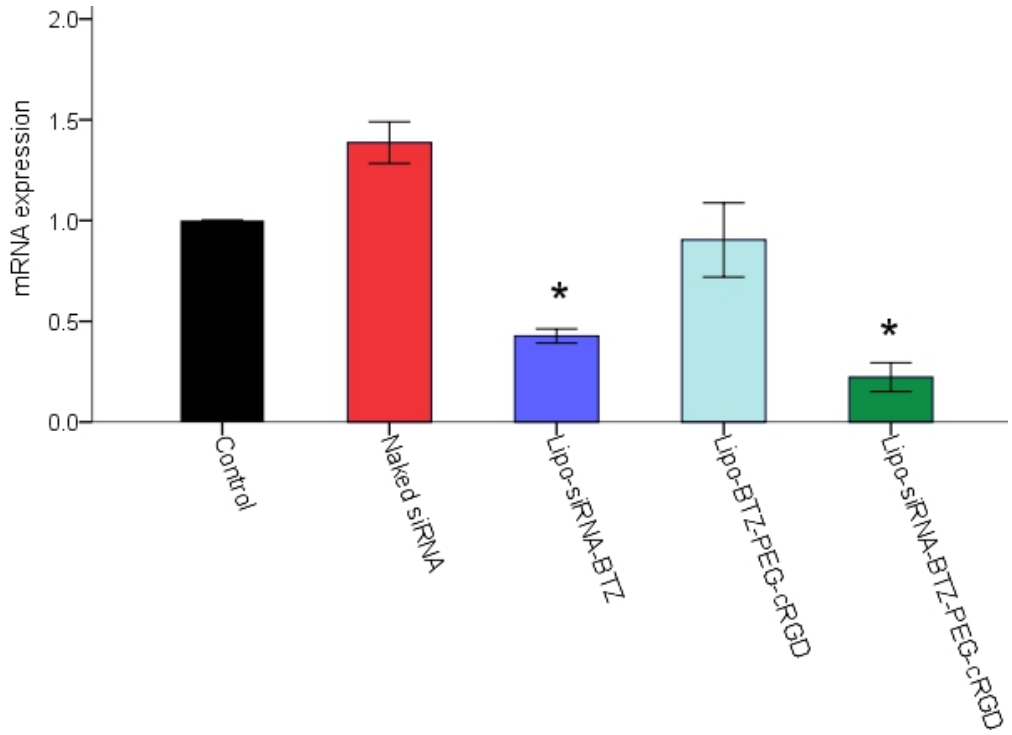

Figure 3.12 qPCR for *SHARP1* mRNA expression in ML-2 cells (mean ± SEM, n = 3); *$p < 0.05$.

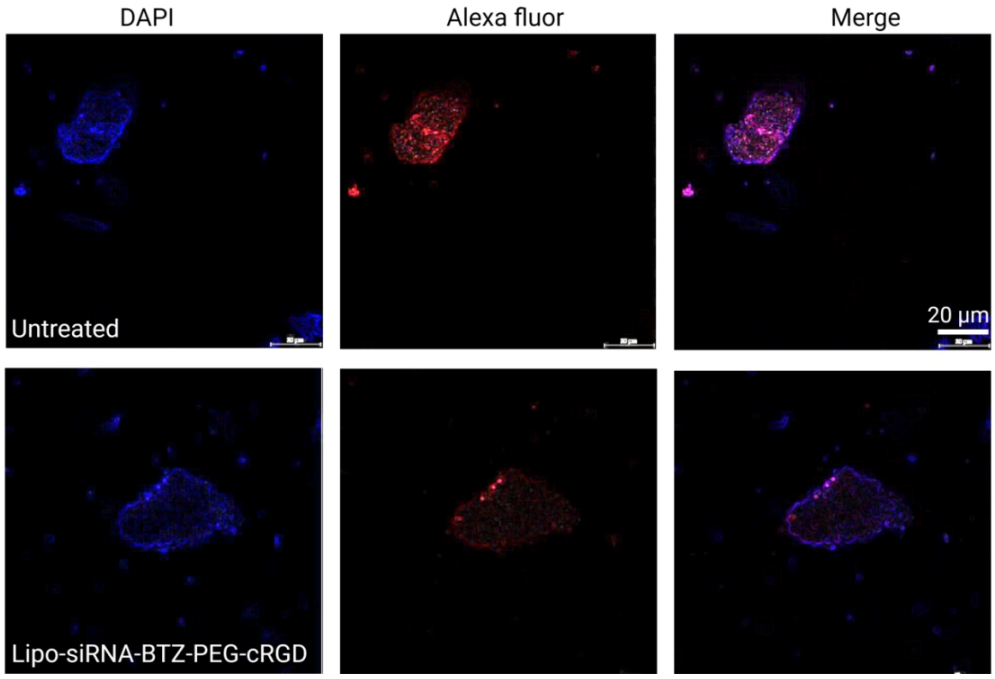

Figure 3.13 Immunofluorescence (IF) of ML-2 cells treated with Lipo-siRNA-BTZ-PEG-cRGD nanostructures relative to untreated cells using red labeled anti-SHARP1 conjugated to Alexa Fluor 568 and DAPI (blue) stains. Scale bar: 20 µm.

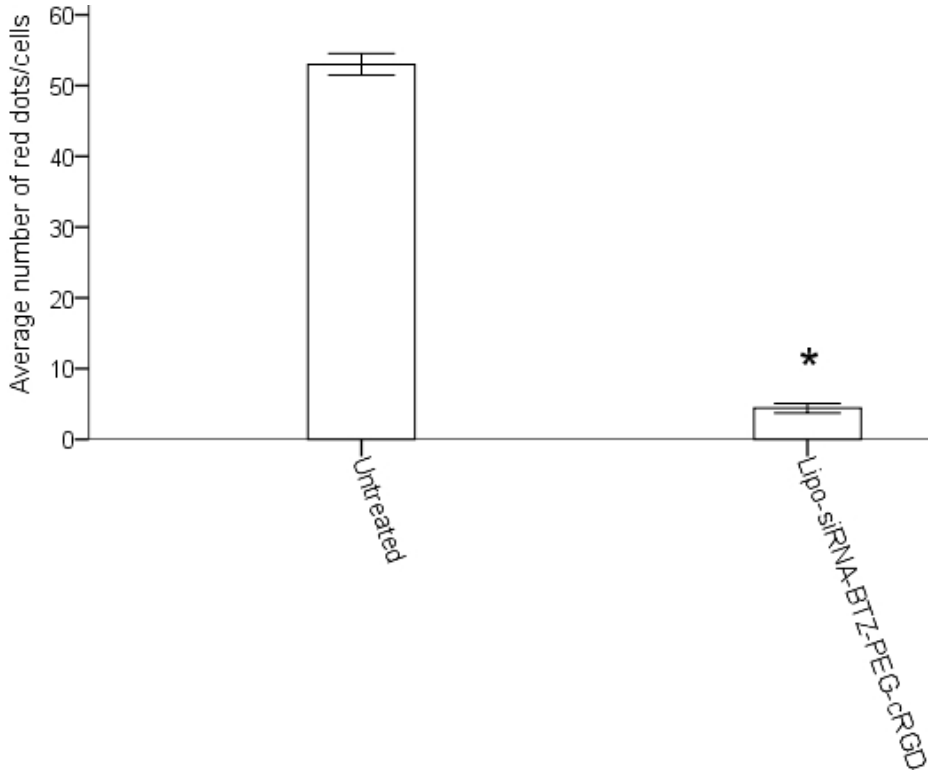

Figure 3.14 Quantification of anti-SHARP1-positive cells in confocal IF images for each group (mean ± SEM). Data are presented as mean ± SEM (n = 5); *$p < 0.05$.

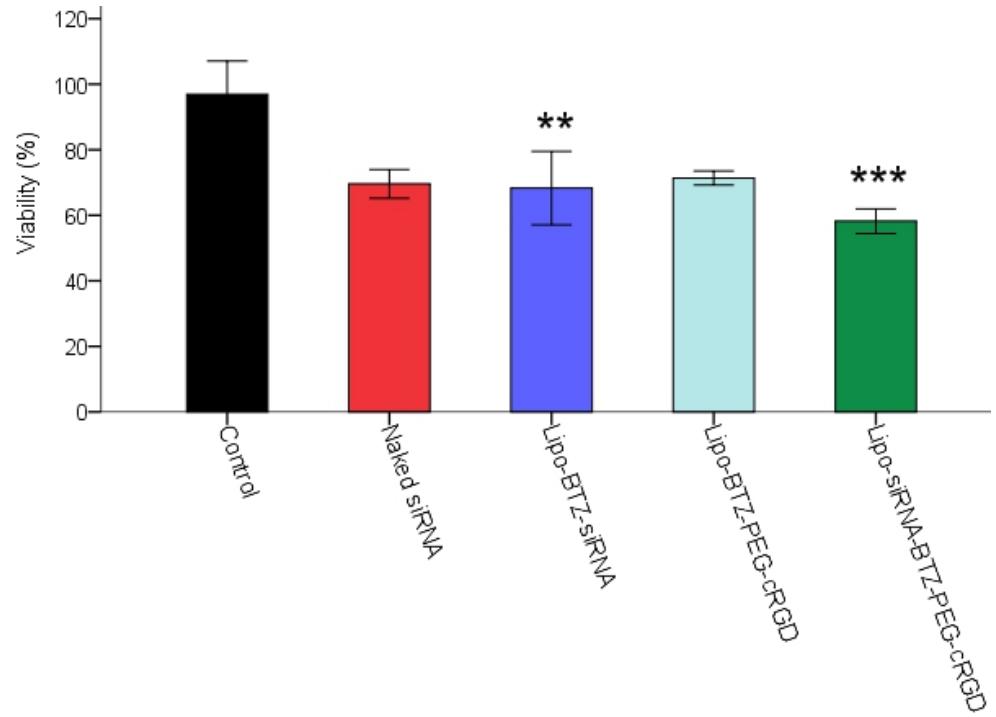

Figure 3.15 Cytotoxicity (via viability assay) were assessed in ML-2 cells. Data are presented as mean ± SEM (n = 5); ***p* <0.01, ****p* <0.001.

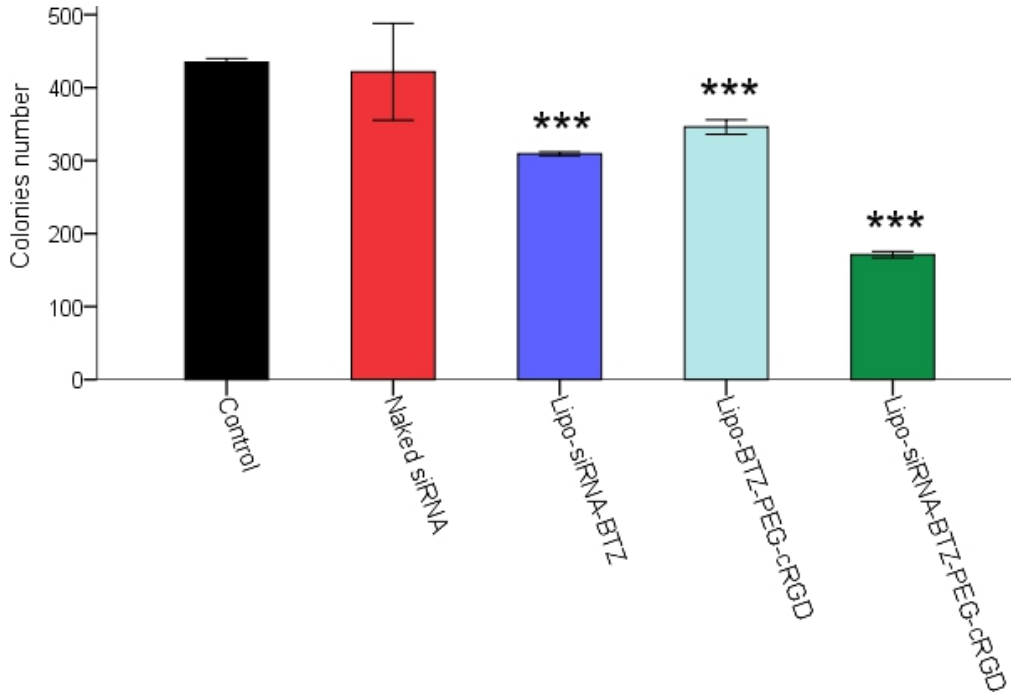

Figure 3.16 Clonogenic growth were assessed in ML-2 cells. Data are presented as mean ± SEM (n = 5); ****p* <0.001.

3.2.4 Cell apoptosis

Flow cytometry using a double-staining assay demonstrated the anti-apoptotic activity of naked siRNA, Lipo-siRNA-BTZ, Lipo-BTZ-PEG-cRGD and Lipo-siRNA-BTZ-PEG-cRGD on ML-2 cells relative to the control (Figures 3.17- 3.19). In detail, the results revealed that naked siRNA, Lipo-siRNA-BTZ, Lipo-BTZ-PEG-cRGD and Lipo-siRNA-BTZ-PEG-cRGD markedly increased ML-2 cell apoptosis to $2.3 \pm 2.3\%$, $2.7 \pm 1.7\%$, $2.5 \pm 1.9\%$ and $2.8 \pm 4.3\%$, respectively (early apoptosis as in Figure 3.18) and $14.5 \pm 3.1\%$, $15.3 \pm 2.4\%$, $14.7 \pm 2.8\%$ and $15.8 \pm 5.3\%$ (total apoptosis as in Figure 3.19).

Fluorescence microscopic images (Figure 3.20) revealed robustly increase ML-2 cell apoptosis in Lipo-siRNA-BTZ- and Lipo-siRNA-BTZ-PEG-cRGD-treated cells relative to the control and naked siRNA- and Lipo-BTZ-PEG-cRGD-treated cells through marked fluorescence signaling for both Annexin V and PI, indicating Lipo-siRNA-BTZ and Lipo-siRNA-BTZ-PEG-cRGD could boost cell apoptosis. Collectively, the cell apoptosis analysis illustrated that Lipo-siRNA-BTZ-PEG-cRGD induced the early and total apoptosis.

Live imaging showed the cell number and growth reduction of Lipo-siRNA-BTZ-PEG-cRGD-treated cells relative to the untreated cells after 1, 5 and 42 h intervals (Figure 3.21). Based on these findings, we plotted an ML-2 cell growth curve to measure cell proliferation, which was found to be strikingly attenuated following Lipo-siRNA-BTZ-PEG-cRGD treatment (Figure 3.22).

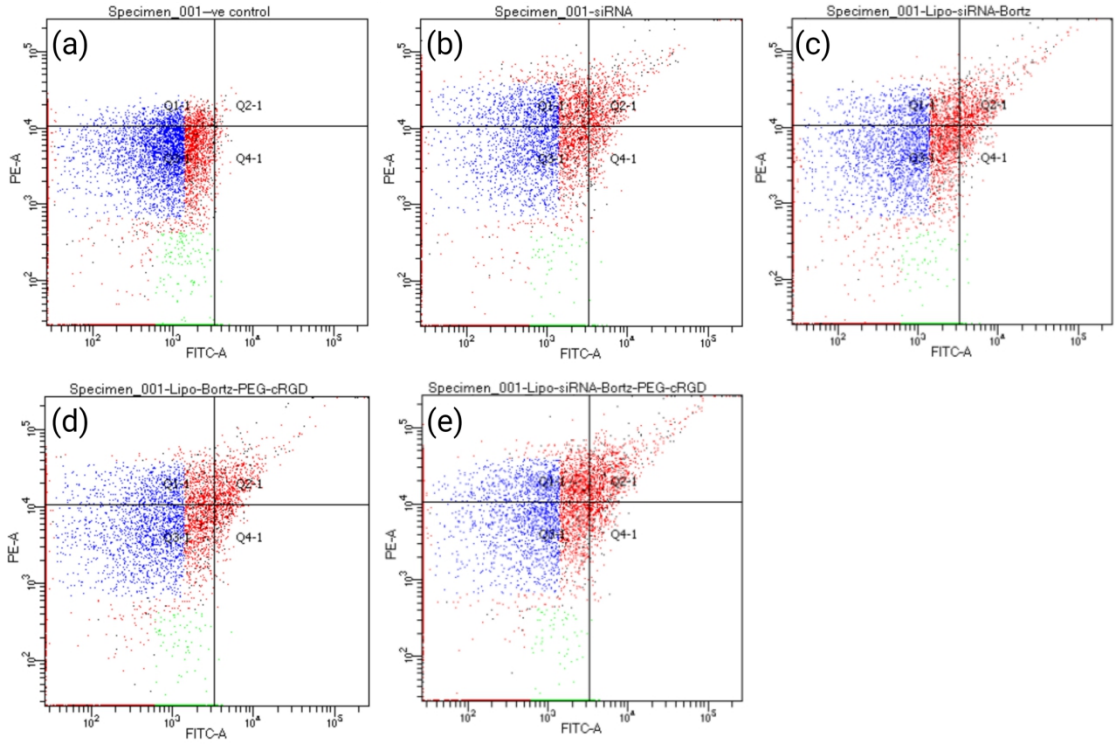

Figure 3.17 Representative flow cytometry plots of treated cells relative to untreated cells for Annexin V and PI, (a) untreated cells; (b) naked siRNA; (c) Lipo-siRNA-BTZ; (d) Lipo-BTZ-PEG-cRGD and (e) Lipo-siRNA-BTZ-PEG-cRGD.

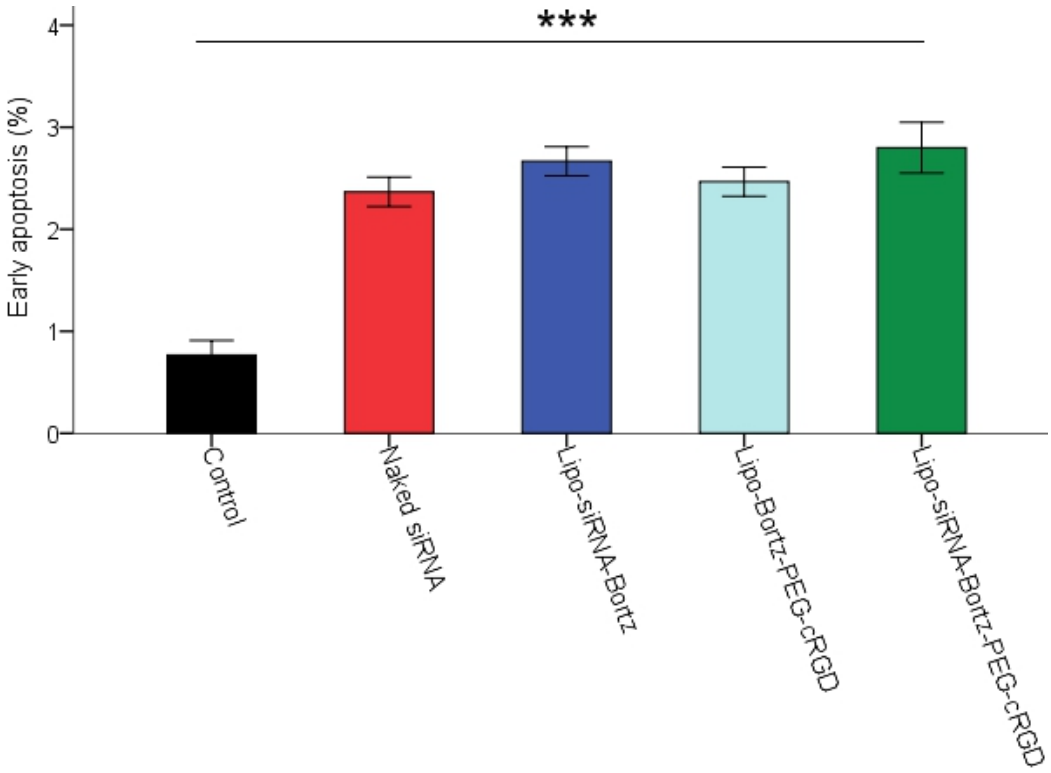

Figure 3.18 Percentage of Annexin V^+ PI^- apoptotic cells. The graphs show mean ± SEM of three independent experiments; ***p <0.001.

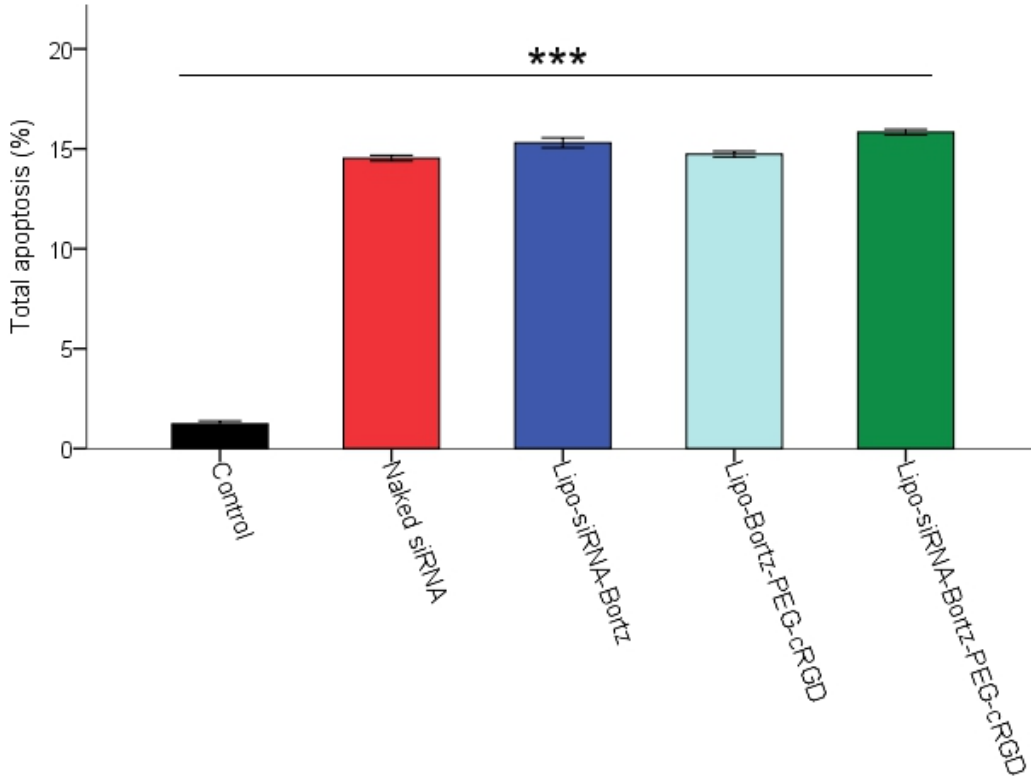

Figure 3.19 Percentage of Annexin V^+ PI^+ apoptotic cells. The graphs show mean ± SEM of three independent experiments; ***p <0.001.

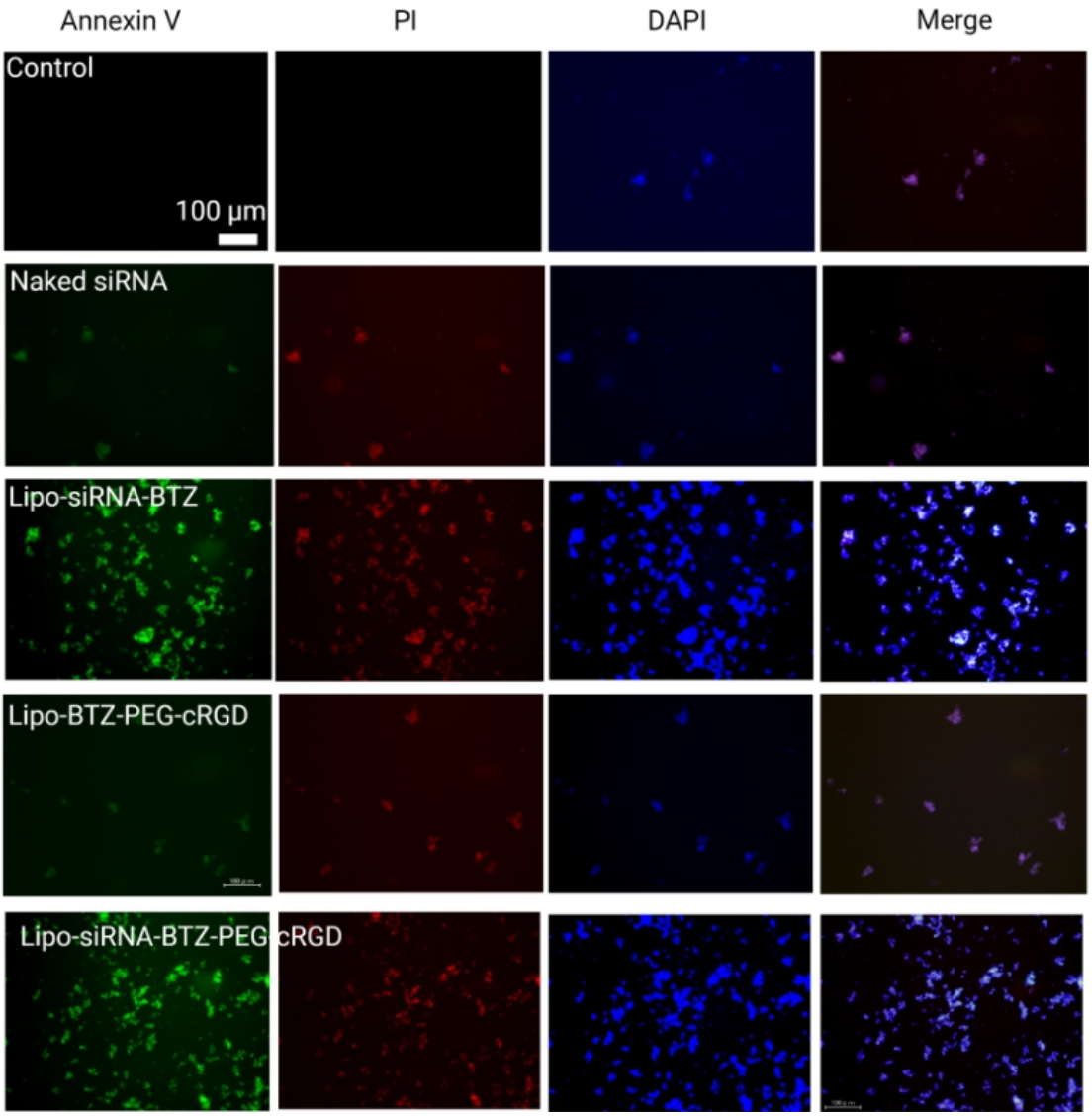

Figure 3.20 Fluorescence imaging of untreated cells; naked siRNA treated cells; Lipo-siRNA-BTZ treated cells; Lipo-BTZ-PEG-cRGD treated cells and Lipo-siRNA-BTZ-PEG-cRGD treated cells using Annexin V, PI, and DAPI staining. Scale bar: 100 µm.

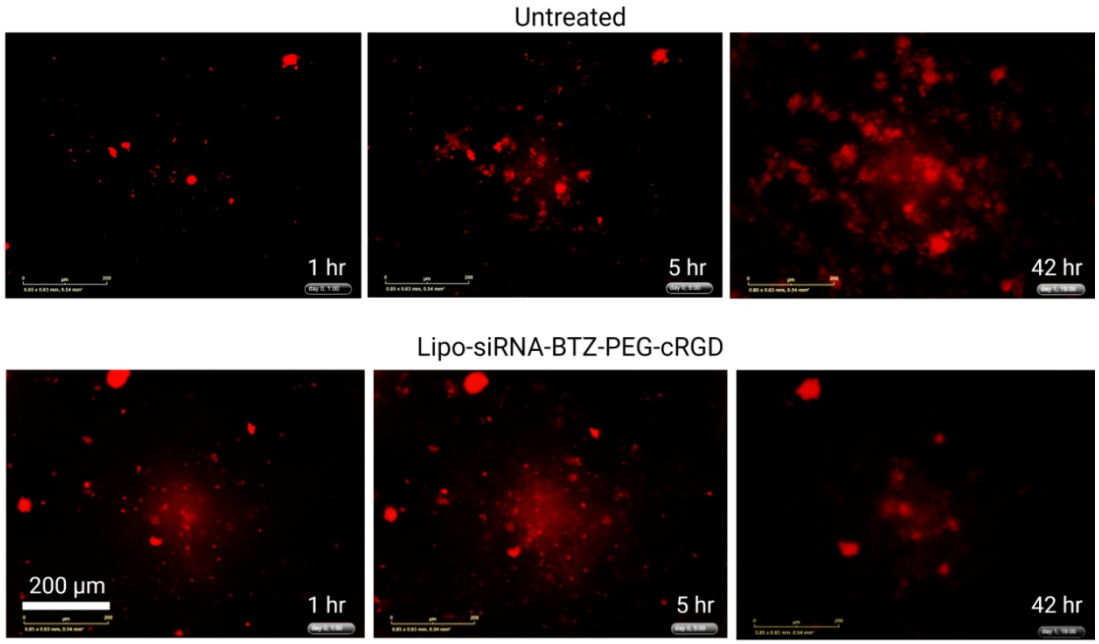

Figure 3.21 Red fluorescence imaging of ML-2 cells treated with Lipo-siRNA-BTZ-PEG-cRGD nanostructures compared to untreated cells using IncuCyte NucLight Rapid Red Reagent for nuclear labeling, showing apoptosis progression after 1, 5 and 42 h intervals (Scale bar = 200 µm). Experiments were repeated three times.

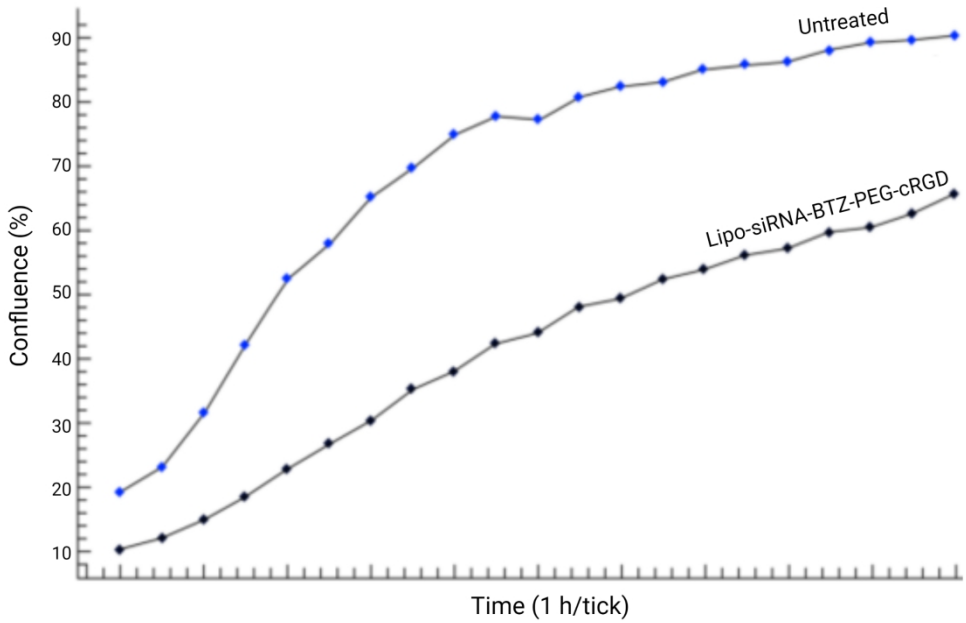

Figure 3.22 Percent growth over time in ML-2 cells after transfection with Lipo-siRNA-BTZ-PEG-cRGD compared with untreated cells. Experiments were performed in triplicate.

3.2.5 Cell autophagy

We hypothesized that DOT1L/MLL-AF6 expression would be suppressed by multifunctional *SHARP1*-targeted Lipo-siRNA-BTZ-PEG-cRGD in MLL-AF6 AML cells. The mRNA expression of DOT1L and MLL-AF6 were profoundly downregulated in Lipo-siRNA-BTZ- and Lipo-siRNA-BTZ-PEG-cRGD-treated cells, while those treated with naked siRNA and Lipo-BTZ-PEG-cRGD were unaffected at $p < 0.05$ (Figures 3.23 and 3.24). Lipo-siRNA-BTZ-PEG-cRGD inhibited DOT1L and MLL-AF6 the most (approximately 80% and 50%, respectively), emphasizing induction of autophagy and indicating a new oncogenic role of *SHARP1* in MLL-AF6 and DOT1L functions in MLL-AF6 AML cells. The MLL-AF6-driven transcriptional machinery correlating with *SHARP1*-related genes for MLL-AF6 AML growth and maintenance are shown in Figure 3.25.

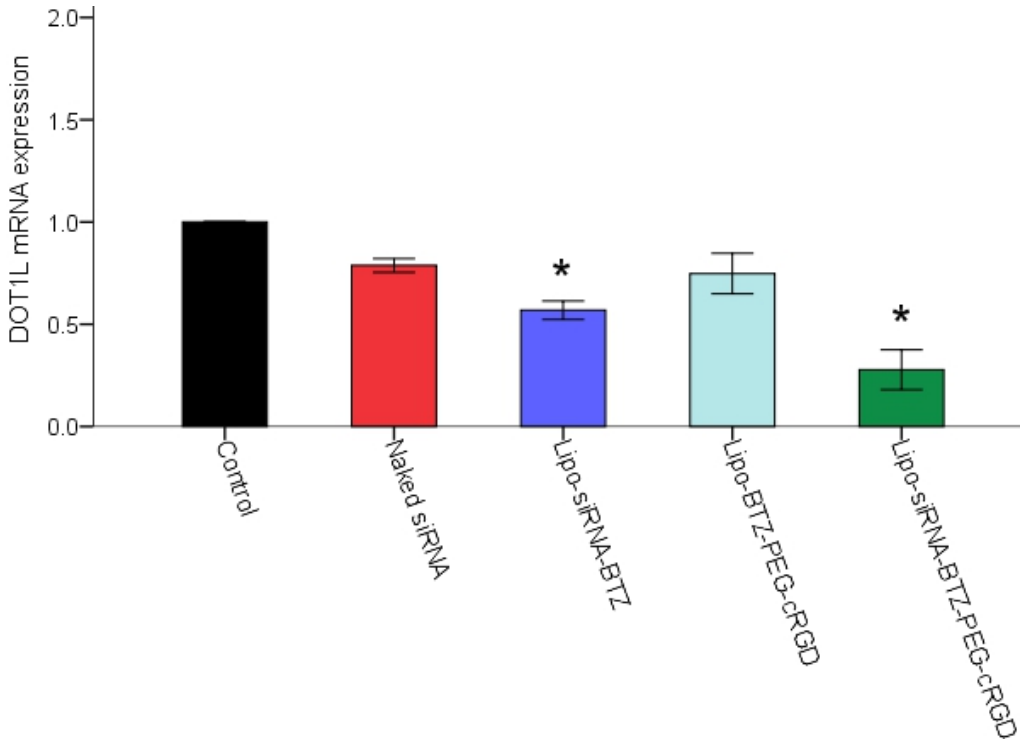

Figure 3.23 qPCR for *DOT1L* mRNA expression in ML-2 cells using all treatments relative to untreated cells (mean ± SEM, n = 3); *$p < 0.05$.

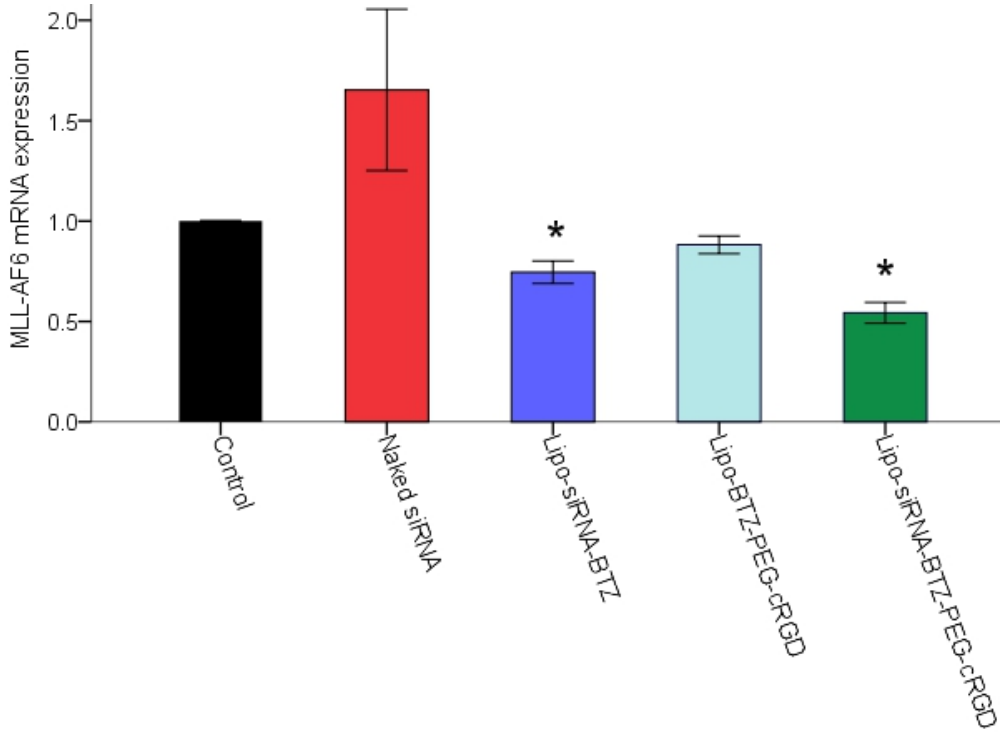

Figure 3.24 qPCR for *MLL-AF6* mRNA expression in ML-2 cells (mean ± SEM, n = 3); *$p < 0.05$.

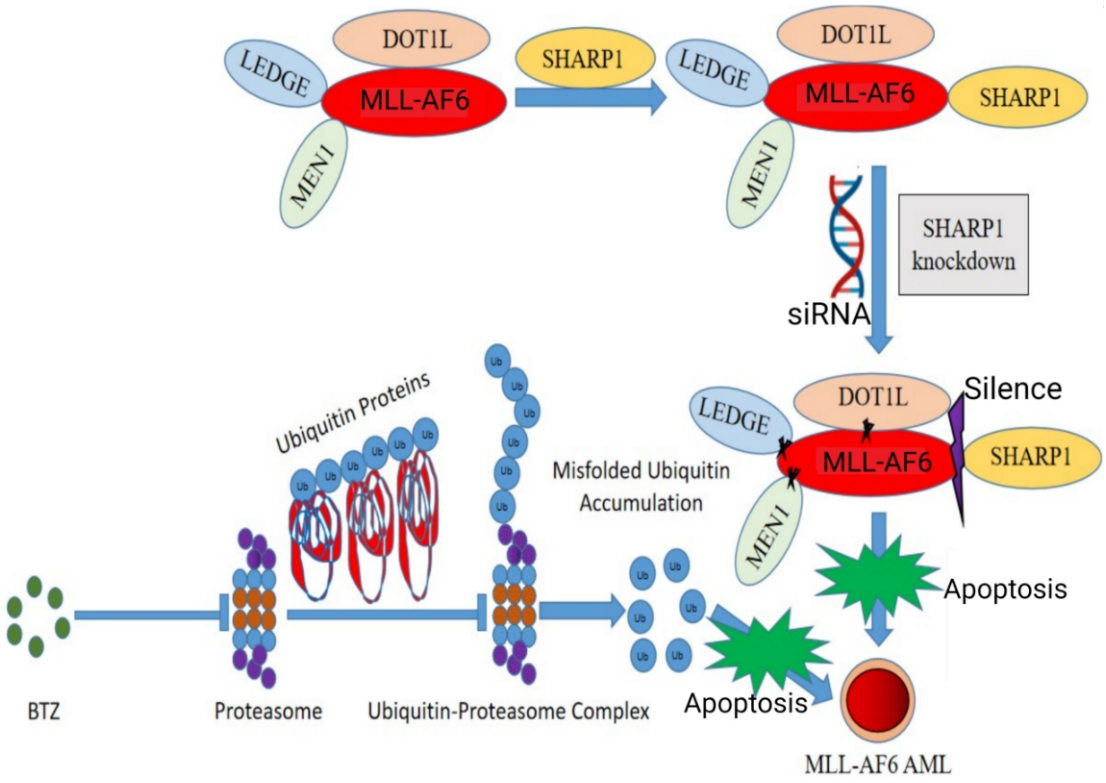

Figure 3.25 A **s**chematic illustration of SHARP1 knockdown and proteasome inhibition-oncogenic functions in MLL-AF6 AML cells. SHARP1 inhibition hindered MLL-FP complex construction following MLL-AF6, LEDGE, and MEN1 accumulation, leading to DOT1L-mediated cell death. BTZ inhibited proteasomes, preventing the ubiquitin-proteasome complex formation and causing cell death by the accumulation of misfolded ubiquitin proteins.

3.3 Discussion

In this study, we demonstrated the role of SHARP1 as an MLL-AF6-dependent leukemogenic driver, as well as the application of multifunctionally bioengineered nanoparticles in SHARP1 downregulation; thus, indicating a potential therapeutic strategy for human MLL-AF6 AML therapy. We fabricated a state-of-the-art biodegradable nanoplatform for siRNA/BTZ co-delivery with targeted *SHARP1* knockdown, demonstrating a potential therapeutic option for MLL-AF6 AML.

Notably, lipid bilayer fusion, endocytosis, drug conjugation, and the facilitated diffusion of a lipofectamine-based formulation [20] with further surface modification by PEGylation allowed the targeting of the $\alpha_v\beta_3$ integrin ligand [21]. These mechanisms were used to allow Lipo-siRNA-BTZ-PEG-cRGD to deliver cargo to ML-2 cells, elucidating how multifunctional bioengineered nanoparticles improve therapeutic efficiency and safety by optimizing delivery in MLL-AF6 AML. Naked siRNA cannot passively diffuse across cell membranes owing to charge instability, high molecular weight, water solubility, and intracellular enzyme degradation [22]. This may lead to producing a large amount of SHARP1 mRNA copies by the cells as a sudden reflex of the possibility of siRNA entrance via the penetration of cell membrane to be able to grow and maintain without threat as shown in Fig 3.3C that revealed that SHARP1 mRNA expression in naked siRNA is higher than that of control. Peptide-guided PEGylated cationic nanoliposomes are effective for siRNA delivery [23]; we showed this strategy is effective for *SHARP1* targeting. Consistently, our cellular uptake results demonstrated that Lipo-siRNA-BTZ-PEG-cRGD undergoes αvβ3 receptor-mediated endocytosis. Our findings corroborate reports of the protective role of *SHARP1* against p53 pathway-mediated DNA-targeting chemotherapeutic cytotoxicity [24]. *SHARP1* knockdown led to p53 pathway-related gene overexpression and ML-2 cell apoptosis. Combination with BTZ inhibits proteasomes, selectively blocking NF-κB target gene expression and activating and stabilizing p21, p27, and p53 signalling [25,26]. These effects suppress cell proliferation and migration and augment synergistic nanoparticle-induced apoptosis.

To investigate the roles of *SHARP1* downregulation-induced autophagy in MLL-AF6 AML, we studied the mRNA expression of MLL-AF6 regulation and DOT1L oncogenic genes affected by *SHARP1* knockdown in ML-2 cells. Mechanistically,

DOT1L and MLL-AF6 are oncogenic proteins that directly regulate *SHARP1* expression. It has been reported that *SHARP1* downregulation does not affect DOT1L gene expression[8]. Therefore, it was suggested that *SHARP1*, together with DOT1L inhibition, may be a favorable treatment modality for MLL-AF6 AML [9], since it is known that DOT1L downregulation can inhibit the regulation of MLL-AF6 AML [27,28]. However, to date, there are no reports regarding *SHARP1* downregulation affecting DOT1L and MLL-AF6 regulation. Lipo-siRNA-BTZ-PEG-cRGD nanoparticles exhibited three fundamental regulatory mechanisms that could initiate autophagic signals for MLL-AF6 AML eradication. First, the BTZ combination disrupted the ubiquitin-proteasome signaling pathway, causing accumulation of unfolded ubiquitin, triggering autophagy [29]. Then, selective *SHARP1* inhibition, which results in the breakdown of oncogenic fusion proteins responsible for DOT1L-dependent MLL-AF6-MEN1-LEDGF complex synthesis crucial for leukemogenesis, was significantly abrogated, strengthening autophagy [30]. Eventually, MLL-AF6 downregulation resulted in considerable RAS-GTP pathway interference. RAS-GTP pathway is necessary for promoting cancer cell survival through binding RAS-GTP selectively to RALB-GTP for overexpressing Bcl-2 [31]. Our nanoparticles primarily interfered with this critical oncogenic pathway, leading to autophagic signals. Thus, Lipo-siRNA-BTZ-PEG-cRGD nanoparticles may be RAS inhibitors, potentiating MLL-AF6 AML therapy. Manipulating autophagy may provide powerful evidence for the effect of Lipo-siRNA-BTZ-PEG-cRGD as a multifunctional targeted therapy in MLL-AF6 AML cells.

3.4 Summary

Chapter 3 provided a comprehensive *in vitro* analysis on new multifunctional bioengineered smart nanoparticles using well-characterized cRGD-conjugated thiolated PEG (NHS-PEG6-maleimide) to effectively co-deliver siRNA/BTZ for targeted *SHARP1* silencing in MLL-AF6 AML cells. These findings indicate that animal experiments may provide useful data for the development of nanomedicines for AML treatment. We demonstrated the effects of *SHARP1* downregulation on *DOT1L* and *MLL-AF6* expression and highlighted a new vital oncogenic role of *SHARP1* in MLL-AF6 AML growth and maintenance. Lipo-siRNA-BTZ-PEG-cRGD are multifunctional particles that reveal versatile regulatory mechanisms, including *SHARP1* silencing, MLL-AF6/DOT1L inhibition, p53 activation, RAS suppression, proteasome inhibition, and apoptosis induction. This approach will foreseeably open new avenues for applying smart biocompatible re-engineered nanostructures *in vivo* and further clinical translation to produce advanced MLL-AF6 AML-targeting therapeutics.

References

1. V. Trujillo-Alonso, *et al*. FDA-approved ferumoxytol displays anti-leukaemia efficacy against cells with low ferroportin levels. *Nat. Nanotechnol*. **14,** 616–622 (2019).
2. E. Ballabio, T.A. Milne Epigenetic control of gene expression in leukemogenesis: cooperation between wild type MLL and M.LL fusion proteins. *Mol. Cell. Oncol*. **1,** e955330 (2014).
3. C. Meyer, *et al*. The MLL recombinome of acute leukemias in 2013. *Leukemia* **27,** 2165–2176 (2013).

4. K.M. Bernt, *et al*. MLL-rearranged leukemia is dependent on aberrant H3K79 methylation by DOT1L inhibitor. *Cancer Cell* **20,** 66–78 (2011).
5. M. Montagner, *et al*. SHARP1 suppresses breast cancer metastasis by promoting degradation of hypoxia-inducible factors. *Nature.* **487,** 380–384 (2012).
6. K. Yamada, K. Miyamoto. Basic helix-loop-helix transcription factors, BHLHB2 and BHLHB3; their gene expressions are regulated by multiple extracellular stimuli. *Front. Biosci*. **10,** 3151–3171 (2005).
7. Z.H. Zhou, *et al*. Roles of SHARP1 in thyroid cancer. *Mol. Med. Rep.* **13**, 5365–5371 (2016).
8. A. Numata, *et al*. The basic helix-loop-helix transcription factor SHARP1 is an oncogenic driver in MLL-AF6 acute myelogenous leukemia. *Nat. Commun.* **9,** 1622 (2018).
9. H. Yin, *et al*. Non-viral vectors for gene-based therapy. *Nat. Rev. Genet.* **15,** 541–555 (2014).
10. G.A. Koning, G.C. Krijger. Targeted multifunctional lipid-based nanocarriers for image-guided drug delivery. *Anticancer Agents Med. Chem.* **7,** 425–440 (2007).
11. X.Y. Pei, Y. Dai, S. Grant. Synergistic induction of oxidative injury and apoptosis in human multiple myeloma cells by the proteasome inhibitor bortezomib and histone deacetylase inhibitors. *Clin. Cancer Res.* **10,** 3839–3852 (2004).
12. Y. Dai, *et al*. Interactions between bortezomib and romidepsin and belinostat in chronic lymphocytic leukemia cells. *Clin. Cancer Res.* **14,** 549–558 (2008).
13. D.E. Denlinger, B.K. Rundall, D.R. Jones. Proteasome inhibition sensitizes non-small cell lung cancer to histone deacetylase inhibitor-induced apoptosis through

the generation of reactive oxygen species. *J. Thorac. Cardiovasc. Surg.* **128,** 740–748 (2004).

14. M. Boccadoro, G. Morgan, J. Cavenagh. Preclinical evaluation of the proteasome inhibitor bortezomib in cancer therapy. *Cancer Cell Int.* **5**, 18 (2005).
15. Y. Dai, M. Rahmani, S. Grant. Proteasome inhibitors potentiate leukemic cell apoptosis induced by the cyclic-dependent kinase inhibitor flavopiridol through a SAPK/JNK- and NF-kappaB-dependent process. *Oncogene* **22,** 7108–7122 (2003).
16. B. Almeida, et al. Recent Progress in Bioconjugation Strategies for Liposome-Mediated Drug Delivery. *Molecules* **25,** 5672 (2020).
17. Y. Xia, J. Tian, X. Chen. Effect of surface properties on liposomal siRNA delivery. *Biomaterials* **79,** 56–68 (2016).
18. D. Vllasaliu, R. Fowler, S. Stolnik. PEGylated nanomedicines: recent progress and remaining concerns. *Expert Opin. Drug Deliv.* **11,** 139–154 (2014).
19. F. Wang, *et al*. The functions and applications of RGD in tumor therapy and tissue engineering. *Int. J. Mol. Sci.* **14,** 13447–13462 (2013).
20. J. Yang, *et al*. Drug delivery via cell membrane fusion using lipopeptide modified liposomes. *ACS Cent. Sci.* **2,** 621–630 (2016).
21. L. Zhang, *et al*. Cytosolic co-delivery of miRNA-34a and docetaxel with core-shell nanocarriers via caveolae-mediated pathway for the treatment of metastatic breast cancer. *Sci. Rep.* **7,** 46186 (2017).
22. J. Wang, Z. Lu, M.G. Wientjes, J.L.S Au. Delivery of siRNA therapeutics: barriers and carriers. *AAPS J.* **12,** 492–503 (2010).
23. F. Mainini, M.R. Eccles. Lipid and Polymer-Based Nanoparticle siRNA Delivery Systems for Cancer Therapy. *Molecules* **25,** 2692 (2020).

24. J.J. Liu, T.K. Chung, J. Li, R. Taneja. Sharp-1 modulates the cellular response to DNA damage. *FEBS Lett.* **584,** 619–624 (2010).

25. C. Li, J. Hu, W. Li, G. Song, J. Shen. Combined bortezomib-based chemotherapy and p53 gene therapy using hollow mesoporous silica nanospheres for p53 mutant non-small cell lung cancer treatment. *Biomater. Sci.* **5,** 77–88 (2017).

26. Y. Xue, *et al*. Bortezomib stabilizes and activates p53 in proliferative compartments of both normal and tumor tissues in vivo. *Cancer. Res.* **79,** 3595–3607 (2019).

27. S.R. Daigle, *et al*. Potent inhibition of DOT1L as treatment of MLL-fusion leukemia. *Blood* **122,** 1017–1025 (2013).

28. C. Dafflon, *et al*. DOT1L inhibition is lethal for multiple myeloma due to perturbation of the endoplasmic reticulum stress pathway. *Oncotarget* **11,** 956 (2020).

29. R. Masaki. Mechanism of action of bortezomib in multiple myeloma therapy. *Int. J. Myeloma* **6,** 1–6 (2016).

30. S.P. Zhang, *et al*. Role of autophagy in acute myeloid leukemia therapy. *Chin. J. Cancer* **32,** 130–135 (2013).

31. E. Manara, *et al*. MLL-AF6 fusion oncogene sequesters AF6 into the nucleus to trigger RAS activation in myeloid leukemia. *Blood* **124,** 263–272 (2014).

Chapter 4. Effect of PLEKHA7-based nanodelivery on behavior and growth of acute myeloid leukemic cells

4.1 Introduction

Acute myeloid leukemia (AML) is characterized by poor survival rates in older adults and children with multiple genetic mutations and high relapse rates in patients [1,2]. In the bone marrow microenvironment, adult normal hematopoiesis could fundamentally induce the maintenance of hematopoietic homeostasis. The interaction balance between bone marrow stromal cells and hematopoietic progenitor cells could result in the regulation of hematopoietic progenitor differentiation and proliferation in the bone marrow microenvironment [3,4]. Stromal cells are readily managed by some important molecules such as cell adhesion molecules [5]. One of these adhesion molecules, PLEKHA7, belonging to PLEKHA7 (Pleckstrin homology domain containing, family A member 7) is a member of the PLEKHA proteins family possessing a functionalized pleckstrin homology domain composing of 120 amino acids which attach membrane phosphoinositides [6]. Pleckstrin homology domains are generated from a broad range of structural proteins participated in cellular signaling and as components of the cytoskeleton [7,8]. PLEKHA7 is regarded as a cytoskeletal modulator or adaptor that essentially regulates protein assembly in the cytoplasmic apical zonula adherens junction (AJ) conjugating cell surface E-cadherin with the microtubule cytoskeleton, hence assuring tight junction integrity and cell-cell adhesion [9,10]. AJ proteins constituted via PLEKHA7 encompass Paracingulin, p120-Catenin, Nezha, Afadin and Cingulin [11,12]. Nectin 1/3

transmembrane adhesion proteins could be protected from proteolysis processes by attachment of Pdz11 protein which also support the tight junction stability [13]. Another study have demonstrated the essential role of PLEKHA7 in the recruitment of Dgcr8 and Drosha, core constituents of the microRNA microprocessor, to apical AJs and also in the suppression of anchorage-independent growth [14,15]. A further PLEKHA7 role has been studied through the contribution in the regulation of RhoA activity which is necessary for the crosstalk among the cytoskeletal organization and intracellular signaling directed by PLEKHA7 binding partners [16] with Paracingulin and Cingulin sequestering Rho to tight junctions [13], and cytosolic 120-catenin conjugation and RhoA inhibition [17]. Recently, RhoA has been demonstrated to regulate the energy metabolism signaling via boosting glycolysis and intracellular glucose transport processes [18] and connected with enhanced cell invasion and migration as well as reduced survival rate, particularly in patients with colon cancer [19]. Tumorigenesis has been generated from PLEKHA7 loss, which interferes with the E-cadherin/EGFR signaling pathway, promoting cancer cell growth and progression [20,21]. Recent studies have reported structural variations between apical AJs and the basolateral areas of cell-cell contact. For instance, the PLEKHA7-binding p120 is mainly located at the apical AJs of well-differentiated epithelial cells, but this PLEKHA7-binding p120 composite is not found in the lateral areas of cell-cell contact [22-24]. Additional reports revealed that basolateral cell-cell complexes without PLEKHA7 could enhance tumorigenesis, while the apical AJs could result in tumor suppression via PLEKHA7 [20,22,25]. Furthermore, E-cadherin is widely expressed in areas of cell-cell contact in kidney and breast cancers, whereas PLEKHA7 is still widely downregulated or mislocalized [20,22] at the apical AJs. In leukemogenesis, adhesion abnormalities can readily induce an imbalance between

hematopoietic progenitor cells and bone marrow stromal cells, altering the normal hematopoietic bone marrow microenvironment into a leukemic microenvironment, enhancing leukemic growth and prohibiting leukemic cell apoptosis [26-28].

In this study, we investigated the effect of PLEKHA7 on the dynamics and behavior of AML cells and how the existence of PLEKHA7 modulates AML characterizations to open a different orientation for the alteration of AML cell growth. Since the role of PLEKHA7 in AML has not been studied previously, we attempted to demonstrate the correlation between PLEKHA7 expression and the incidence of AML growth. We delivered PLEKHA7 protein harnessing cRGD-mediated PEGylated cationic lipid nanoparticles to restore adhesion normality and integrity in AML cells, thereby resulting in the regulated induction of AML behavior alteration for normal homeostasis.

Outstandingly, targeted drug delivery systems, such as multifunctional biodegradable lipid nanoparticles, have been engineered to manifest considerable strategies to ameliorate many cargo loading challenges [29-31]. Incorporation of inert polymers such as polyethylene glycol (PEG) robustly reinforces the surface functionalization of cationic nanoliposomal nanostructures to form more sterically stabilized nanoparticles [32-34] and protect them from macrophage capture, aggregation, and reticuloendothelial system clearance, thereby prolonging retention time in the blood stream [35,36]. For selective targeting, surface ligands such as cyclic arginine-glycine-aspartate (RGD), which combines explicitly with αvβ3 integrin with high affinity, could promote cell-nanomaterial interactions, allowing cargo penetration into the pathologic location [37-39]. The RGD{d-Phe}{Lys(PEG-Mal)} sequence was synthesized from the chemical linkage of c(RGDfK) with thiolated PEG (NHS-PEG6-maleimide) associated with head-to-tail cyclic

modification to acquire a bioengineered surface for optimal functionalization of the fabricated nanostructures.

In our current study, we synthesized cRGD-tagged PEGylated cationic nanoliposomes for PLEKHA7 delivery to regulate the induction of AML behavior alteration and growth retardation to emerge as a potential target for AML modulation (Figure 4.1). This research is the first preclinical trial of PLEKHA7-based AML. Lipo-PLEKHA7-PEG-cRGD mainly displayed a significant mitigating effect on cell proliferation and colony formation with noticeable adhesion integrity. Therefore, our findings shed new light on PLEKHA7 as an AML behavior and growth modulator, consistent with the application of bioengineered PLEKHA7 nanoparticles, representing a prospective insight for human AML behavior alteration and modulation.

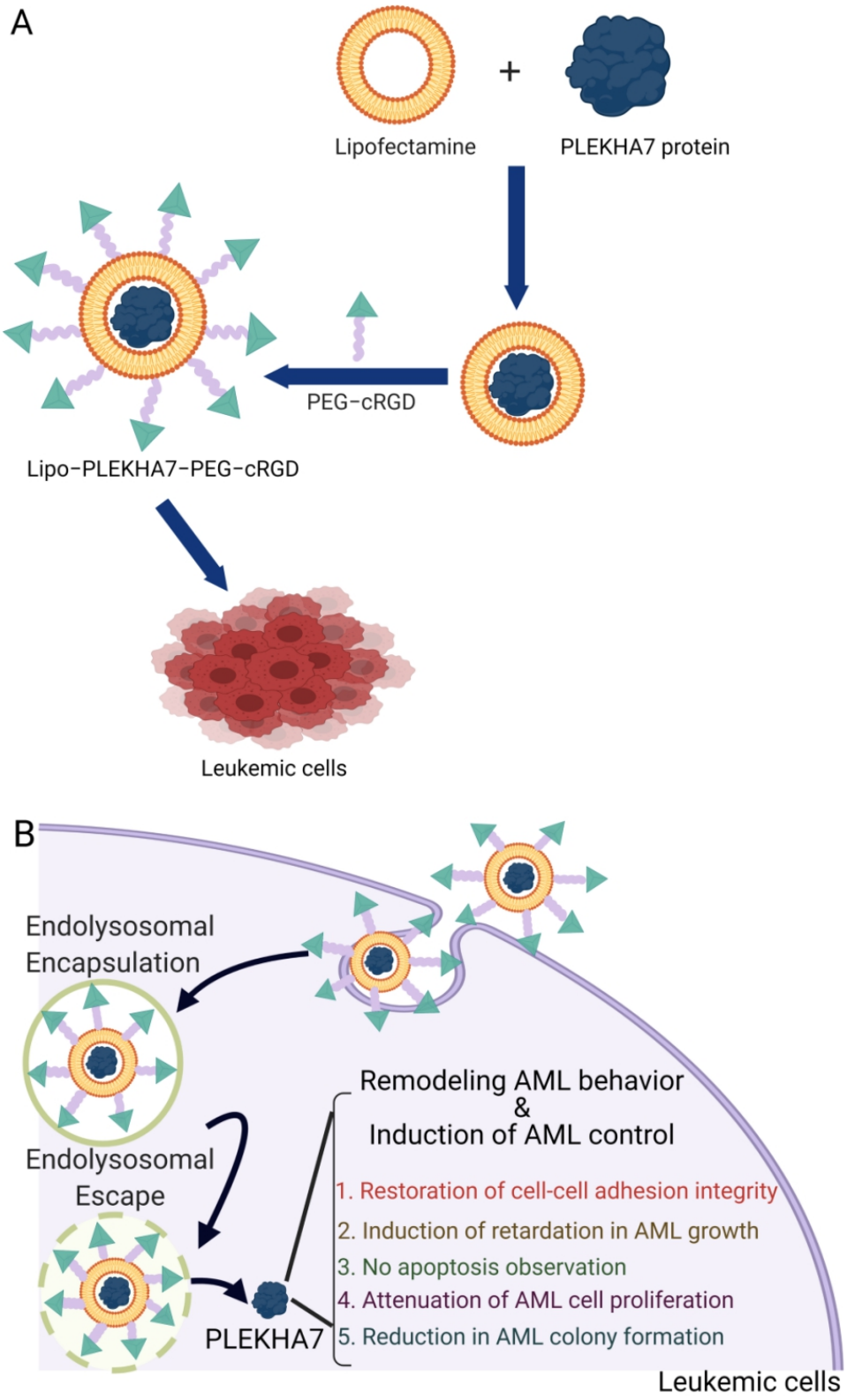

Figure 4.1 Synthesis of Lipo-PLEKHA7-PEG-cRGD nanoparticles for efficient delivery to leukemic cells. (A) Schematic illustration of synthetic Lipo-PLEKHA7-PEG-cRGD nanoparticles for AML delivery. (B) Proposed mechanism of the cellular uptake of Lipo-PLEKHA7-PEG-cRGD nanoparticles for behavior alteration and growth retardation of AML cells.

4.2 Results

4.2.1 Nanoparticle synthesis and characterization

To provide a biodegradable nanoplatform for PLEKHA7 delivery to AML cells, cRGD-guided PEGylated cationic lipid nanoparticles were prepared. Nanoparticles were conjugated with cyclic RGD peptide as a surface ligand for $\alpha_v\beta_3$ integrin targeting to avoid the PEG dilemma and expedite targeted, efficient delivery. The particle size and zeta potential values are listed in Table 4.1.

Table 4.1 Size and zeta potential characterizations (mean ± SEM) of Lipo-PLEKHA7-PEG-cRGD nanoparticles

Groups	Size (nm)	PDI	Zeta potential (mV)
Lipo-PLEKHA7-PEG-cRGD	172.3 ± 12.1	0.477 ± 0.011	29.22 ± 1.3

The average diameter of Lipo-PLEKHA7-PEG-cRGD was 172.3 ± 12.1 nm, while the zeta potential was 29.22 ± 1.3 mV (Figure. 4.2A and B). The resultant polydispersity index indicated that the synthesized nanoparticles were stable in water with a narrow size dispersion. As shown in the TEM images (Figure 4.3), the prepared nanoparticles were spherical and manifested a proper structure and configuration. The morphology of Lipo-PLEKHA7-PEG-cRGD revealed a uniform spherical shape and narrow size distribution. Altogether, these results highlight that PLEKHA7 was encapsulated in the nanoparticles without bulky aggregation or degradation.

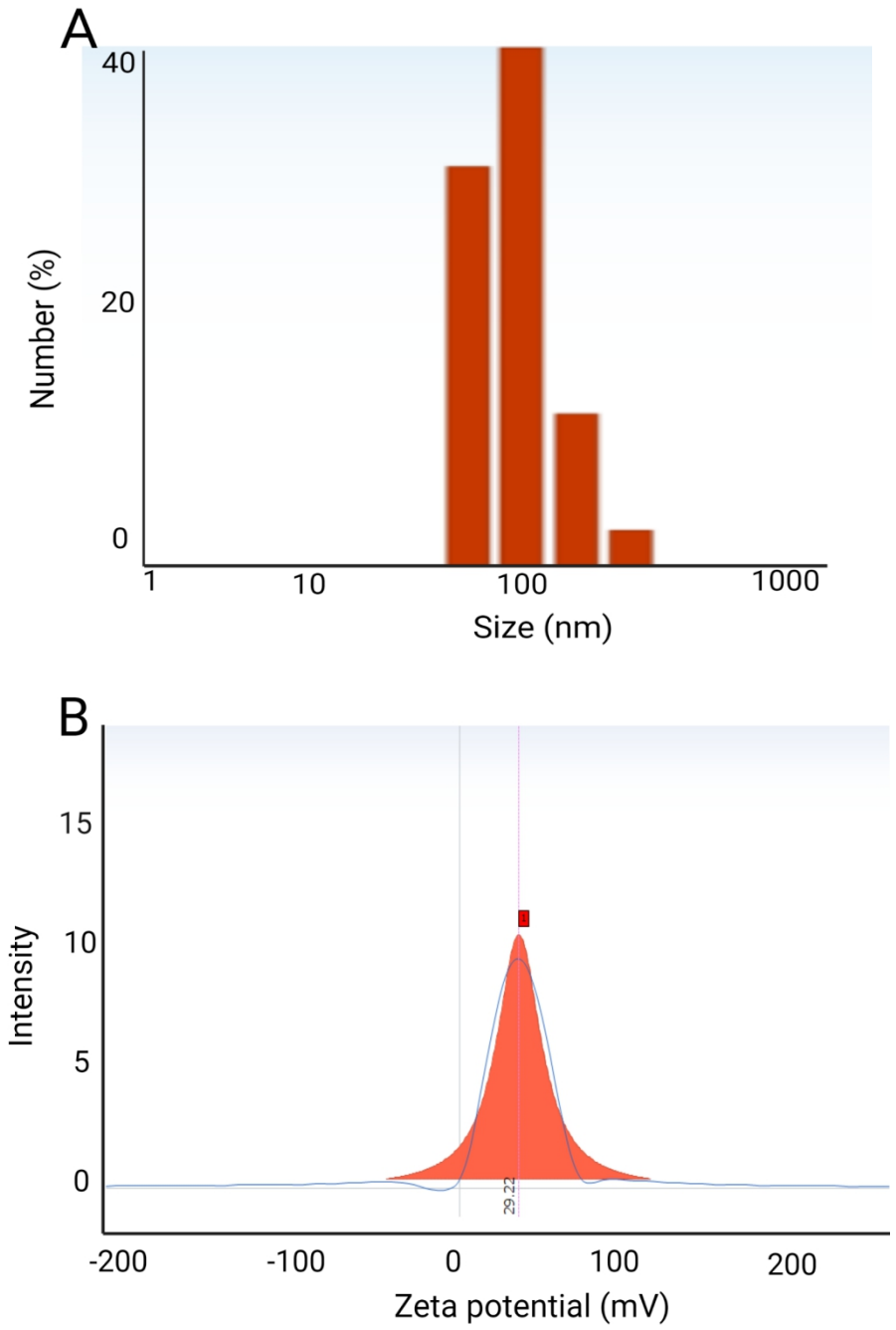

Figure 4.2 (A) Dynamic light scattering plot of Lipo-PLEKHA7-PEG-cRGD (n = 3). (B) Zeta potential measurement of Lipo-PLEKHA7-PEG-cRGD (n = 3).

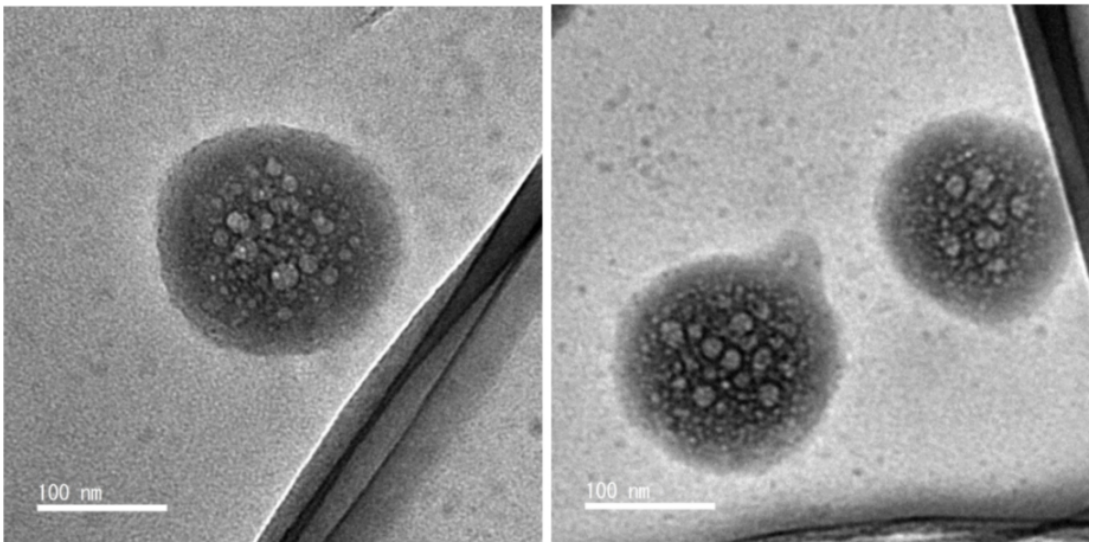

Figure 4.3 Transmission electron microscope images of Lipo-PLEKHA7-PEG-cRGD. (Scale bar = 100 nm, n = 3).

4.2.2 Intracellular uptake and colocalization analysis

Effective intracellular uptake of synthetic nanoparticles is a fundamental necessity for evidence of therapeutic efficiency. Lipo-PLEKHA7-PEG-cRGD uptake by KG-1a cells was examined by confocal microscopy (Figures 4.4 and 4.5). KG-1a cells were successfully transfected with ATTO 550 red-labeled Lipo-PLEKHA7-PEG-cRGD, accompanied by the observation of Lipo-PLEKHA7-PEG-cRGD located in the cytoplasm after 4 h of incubation. As demonstrated in the merged image for investigating the comprehensive cellular uptake, the aggregated dots of ATTO 550 red-labeled Lipo-PLEKHA7-PEG-cRGD were largely displayed in the cytoplasm.

Moreover, 3D images in Figure 4.6 revealed a considerable boost of ATTO 550 red-labeled Lipo-PLEKHA7-PEG-cRGD; thus, these findings also confirmed higher intracellular uptake efficiency of Lipo-PLEKHA7-PEG-cRGD inside KG-1a cells. Our results showed that Lipo-PLEKHA7-PEG-cRGD undergoes $\alpha_v\beta_3$ receptor-mediated endocytosis.

The performance of colocalization analysis was indispensably required to emphasize high transfection and distribution of Lipo-PLEKHA7-PEG-cRGD nanoparticles inside KG-1a cells after 12 h incubation. As shown in Figure 4.7, the visible colocalization between FITC-labeled Lipo-PLEKHA7-PEG-cRGD (green) and phalloidin-labeled actin filaments (red) was exhibited for the regulated distribution of PLEKHA7 at the apical ZA location, indicating effective transfection of the fabricated nanoparticles for efficient PLEKHA7 delivery.

To elucidate PLEKHA7 expression in KG-1a cells before and after transfection with Lipo-PLEKHA7-PEG-cRGD nanoparticles, immunoblotting experiment was performed to assess the comparison between KG-1a untreated cells with cells treated with Lipo-PLEKHA7-PEG-cRGD nanoparticles. The results confirmed our claim displaying that PLEKHA7 was lost (in lower expression level) or mis-localized in KG-1a cells while after the addition of nanoparticle-mediated PLEKHA7 delivery, it significantly resulted in PLEKHA7 re-expression inside the cells. As demonstrated in (Figures 4.8 and 4.9), PLEKHA7 protein expression was significantly upregulated and re-stored in cells treated with Lipo-PLEKHA7-PEG-cRGD with approximately 50% PLEKHA7 protein expression increase in comparison with untreated cells at $p < 0.05$.

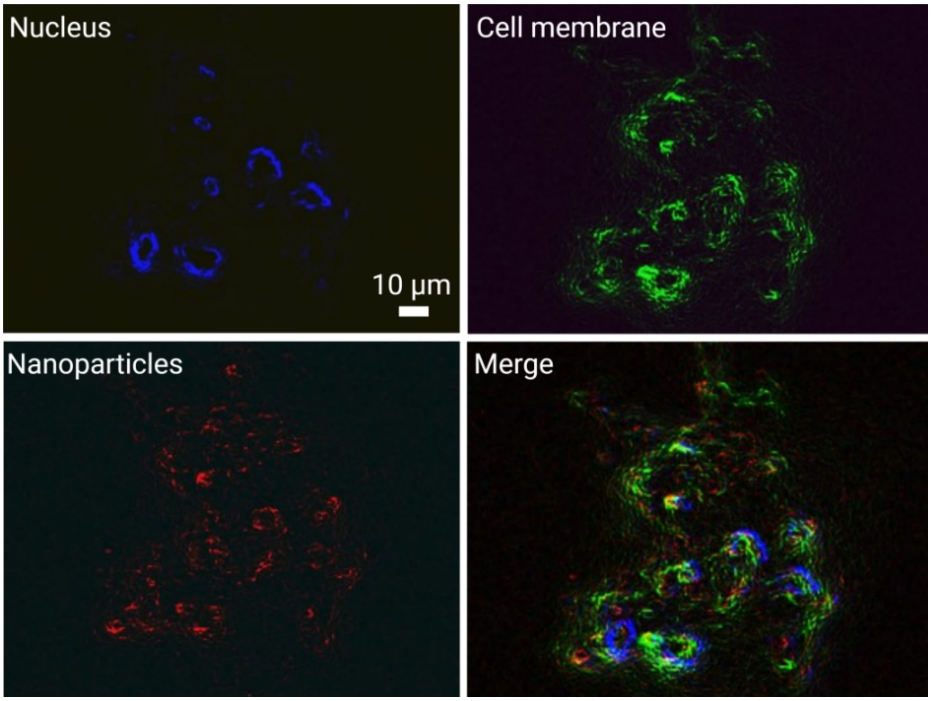

Figure 4.4 Cellular uptake of fluorescently labeled Lipo-PLEKHA7-PEG-cRGD into KG-1a cells. Scale bar = 10 µm. The color representatives are blue (Hoechst 33342) for nuclei, green (Concanavalin A-FITC) for cell membrane, and red (ATTO 550) for Lipo-PLEKHA7-PEG-cRGD nanoparticles.

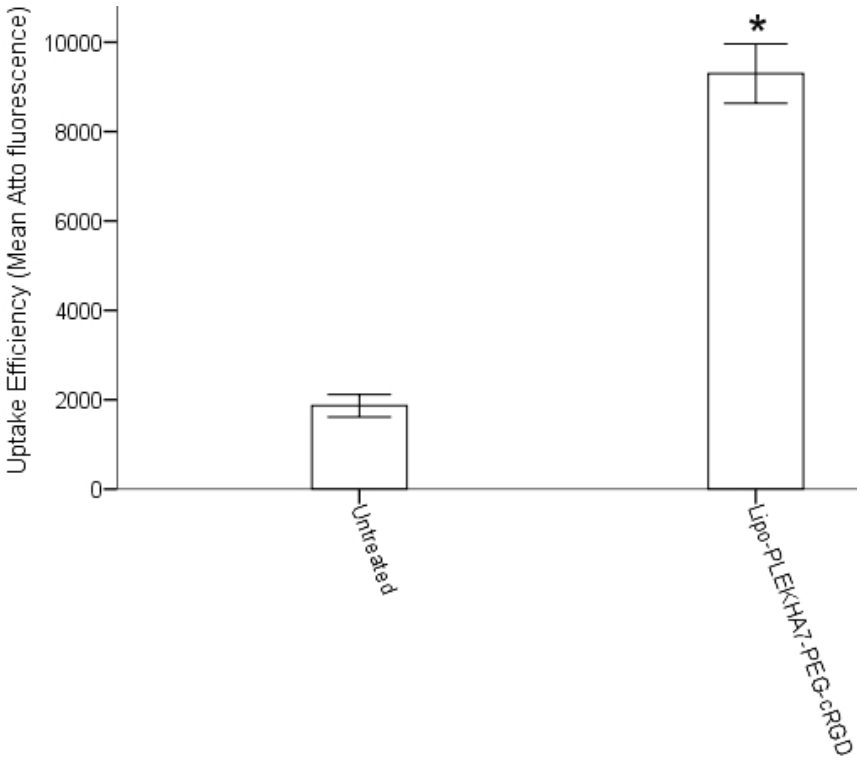

Figure 4.5 Cellular uptake efficiency of Lipo-PLEKHA7-PEG-cRGD in KG-1a cells. Data are presented as mean ± SEM (n = 3 biological replicates). Statistical significance was set at *p < 0.05.

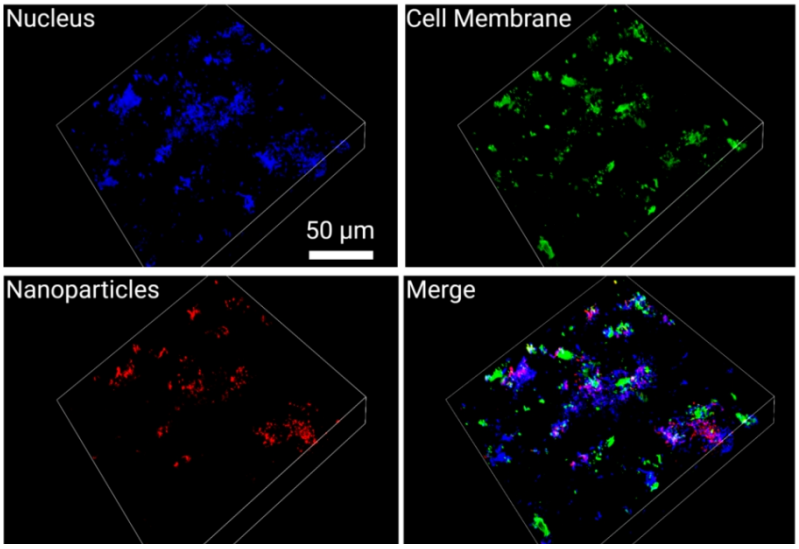

Figure 4.6 3D cellular uptake snapshots of fluorescently labeled Lipo-PLEKHA7-PEG-cRGD into KG-1a cells. Scale bar = 50 µm. The color representatives are blue (Hoechst 33342) for nuclei, green (Concanavalin A-FITC) for cell membrane, and red (ATTO 550) for Lipo-PLEKHA7-PEG-cRGD nanoparticles.

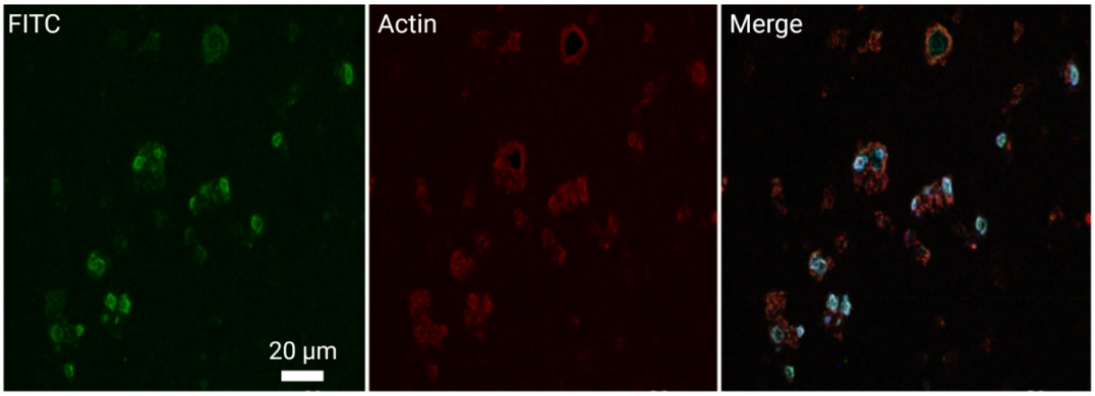

Figure 4.7 Colocalization study of of FITC-labeled Lipo-PLEKHA7-PEG-cRGD nanoparticles for efficient transfection in leukemic cells. Fluorescently labeled Lipo-PLEKHA7-PEG-cRGD were monitored in KG-1a cells. Scale bar = 20 µm. The color representatives are green (FITC) for PLEKHA7 and red (phalloidin) for actin.

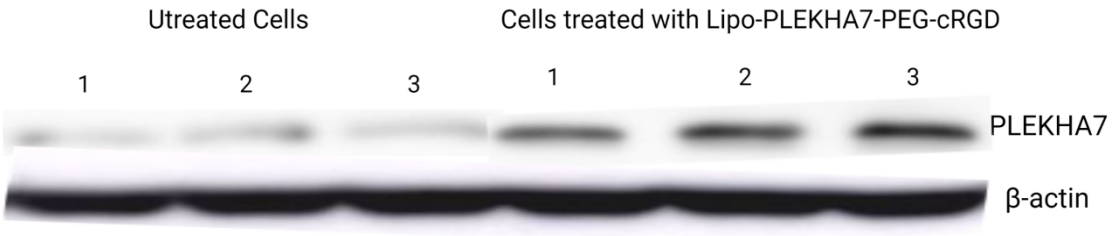

Figure 4.8 Western blots showing PLEKHA7 protein expression in KG-1a cells prior to and after transfection with Lipo-PLEKHA7-PEG-cRGD compared to untreated cells (n = 3).

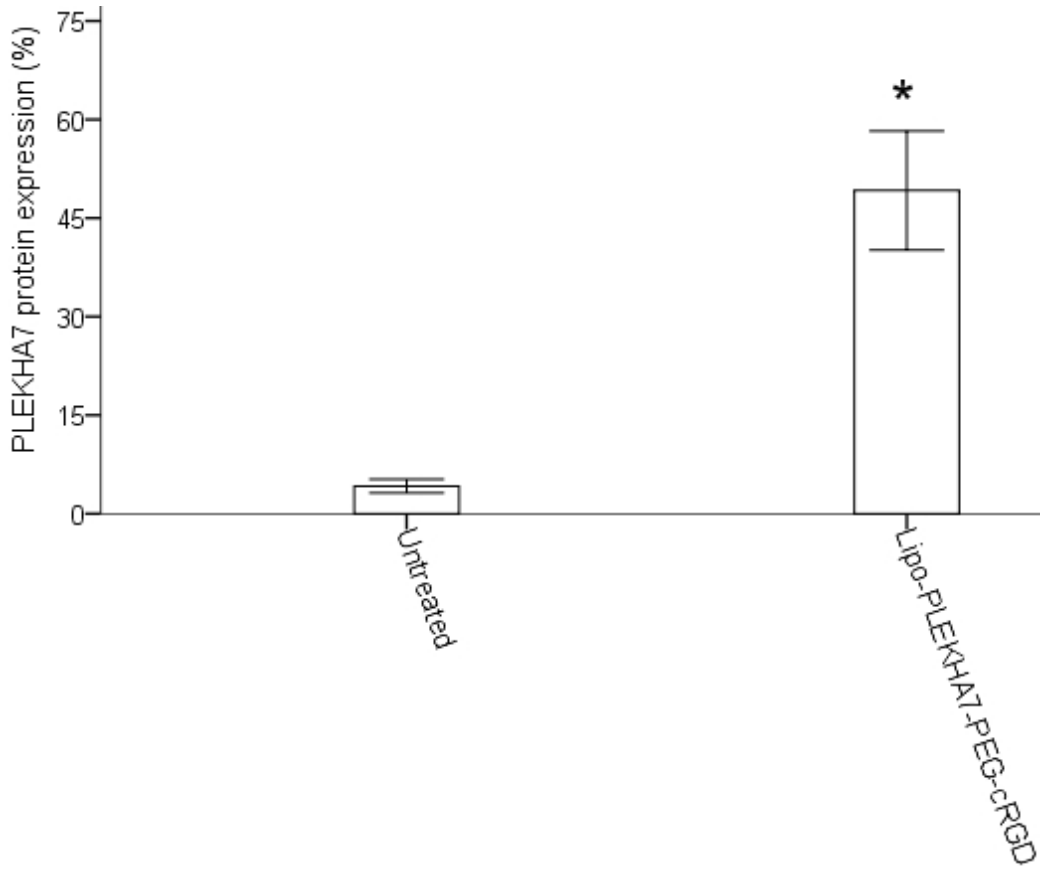

Figure 4.9 Quantification of PLEKHA7 protein expression in KG-1a cells. Data are presented as mean ± SEM (n = 3 biological replicates); *$p < 0.05$.

4.2.3 Cell proliferation and clonogenic growth

As demonstrated in Figures 4.10 and 4.11, cell counting revealed that Lipo-PLEKHA7-PEG-cRGD nanoparticles considerably reduced the proliferation rate in KG-1a and ML-2 cells compared to control cells. We observed a significant alleviation of AML cell proliferation caused by Lipo-PLEKHA7-PEG-cRGD compared with naked PLEKHA7, Lipo-PLEKHA7 and Lipo-PEG-cRGD. We also noticed that the relative number of colonies formed by naked PLEKHA7, Lipo-PLEKHA7, Lipo-PEG-cRGD and Lipo-PLEKHA7-PEG-cRGD were 592 ± 15, 455 ± 16, 593 ± 13 and 189 ± 11, respectively in KG-1a cells (Figure 4.12) while 786 ± 11, 532 ± 15, 843 ± 10 and 309 ± 12, respectively in ML-2 cells (Figure 4.13). Lipo-

PLEKHA7-PEG-cRGD nanoparticles were correlated with the lowest average colony numbers, roughly 70% reduction in both leukemic cell lines compared to control cells ($p < 0.001$). Our findings indicate that Lipo-PLEKHA7-PEG-cRGD markedly attenuated cell proliferation, as evidenced by a dense decline in clonogenic growth of KG-1a and ML-2 cells.

4.2.4 Cell apoptosis

After demonstrating the proliferation-inhibiting function of Lipo-PLEKHA7-PEG-cRGD nanoparticles on AML cells, the effectiveness of naked PLEKHA7, Lipo-PLEKHA7, Lipo-PEG-cRGD and Lipo-PLEKHA7-PEG-cRGD nanoparticles on cell apoptosis was also investigated. Flow cytometric analysis with Annexin V-FITC/PI double staining was used to evaluate transfected KG-1a cells (Figure 4.14). There was no induction of cell apoptosis when KG-1a cells were transfected with naked PLEKHA7, Lipo-PLEKHA7, Lipo-PEG-cRGD or Lipo-PLEKHA7-PEG-cRGD nanoparticles, showing no significant difference compared to untreated cells. Interestingly, the cell apoptosis study results illustrated that Lipo-PLEKHA7-PEG-cRGD possesses a different direction, completely different from conventional chemotherapeutics.

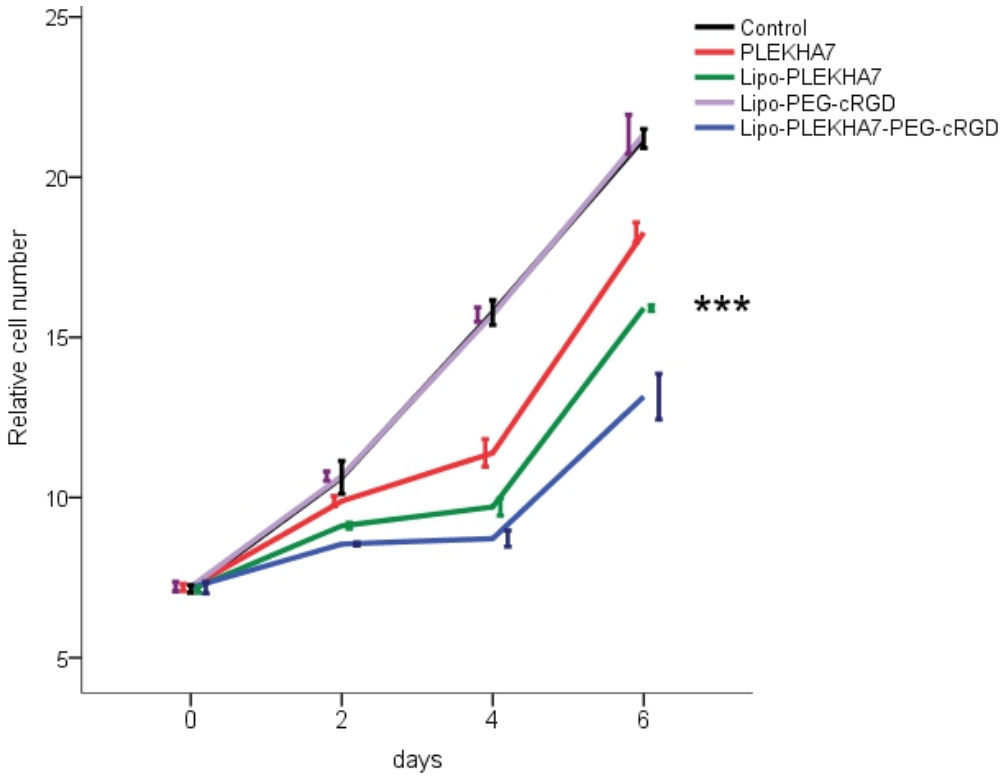

Figure 4.10 Cell count of KG-1a cells transfected with naked PLEKHA7, Lipo-PLEKHA7, Lipo-PEG-cRGD and Lipo-PLEKHA7-PEG-cRGD nanoparticles in culture comparable to untreated cells. The value is determined as the fold increase in cell number relative to the number of cells initially plated. Data are presented as mean ± SEM (n = 5) at ***$p < 0.01$.

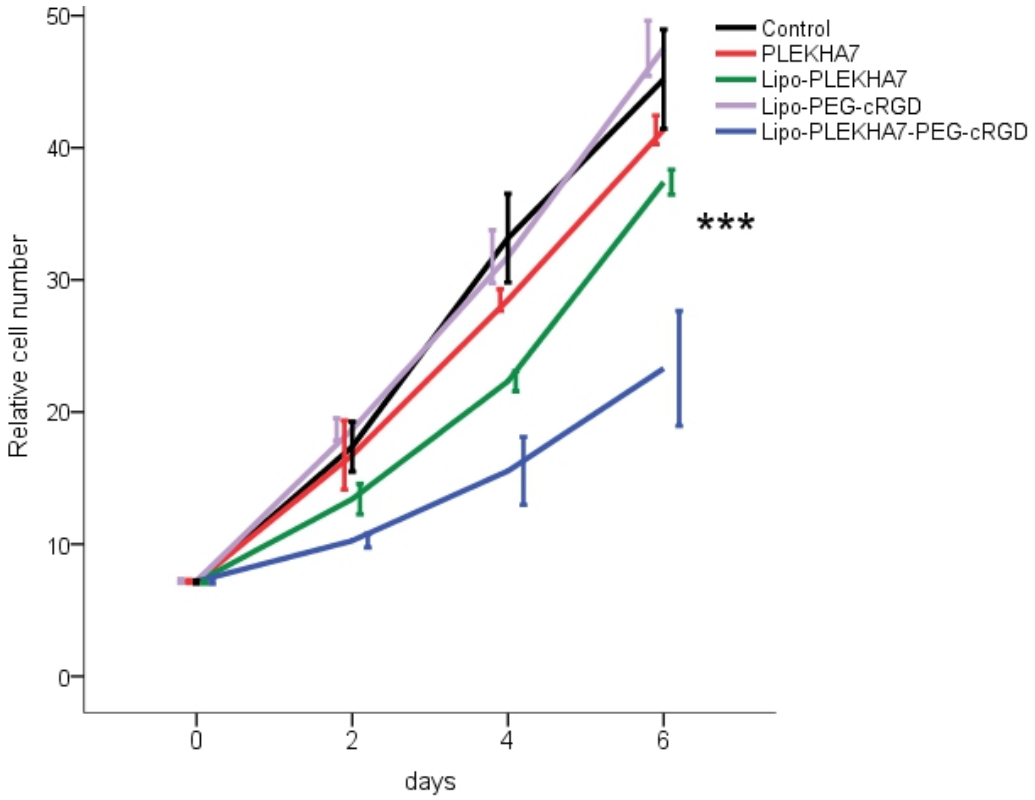

Figure 4.11 Cell count of ML-2 cells transfected with naked PLEKHA7, Lipo-PLEKHA7, Lipo-PEG-cRGD and Lipo-PLEKHA7-PEG-cRGD nanoparticles in culture comparable to untreated cells. The value is determined as the fold increase in cell number relative to the number of cells initially plated. Data are presented as mean ± SEM (n = 5) at ***$p < 0.01$.

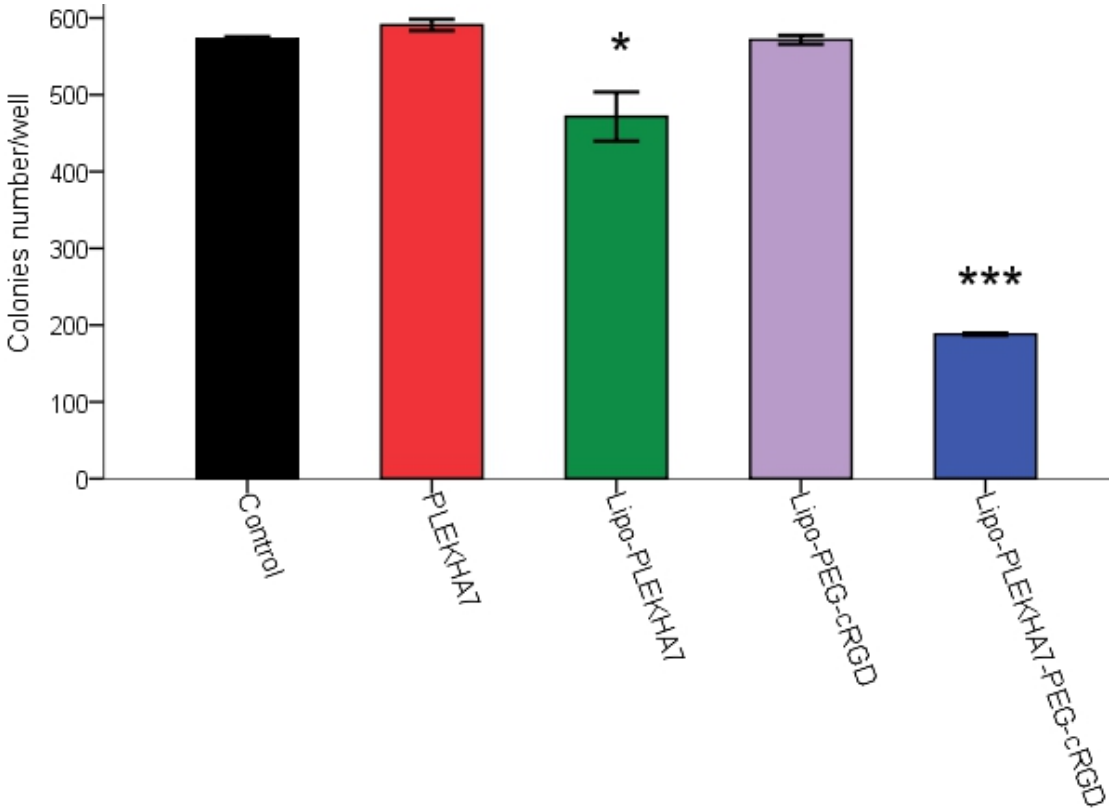

Figure 4.12 Clonogenic growth of KG-1a cells transfected with naked PLEKHA7, Lipo-PLEKHA7, Lipo-PEG-cRGD and Lipo-PLEKHA7-PEG-cRGD nanoparticles relative to untreated cells. The number of colonies observed 7 d after plating. Data are presented as mean ± SEM (n = 5); *$p < 0.05$, ***$p < 0.001$.

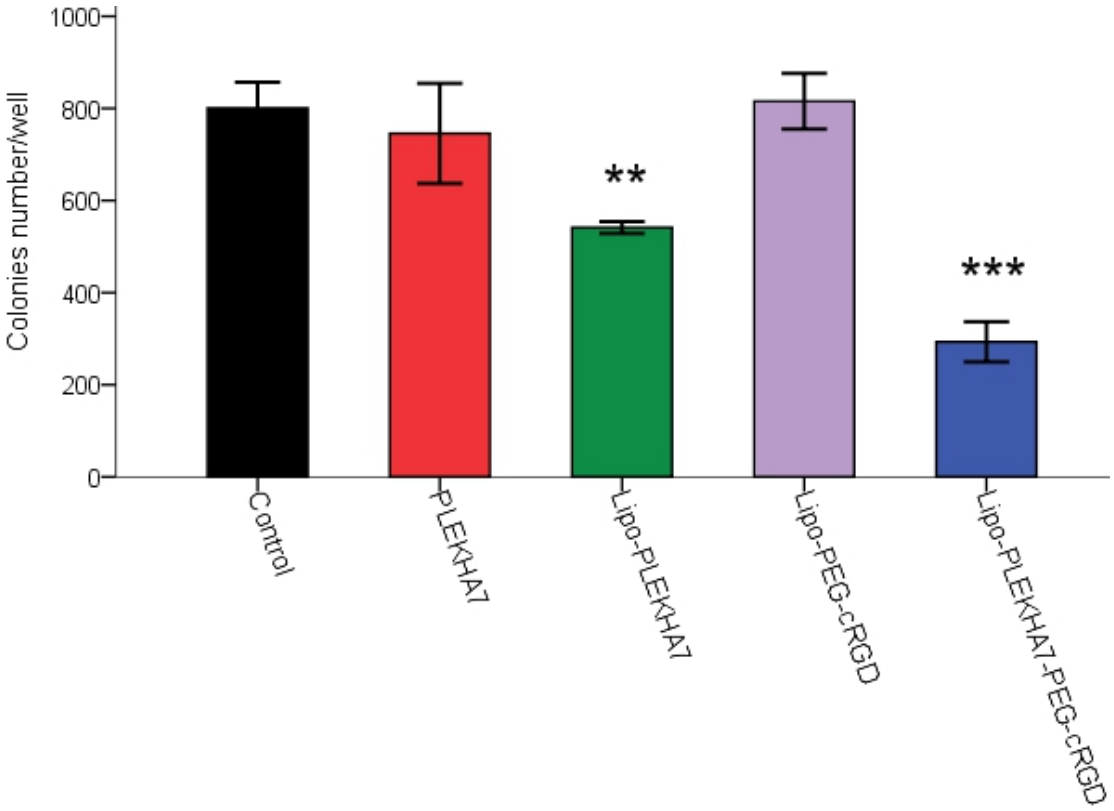

Figure 4.13 Clonogenic growth of ML-2 cells transfected with naked PLEKHA7, Lipo-PLEKHA7, Lipo-PEG-cRGD and Lipo-PLEKHA7-PEG-cRGD nanoparticles relative to untreated cells. The number of colonies observed 7 d after plating. Data are presented as mean ± SEM (n = 5); **p < 0.01, ***p < 0.001.

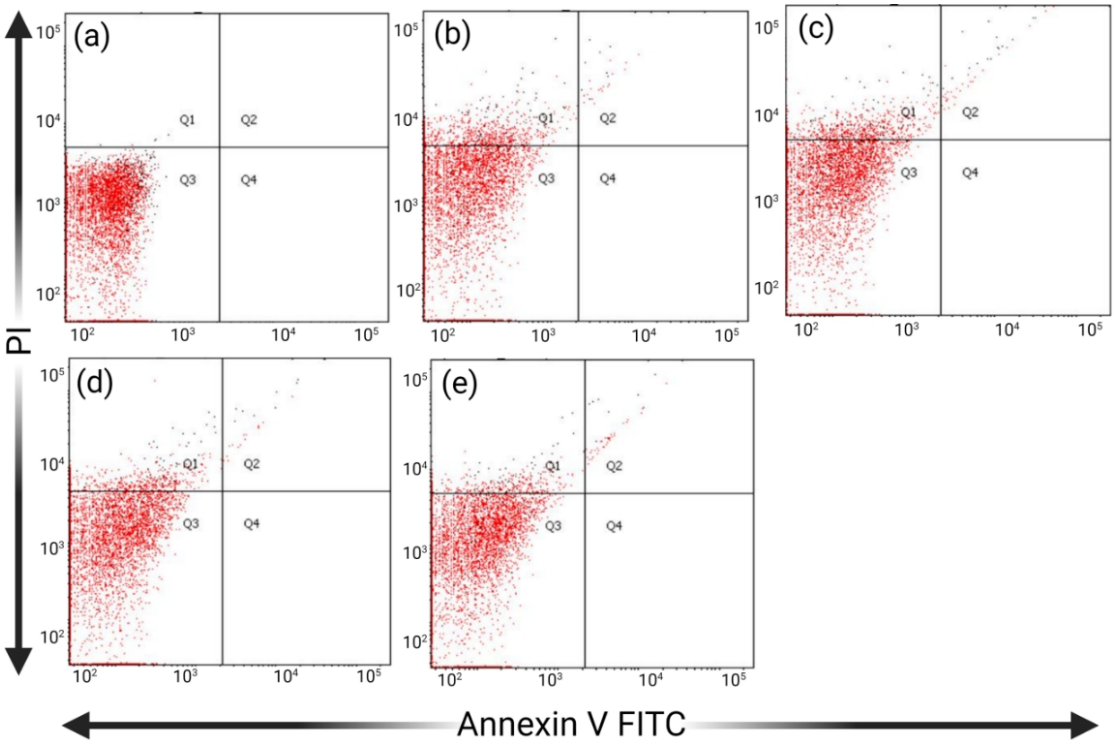

Figure 4.14 Effect of naked PLEKHA7, Lipo-PLEKHA7, Lipo-PEG-cRGD and Lipo-PLEKHA7-PEG-cRGD nanoparticles on AML cell apoptosis. Representative flow cytometry plots of treated cells relative to untreated cells for Annexin V and PI, (a) untreated cells; (b) naked PLEKHA7; (c) Lipo-PLEKHA7; (d) Lipo-PEG-cRGD and (e) Lipo-PLEKHA7-PEG-cRGD.

4.2.5 Cell adhesion morphology

We investigated the significant roles of PLEKHA7 in KG-1a cells transfected with Lipo-PLEKHA7-PEG-cRGD nanoparticles, compared to untreated cells and cells transfected with naked PLEKHA7 and Lipo-PEG-cRGD, by inducing the enhancement of surface adhesion of PLEKHA7-mediated cells. As shown in Figures 4.15 ─ 4.18, our results revealed that PLEKHA7 re-expression could restore cell surface morphologic changes associated with surface adhesion in KG-1a cells particularly in Lipo-PLEKHA7-PEG-cRGD treated cells. However, there is no a significant change in untreated cells, naked PLEKHA7 and Lipo-PEG-cRGD groups.

To monitor PLEKHA7 location within KG-1a cells, FITC-labeled Lipo-PLEKHA7-PEG-cRGD nanoparticles were selectively located at the ZA along with the nucleus (as shown in Figure 4.18). PLEKHA7 was recruited to the cell-cell contact locations in the ZA to regulate ZA integrity, which was lost in AML cells. Where, the superimposed ovals indicate the cell-cell surface adhesion which is created with the contacting of KG-1a cells after PLEKHA7 restoration in its intracellular location. The PLEKHA7 effect was observed that is the induction of cell to cell surface contact and adhesion through the morphological changes associated with adhesion to attach together and to restore the normal cell behavior. This effect took place once PLEKHA7 had been re-expressed within leukemic cells. These results were also emphasized by the quantification of cellular adhesion as revealed in Figure 4.19. KG-1a cells transfected with Lipo-PLEKHA7 and Lipo-PLEKHA7-PEG-cRGD nanoparticles exhibited a significant enhancement in the percentage of cellular adhesion which was measured as mentioned in section 2.13., approximately 55% and 75% higher than that in control cells ($p < 0.001$). Contrarily, there is no significant change in naked PLEKHA7 and Lipo-PEG-cRGD groups compared to untreated cells. These results were also confirmed by red fluorescence images in Figure 4.20 for revealing the cell-cell surface adhesion of cells transfected with Lipo-PLEKHA7-PEG-cRGD nanoparticles. The arrows indicated that the two adjacent cells treated with Lipo-PLEKHA7-PEG-cRGD nanoparticles were attached together to contact each other after 12 and 24 h. While there is no significant change in untreated cells. Intriguingly, restabilization of PLEKHA7 in AML cells could restore the capability cell-cell adhesion, corroborating our PLEKHA7 nanoconstruct concept for acquiring some characteristic features of healthy normal cells to curb the aggressive behavior of AML cells in growth.

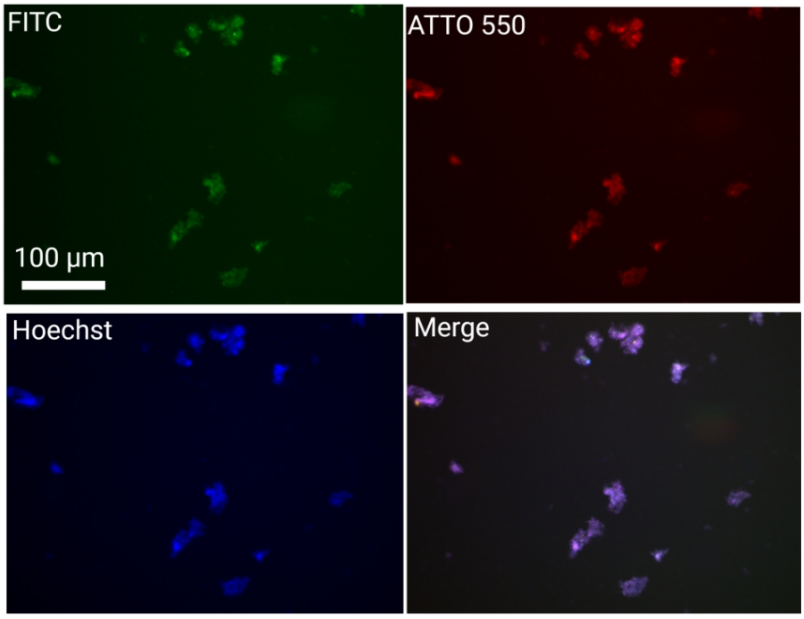

Figure 4.15 Morphologic appearance associated with adhesion in untreated cells. The stain color representatives are green (FITC) for cell membrane, red (ATTO 550) for actin and blue (Hoechst 33342) for nuclei. Scale bar = 100 µm.

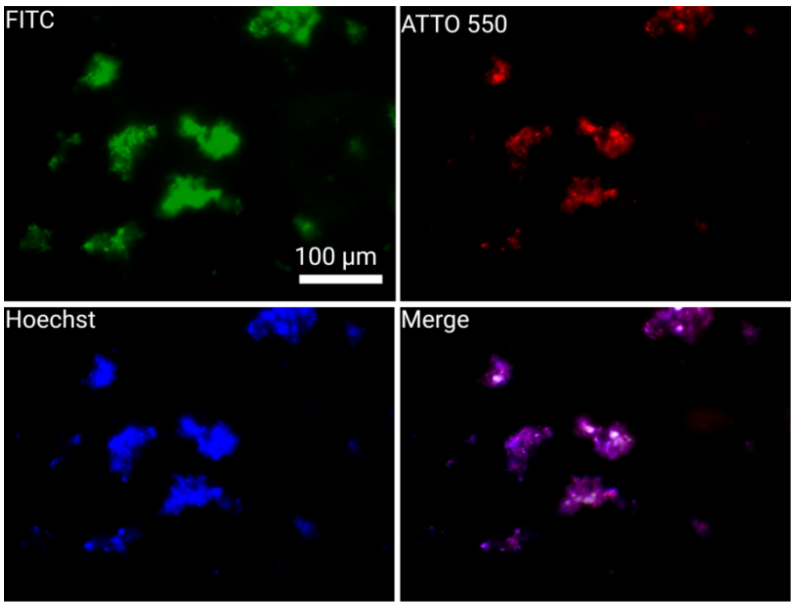

Figure 4.16 Morphologic appearance associated with adhesion in naked PLEKHA7 treated cells. The stain color representatives are green (FITC) for cell membrane, red (ATTO 550) for actin and blue (Hoechst 33342) for nuclei. Scale bar = 100 µm.

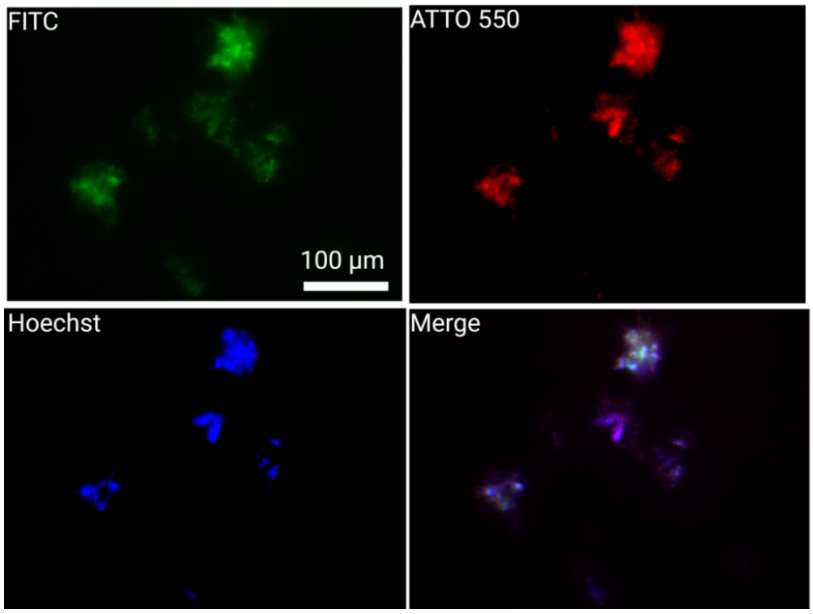

Figure 4.17 Morphologic appearance associated with adhesion in Lipo-PEG-cRGD treated cells. The stain color representatives are green (FITC) for cell membrane, red (ATTO 550) for actin and blue (Hoechst 33342) for nuclei. Scale bar = 100 µm.

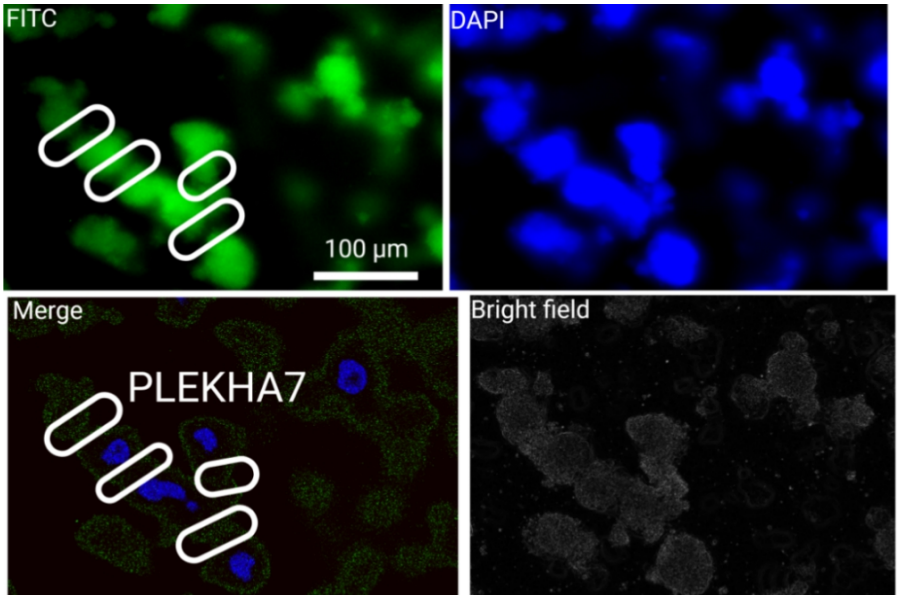

Figure 4.18 Effect of Lipo-PLEKHA7-PEG-cRGD nanoparticles on the restoration of normal cell functions with observation of the exact location of PLEKHA7 within KG-1a cells. Restoration of cell surface adhesion in KG-1a cells transfected with FITC-labeled Lipo-PLEKHA7-PEG-cRGD nanoparticles. The color representatives are green (FITC) for PLEKHA7 and blue (DAPI) for nuclei. Scale bar = 100 µm.

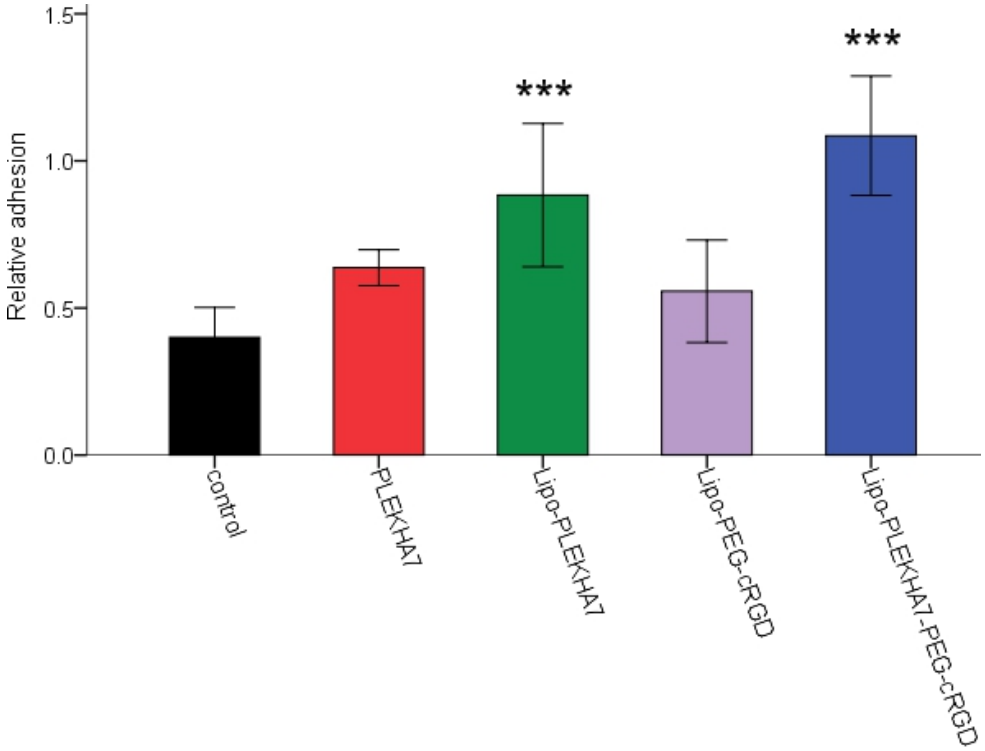

Figure 4.19 Enhancement effects of PLEKHA7, Lipo-PLEKHA7, Lipo-PEG-cRGD and Lipo-PLEKHA7-PEG-cRGD on the cell adhesion of KG-1a cells in comparison with untreated control. Data are expressed as mean ± SEM (n = 3 biological replicates). Statistical significance was set at ***$p < 0.001$.

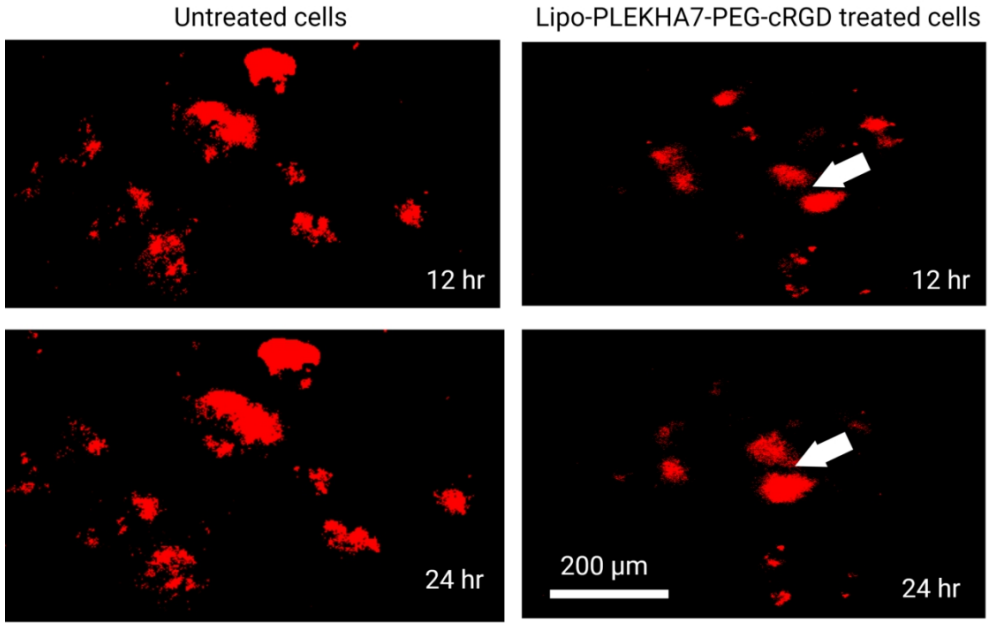

Figure 4.20 Red fluorescence imaging of KG-1a cells transfected with Lipo-PLEKHA7-PEG-cRGD nanoparticles compared with untreated cells after 12 and 24 h intervals using IncuCyte NucLight Rapid Red Reagent for nuclear labeling showing cell to cell surface adhesion. (Scale bar = 200 µm).

4.2.6 Cell growth retardation

The presence of PLEKHA7 plays a pivotal role in AML cell growth. During the IncuCyte schedule scans, we revealed noticeable growth retardation of Lipo-PLEKHA7-PEG-cRGD-treated cells compared to untreated cells, as displayed in Figures 4.21 and 4.22 which were mainly emphasized by the cell growth curve in Figure 4.23 The cell proliferation rate was strikingly attenuated upon transfection with Lipo-PLEKHA7-PEG-cRGD nanoparticles. These findings were supported by Figure 4.24 which showed a significant attenuation in cell growth in cells transfected with Lipo-PLEKHA7-PEG-cRGD nanoparticles when compared with untreated cells, highlighting the controllable effect of Lipo-PLEKHA7-PEG-cRGD on ML-2 cell

growth. Ultimately, the restoration of PLEKHA7 could re-establish the growth retardation in AML cells to curb the AML aggressiveness.

These findings provide us evidence for the controllable effect of Lipo-PLEKHA7-PEG-cRGD on AML cell growth. Ultimately, the restoration of PLEKHA7 could re-establish the growth retardation in KG-1a and ML-2 cells to alter the growth mode and restore the function of normal cells.

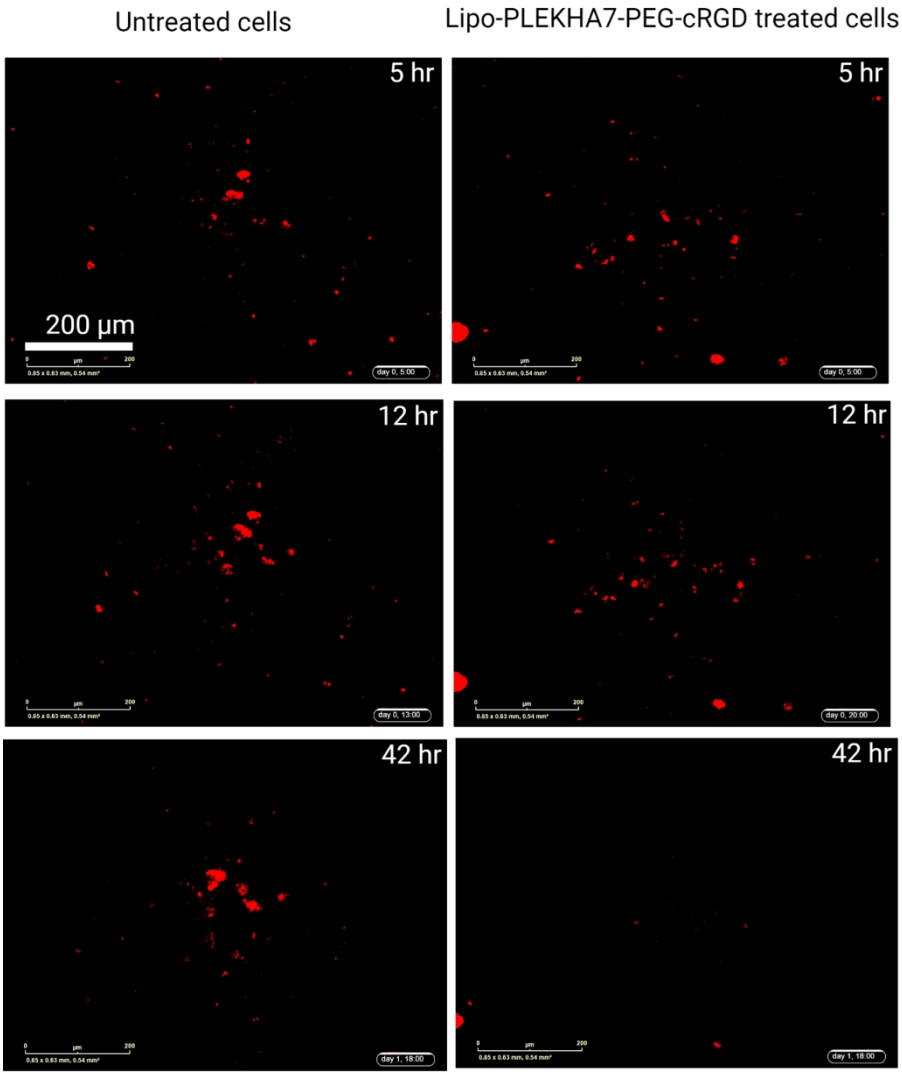

Figure 4.21 Red fluorescence imaging of KG-1a cells transfected with Lipo-PLEKHA7-PEG-cRGD nanoparticles compared to untreated cells after 5, 12 and 42 h intervals using IncuCyte NucLight Rapid Red Reagent for nuclear labeling showing cell growth retardation. (Scale bar = 200 µm).

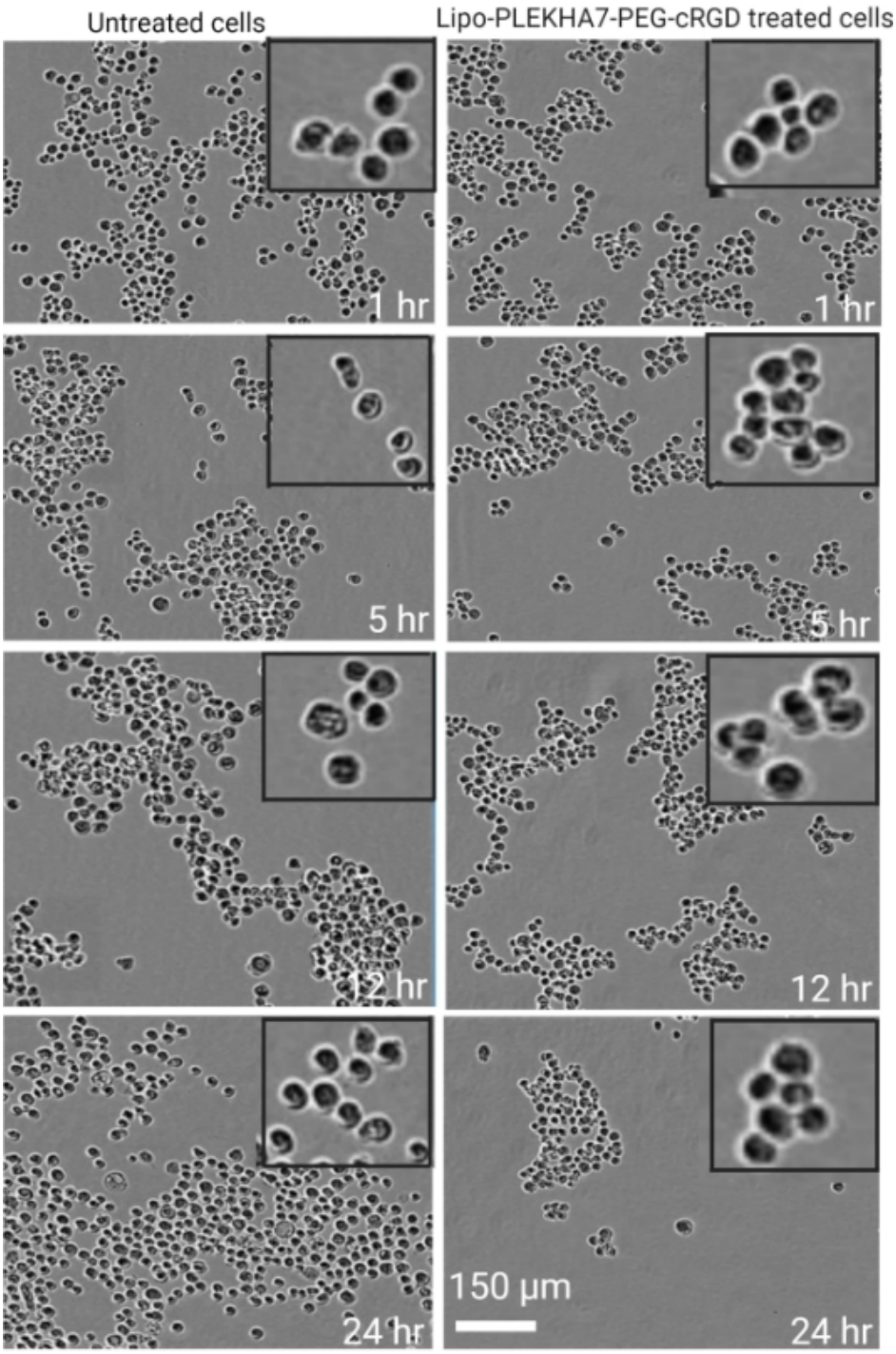

Figure 4.22 Live imaging (phase contrast) of KG-1a cells transfected with Lipo-PLEKHA7-PEG-cRGD nanoparticles relative to untreated cells after 1, 5, 12, 24 h intervals demonstrating the induction of AML growth attenuation. (Scale bar = 150 µm).

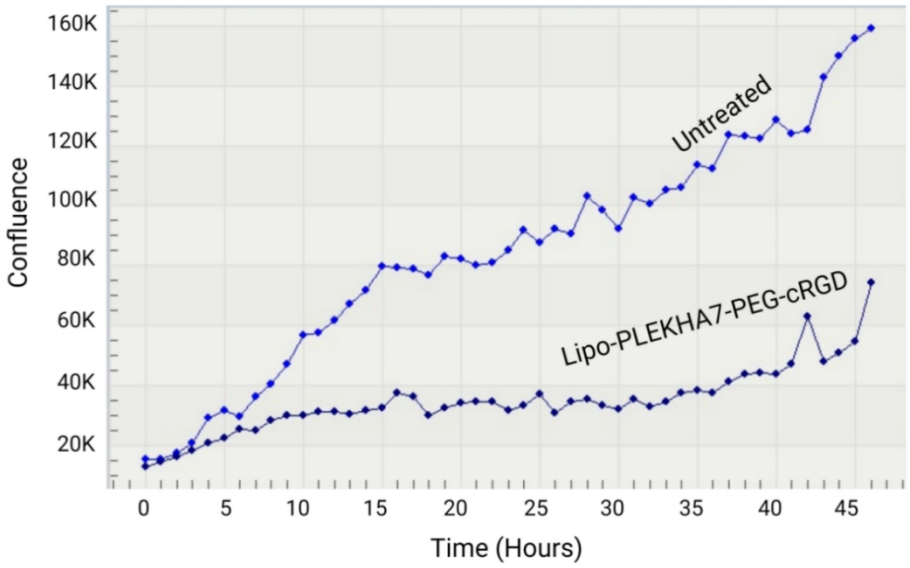

Figure 4.23 Overall growth over time in KG-1a after transfection with Lipo-PLEKHA7-PEG-cRGD nanoparticles compared with untreated cells. Experiments were performed in triplicate.

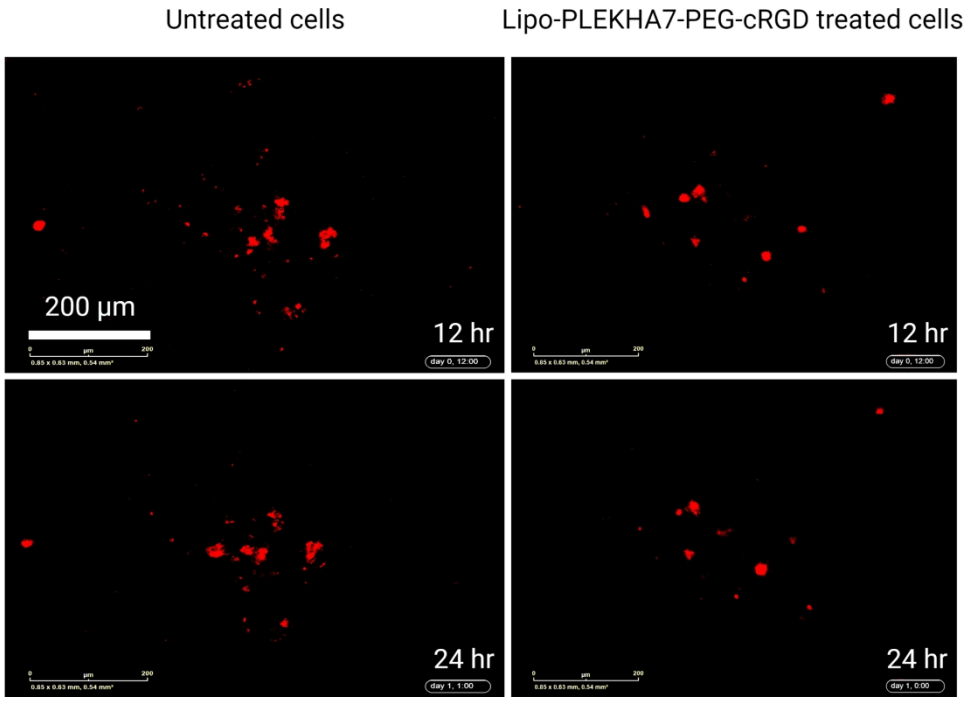

Figure 4.24 Red fluorescence imaging of ML-2 cells transfected with Lipo-PLEKHA7-PEG-cRGD nanoparticles compared to untreated cells after 12 and 24 h intervals using IncuCyte NucLight Rapid Red Reagent for nuclear labeling showing growth retardation of the cells (Scale bar = 200 µm).

4.3 Discussion

PLEKHA7, one of the most important molecules involved in tissue morphogenesis and maintenance of tissue integrity, also functions as a tumor suppressor protein [8,40]. Numerous studies have reported a strong correlation between PLEKHA7 loss and the initiation of tumors [20, 21, 25, 41]. We have firstly studied the PLEKHA7 expression in leukemic cells to assess the growth capability of leukemic cells under the condition of loss or mis-localization of PLEKHA7, and estimated the efficacy of PLEKHA7-loaded cRGD-mediated PEGylated cationic lipid nanoparticles for efficient PLEKHA7 delivery in leukemic cells as well as the effect of PLEKHA7 on the regulated induction of AML behavior and growth alterations. To further investigate the significance of PLEKHA7 protein in leukemia, we treated leukemia cells with PLEKHA7-loaded cRGD-mediated PEGylated cationic lipid nanoparticles to restore PLEKHA7 expression and examined its effects on PLEKHA7-mediated cellular adhesion and proliferation. The restoration of adhesion normality and integrity, which was lost in AML cells, could result in normal homeostasis through regulated induction of AML behavior and growth alterations.

Specifically, we tested PLEKHA7 expression in AML cells prior to the transfection to understand the importance of PLEKHA7 loss or mis-localization for survival and aggressiveness of AML cells and we also demonstrated that the restoration of PLEKHA7 strengthens apical ZA and restrains AML growth. The results of the current study illustrated that AML cells could be efficiently transfected with Lipo-PLEKHA7-PEG-cRGD nanoparticles, suggesting their internalization assimilation to alter AML behavior and dynamics to control growth.

Notably, lipid bilayer fusion, endocytosis, drug conjugation, and facilitated diffusion of lipofectamine-based formulation [42] with further surface modification

by PEGylation allowed the targeting of the $\alpha_v\beta_3$ integrin ligand [43]. These mechanisms demonstrated that Lipo-PLEKHA7-PEG-cRGD could facilitate the entry of the cargo by liposomes (lipid-based nanocarriers) and cRGD peptide which promotes cell-nanomaterial conjugations to allow cargo penetration into the pathologic location to supply optimum delivery of PLEKHA7 for AML normal homeostasis. These important functions of these biocompatible materials have clearly appeared in cell proliferation, colony formation, and adhesion results. Lipo-PLEKHA7 and Lipo-PLEKHA7-PEG-cRGD nanoparticles have significant effects on AML cells when compared to untreated and other groups. Consistent with the hypothesis that PLEKHA7 acts as an adhesion relative modulator, its re-expression in KG-1a and ML-2 cell lines significantly attenuated the cell growth rate. The cell proliferation results of Lipo-PLEKHA7-PEG-cRGD nanoparticles demonstrated a considerable decrease in cell counting or colony-forming ability, thus displaying high transfection efficiency of nanoparticles in particularly liposomes and cRGD moiety.

Lipo-PLEKHA7-PEG-cRGD showed the highest reduction in viable cells (approximately half of total cell numbers) and the lowest clonogenic growth relative to untreated and other indicated groups., promoting efficient PLEKHA7 nanodelivery. The materials utilized in Lipo-PLEKHA7-PEG-cRGD nanostructure for PLEKHA7 delivery have contributed as a biodegradable non-viral vector to efficiently deliver PLEKHA7 cargo to cancer cells without the appearance of therapeutic activity of these biomaterials inside the cells that may cause interference with PLEKHA7 effects. This was evidenced by the results of Lipo-PEG-cRGD in cell proliferation, colony formation and apoptosis experiments. However, it may still have a possibility that the effects of PLEKHA7 protein could be affected by the simultaneous integrin stimulation caused by the nanoparticles. We have observed the appearance of cell to

cell adhesion in AML cells after transfection with Lipo-PLEKHA7-PEG-cRGD nanoparticles compared to untreated, naked PLEKHA7 and Lipo-PEG-cRGD groups. These morphological changes in the cells may be related to PLEKHA7 re-expression because it is an apical AJ-specific conjugating partner of p120 catenin to form a regulatory complex which responsible for stabilization of cell to cell surface adhesion and interactions [22,23]. Cell adhesion is a regulatory process of cell to establish interactions with the neighboring cells through specific protein complexes which could be mediated by adherent junctions [22]. PLEKHA7 is one of these regulatory proteins that directly contributes in the cell to cell adhesion function via p120-specific interacting complex, thus its loss can cause disturbance in cellular interaction and adhesion [23,24]. Moreover, a recent study have reported that PLEKHA7 expression in breast cancer can induces E-cadherin and p120 upregulations which could promote cell to cell adhesion and also inhibit the cancer cell proliferation [20]. We did not investigate the causative mechanism by which PLEKHA7 achieves these behaviors and growth modulator roles in AML. However, previous studies have shown that PLEKHA7 employs the RNAi machinery to the apical AJs to stimulate miRNA maturation and conjugation with an apically localized RNA-induced silencing complex (RISC) [22,44]. This PLEKHA7 role inhibited the expression of pro-tumor-promoting proteins such as cyclin D1, Snail, and c-Myc [22]. A recent study reported concomitant dysfunction of PLEKHA7 and the RNAi machinery at the apical AJs in colon cancer patient samples. Moreover, the RNAi machinery was restored to apical AJs, and PLEKHA7-expressing xenografts showed a reduced tumor burden once PLEKHA7 was restored in colon cancer cell lines [45]. Inhibition of E-cadherin/epidermal growth factor receptor (EGFR) signaling and p120 signaling are the contributing mechanisms that indicate the fundamental role of PLEKHA7 in

tumor suppression [20]. In ovarian epithelial cancer, E-cadherin induces EGFR signaling, which is inhibited by PLEKHA7 expression [20]. In AML cells, E-cadherin suppression significantly reduced cell-cell adhesion and enhanced cell growth and colony formation, indicating the function of E-cadherin in homophilic adhesion stimulation and cell proliferation retardation by an E-cadherin-mediated connection with stromal cells [46]. Furthermore, E-cadherin could also suppress the Wnt signaling pathway via β-catenin interaction from the nuclear signaling pool, contributing to its tumor suppression function [47-49]. Prior studies have reported that cell adhesion plays a main role in the interaction between developing hematopoietic cells and their microenvironment, which regulates the destiny of hematopoietic stem cells [50-53]. Zhou et al. demonstrated that the adhesion capacity to bone marrow stroma was impaired in leukemia cells. Hence, the modulation of the adhesion behavior of hematopoietic stem cells may change the hematopoietic cell homeostasis with the bone marrow microenvironment, leading to leukemic transformation [54]. Our results have been agreed with Pence and coauthors that discussed the induction of cancer cells for PLEKHA7 loss or cytoplasmic translocation in order to avoid PLEKHA7 tumor suppression thereby, this suppression caused an extensive burden on cancer cells to eradicate the expression of apical PLEKHA7 [55].

Our study revealed that PLEKHA7 re-expression restores apical ZA integrity and cellular adhesion and attenuates AML growth rate. Taken together, these findings indicate that animal experiments may provide useful data for developing PLEKHA7 nanomedicines for AML regulation and reprogramming.

4.4 Summary

In this chapter, we uncovered the important function of PLEKHA7 as a behavior and growth modulator in AML via an in vitro study on new bioengineered smart nanoparticles that are well-characterized, cRGD-conjugated with thiolated PEG (NHS-PEG6-maleimide) to effectively deliver PLEKHA7 to induce normal homeostasis in AML cells. Our study revealed that PLEKHA7 re-expression restores apical ZA integrity and cellular adhesion and attenuates AML growth rate without appearance of apoptosis signals occurred to AML cells. Altogether, This approach will foreseeably open new avenues for applying smart biocompatible PLEKHA7 re-engineered nanoconstructs *in vivo* via implementation of experimental animal models and further passing into clinical trials for efficient translation and production of advanced PLEKHA7 nanomedicines for AML regulation and reprogramming.

References

1. M. Dorrance, Targeting leukemia stem cells in vivo with antagomiR-126 nanoparticles in acute myeloid leukemia. *Leukemia,* **29**, 2143–2153 (2015).
2. V. Trujillo-Alonso, et al., FDA-approved ferumoxytol displays anti-leukaemia efficacy against cells with low ferroportin levels. *Nat. Nanotechnol..* **14**, 616–622 (2019).
3. J. Zhu, S. G. Emerson, A new bone to pick: osteoblasts and the haematopoietic stem-cell niche. *Bioessays,* **26**, 595–599 (2004).
4. R. S. Taichman, Blood and bone: two tissues whose fates are intertwined to create the hematopoietic stem-cell niche. *Blood,* **105**, 2631–3639 (2005).
5. J. P. Levesque, I. G. Winkler, Cell adhesion molecules in normal and malignant hematopoiesis: from bench to bedside. *Curr. Stem Cell Rep.,* **2**, 356–367 (2016).

6. S. Jungmichel, B. Sylvestersen, C. Choudhary, S. Nguyen, M. Mann, M. Nielsen, Specificity and commonality of the phosphoinositide-binding proteome analyzed by quantitative mass spectrometry, *Cell Rep.,* **6**, 578- 591 (2014).
7. B. J. Mayer, R. Ren, K. L. Clark, D. Baltimore, A putative modular domain present in diverse signaling proteins, *Cell,* **73**, 629–630 (1993).
8. M. Lemmon, Pleckstrin homology (PH) domains and phosphoinositides, *Biochem Soc Symp.,* **74**, 81–93 (2007).
9. J. Shah, D. Guerrera, E. Vasileva, S. Sluysmans, E. Bertels, S. Citi, PLEKHA7: cytoskeletal adaptor protein at center stage in junctional organization and signaling, *Int J Biochem.,* **75**, 112–116 (2016).
10. S. Paschoud, L. Jond, D. Guerrera, S. Citi, PLEKHA7 modulates epithelial tight junction barrier function, *Tissue Barriers,* **2**, e28755 (2014).
11. S. Kurita, T. Yamada, E. Rikitsu, W. Ikeda, Y. Takai, Takai Binding between the junctional proteins afadin and PLEKHA7 and implication in the formation of adherens junction in epithelial cells. *J Biol Chem.,* **288**, 29356–29368 (2013).
12. S. Citi, P. Pulimeno, S. Paschoud, Cingulin, paracingulin, and PLEKHA7: signaling and cytoskeletal adaptors at the apical junctional complex, *Ann N Y Acad Sci.,* **1257**, 125–132 (2012).
13. D. Guerrera, J. Shah, E. Vasileva, S. Sluysmans, I. M´ean, L. Jond, et al., PLEKHA7 recruits PDZD11 to adherens junctions to stabilize nectins, *J Biol Chem.,* **291**, 11016–11029 (2016).
14. A. Kourtidis, S.P. Ngok, P. Pulimeno, R.W. Feathers, L.R. Carpio, T.R. Baker, et al., Distinct E-cadherin-based complexes regulate cell behavior through miRNA processing or Src and p120 catenin activity, *Nat Cell Biol.,* **17**, 1145–1157 (2015).

15. A. Kourtidis, P.Z. Anastasiadis, PLEKHA7 defines an apical junctional complex with cytoskeletal associations and miRNA-mediated growth implications, *Cell Cycle.* **15**, 498–505 (2016).

16. S. Citi, D. Guerrera, D. Spadaro, J. Shah, Epithelial junctions and Rho family GTPases: the zonular signalosome, *Small.* **5**, 1–15 (2014).

17. P. Anastasiadis, p120-ctn: A nexus for contextual signaling via Rho GTPases, *Biochim Biophys Acta.* **1773**, 34–46 (2007).

18. D. Wu, D. Harrison, T. Szasz, C. Yeh, T. Shentu, A. Meliton, et al., Single-cell metabolic imaging reveals a RhoA triggered glycolytic burst in motile endothelial cells, *Nat Metab.,* **3**, 714–727 (2021).

19. D. Jeong, S. Park, H. Kim, C. Kim, T. Ahn, S. Bae, et al., RhoA is associated with invasion and poor prognosis in colorectal cancer, *Int J Oncol.,* **48**, 714–722 (2016).

20. K. Rea, et al, Simultaneous E-cadherin and PLEKHA7 expression negatively affects E-cadherin/EGFR mediated ovarian cancer cell growth. *J. Exp. Clin. Cancer Res.,* **37**, 146 (2018).

21. A. M. Mendonsa, T. Y. Na, B. M. Gumbiner, E-cadherin in contact inhibition and cancer. *Oncogene,* **37**, 4769–4780 (2018).

22. A. Kourtidis, et al, Distinct E-cadherin-based complexes regulate cell behaviour through miRNA processing or Src and p120 catenin activity. *Nat. Cell Biol.,* **17**, 1145–1157 (2015).

23. W. Meng, Y. Mushika, T. Ichii, M. Takeichi, Anchorage of microtubule minus ends to adherens junctions regulates epithelial cell-cell contacts. *Cell.,* **135**, 948–959 (2008).

24. P. Pulimeno, C. Bauer, J. Stutz, S. Citi, PLEKHA7 is an adherens junction protein with a tissue distribution and subcellular localization distinct from ZO-1 and E-cadherin. *PLoS One,* **5**, e12207 (2010).

25. A. Kourtidis, P. Z. Anastasiadis, PLEKHA7 defines an apical junctional complex with cytoskeletal associations and miRNA-mediated growth implications. *Cell Cycle,* **15**, 498–505 (2016).

26. E. E. Ladikou, H. Sivaloganathan, A. Pepper, T. Chevassut, Acute myeloid leukaemia in its niche: the bone marrow microenvironment in acute myeloid leukaemia. *Curr. Oncol. Rep.,* **22**, 27 (2020).

27. T. Yamaguchi, E. Kawamoto, A. Gaowa, E. J. Park, M. Shimaoka, Remodeling of bone marrow niches and roles of exosomes in leukemia. *Int. J. Mol. Sci.,* **22**, 1881 (2021).

28. N. Asada, Regulation of malignant hematopoiesis by bone marrow microenvironment. *Front. Oncol.,* **8**, 119 (2018).

29. A. A. Yetisgin, S. Cetinel, M. Zuvin, A. Kosar, O. Kutlu, Therapeutic nanoparticles and their targeted delivery applications. *Molecules,* **25**, 2193 (2020).

30. S. S. Hallan, M. Sguizzato, E. Esposito, R. Cortesi, Challenges in the physical characterization of lipid nanoparticles. *Pharmaceutics,* **13**, 549 (2021).

31. A. M. Matei, Applications of nanosized-lipid-based drug delivery systems in wound Care. *Appl. Sci.,* **11**, 4915 (2021).

32. B. Pelaz, et al., Surface functionalization of nanoparticles with polyethylene glycol: effects on protein adsorption and cellular uptake. *ACS Nano,* **9**, 6996–7008 (2015).

33. J. S. Suk, Q. Xu, N. Kim, J. Hanes, L.M. Ensign, PEGylation as a strategy for improving nanoparticle-based drug and gene delivery. *Adv. Drug Deliv. Rev.,* **99**, 28–51 (2016).

34. S. Y. Fam, C. F. Chee, C. Y. Yong, K. L. Ho, A. R. Mariatulqabtiah, W. S. Tan, Stealth coating of nanoparticles in drug-delivery systems. *Nanomaterials*, **10**, 787 (2020).

35. U. Termsarasab, I. S. Yoon, J. H. Park, H. T. Moon, H. J. Cho, D. D. Kim, Polyethylene glycol-modified arachidyl chitosan-based nanoparticles for prolonged blood circulation of doxorubicin. *Int. J. Pharm.,* **464**, 127–134 (2014).

36. T. T. Hoang Thi, E. H. Pilkington, D. H. Nguyen, J. S. Lee, K. D. Park , N. P. Truong, The importance of poly(ethylene glycol) alternatives for overcoming PEG immunogenicity in drug delivery and bioconjugation. *Polymers,* **12**, 298 (2020).

37. J. Zhao, F. Santino, D. Giacomini, L. Gentilucci. Integrin-targeting peptides for the design of functional cell-responsive biomaterials. *Biomedicines*, **8**, 307 (2020).

38. F. Danhier, A. Le Breton, V. Préat, RGD-based strategies to target alpha(v) beta(3) integrin in cancer therapy and diagnosis. *Mol. Pharm.*, **9**, 2961–2973 (2012).

39. J. M. Rios De La Rosa, et al., Microfluidic-assisted preparation of RGD-decorated nanoparticles: exploring integrin-facilitated uptake in cancer cell lines. *Sci. Rep.,* **10**, 14505 (2020).

40. F. Rouaud, S. Sluysmans, A. Flinois, J. Shah, E. Vasileva, S. Citi, Scaffolding proteins of vertebrate apical junctions: structure, functions and biophysics. *Biochim. Biophys. Acta. Biomembr.,* **1862**, 183399 (2020).

41. A. Kourtidis, et al., Cadherin complexes recruit mRNAs and RISC to regulate epithelial cell signaling. *J. Cell Biol.,* **216**, 3073–3085 (2017).

42. J. Yang, et al., Drug delivery via cell membrane fusion using lipopeptide modified liposomes. *ACS Cent. Sci.*, **2**, 621–630 (2016).

43. L. Zhang, et al., Cytosolic co-delivery of miRNA-34a and docetaxel with core-shell nanocarriers via caveolae-mediated pathway for the treatment of metastatic breast cancer. *Sci. Rep.,* **7**, 46186 (2017).

44. A. Kourtidis, et al., Distinct E-cadherin-based complexes regulate cell behaviour through miRNA processing or Src and p120 catenin activity. *Nat. Cell Biol.,* **17**, 1145–1157 (2015).

45. J. Nair-Menon, et al., Predominant distribution of the RNAi machinery at apical adherens junctions in colonic epithelia is disrupted in cancer. *Int. J. Mol. Sci.,* **21**, 2559 (2020).

46. Q. Rao, et al., Low-expression of E-cadherin in leukaemia cells causes loss of homophilic adhesion and promotes cell growth. *Cell Biol. Int.,* **35**, 945-951 (2011).

47. Q. Rao, et al., Leukemia cell surface expression of E-cadherin and its correlation with membrane localization of beta-catenin. Zhonghua Xue Ye Xue Za Zhi (in Chinese) **29**, 592–594 (2008).

48. B. Wang, X. Li, L. Liu, M. Wang, β-Catenin: oncogenic role and therapeutic target in cervical cancer. *Biol. Res.,* **53**, 33 (2020).

49. Y. Azbazdar, M. Karabicici, E. Erdal, G. Ozhan, Regulation of Wnt signaling pathways at the plasma membrane and their misregulation in cancer. *Front. Cell Dev. Biol.,* **9**, 631623 (2021).

50. R. N. Kaplan, B. Psaila, D. Lyden. Niche-to-niche migration of bone-marrow-derived cells. *Trends Mol. Med.,* **13**, 72–81 (2007).

51. P. Zhang, C. Zhang, J. Li, J. Han, X. Liu, H. Yang, The physical microenvironment of hematopoietic stem cells and its emerging roles in engineering applications. *Stem Cell Res. Ther.,* **10**, 327 (2019).

52. R. Kulkarni, V. Kale, Physiological cues involved in the regulation of adhesion mechanisms in hematopoietic stem cell fate decision. *Front. Cell Dev. Biol.,* **8**, 611 (2020).

53. S. Chen, M. Lewallen, T. Xie, Adhesion in the stem cell niche: biological roles and regulation. *Development,* **140**, 255–265 (2013).

54. J. Zhou, K. Mauerer, L. Farina, J. G. Gribben, The role of the tumor microenvironment in hematological malignancies and implication for therapy. *Front. Biosci.,* **10**, 1581–1596 (2005).

55. L. J. Pence, et al, PLEKHA7, an apical adherens junction protein, suppresses inflammatory breast cancer in the context of high E-cadherin and p120-catenin expression. *Int. J. Mol. Sci.,* **22**, 1275 (2021).

Chapter 5. Conclusions

In this study, we investigated *SHARP1* knockdown in ML-2 cells in stimulating apoptosis to determine the oncogenic role of *SHARP1* as an MLL-AF6-dependent leukemogenic driver in MLL-AF6 AML growth and maintenance, as well as the application of multifunctionally bioengineered nanoparticles in *SHARP1* downregulation; thus, indicating a potential therapeutic strategy for human MLL-AF6 AML therapy. We fabricated a state-of-the-art biodegradable nanoplatform for siRNA/BTZ co-delivery with targeted *SHARP1* knockdown, demonstrating a potential therapeutic option for MLL-AF6 AML. This efficient co-delivery of siRNA and BTZ resulted in remarkable inhibition in cell viability and clonogenic growth as well as triggering apoptosis *in vitro.* We hypothesized that *SHARP1* downregulation induced the accumulation of non-functional MLL-AF6, DOT1L, MEN1, and LEDGF fusion proteins, preventing MLL-AF complex formation and downregulating RAS-GTP and Bcl-2 expression, consequently triggering apoptosis. The BTZ combination substantially augmented therapeutic synergy and enhanced apoptotic events. The results demonstrated the effects of *SHARP1* downregulation on *DOT1L* and *MLL-AF6* expression and highlighted a new vital oncogenic role of *SHARP1* in MLL-AF6 AML growth and maintenance. Taken together, Lipo-siRNA-BTZ-PEG-cRGD are multifunctional particles that reveal versatile regulatory mechanisms, including *SHARP1* silencing, MLL-AF6/DOT1L inhibition, p53 activation, RAS suppression, proteasome inhibition, and apoptosis induction. This approach will foreseeably open new avenues for applying smart biocompatible re-engineered nanostructures *in vivo*

and further clinical translation to produce advanced MLL-AF6 AML-targeting therapeutics.

On the other hands, we have firstly studied the PLEKHA7 expression in leukemic cells to assess their growth capability affected by the restoration of PLEKHA7 in the cells. The efficacy of PLEKHA7-loaded cRGD-mediated PEGylated cationic lipid nanoparticles for efficient PLEKHA7 delivery in leukemic cells as well as the effect of PLEKHA7 on the regulated induction of AML behavior alteration and growth retardation were investigated. PLEKHA7 re-expression inhibited cell proliferation, diminished colony-forming ability and reinforced the incidence of growth retardation without apoptosis in AML cell lines. PLEKHA7 regulated the restoration of cell surface adhesion and integrity during normal homeostasis. To our knowledge, the role of PLEKHA7 in AML had not been studied previously and our data could be exploited for further mechanistic studies and insights into altering human AML behavior and attenuating its aggressiveness. Our findings uncover the important function of PLEKHA7 as a adhesion relative modulator and growth attenuator in AML via an in vitro study on new bioengineered smart nanoparticles that are well-characterized, cRGD-conjugated with thiolated PEG (NHS-PEG6-maleimide) to effectively deliver PLEKHA7 to induce normal homeostasis in the KG-1a cell line. This study revealed that PLEKHA7 re-expression could restore apical ZA integrity and cellular adhesion and attenuate AML growth rate. Altogether, these findings indicated that animal experiments may provide useful data for developing PLEKHA7 nanomedicines for AML regulation and reprogramming.

Acknowledgements

First and foremost, I would like to express my sincere gratitude and profound thanks to my supervisor, Prof. Yang Ju, for giving me an opportunity to work in his laboratory. He is not only an exceptional researcher and a respected professor, but also a wonderful advisor and mentor. His support, careful revision, excellent technical advices, endless enthusiasm and inspiration has given me full confidence in the implementation of this doctoral research.

I would like to thank Prof. Noritsugu Umehara, Prof. Guanbin Song, Prof. Yasuyuki Morita, and Prof. Hisataka Maruyama for their time and precious suggestions in the preparation of this dissertation.

I am very grateful to Prof. Yuhki Toku for the valuable suggestions and instructive discussions. His knowledge, expertise and willingness are instrumental in assisting me accomplish my goals.

Really, my sincere gratitude is offered to Prof. Yasuhiro Kimura for his excellent technical advices, generous assistance, careful revision and great efforts throughout all stages of this study.

Last but not least my heartful gratitude should be extended to include my labmates, colleagues and all the members in Ju laboratory for their encouragement, help and cooperation.

I would also like to acknowledge Government of Japan's Ministry of Education, Culture, Sports, Science and Technology (Monbukagakusho: MEXT) for supporting my research and study in Japan.

Also, I would like to impart my sincere thanks to Yorifuji Eri for excellent technical assistance and training courses on live-cell imaging systems and confocal microscopy.

All my great thanks to my God (Allah) who helped me endlessly to finish this work.

My sincere gratitude is offered to my parents, I can't forget their endless love, everlasting support, prayer and taking care of me. Words fail to express my appreciation to them. Really, they tolerate a lot for me throughout understanding my entire academic carrier., I ask Allah to keep them in a good health.

All my great thanks to my beloved wife, Esraa Shaaban, I would like to express my great gratitude for her endless love, help, patience and emotional support. All the time I ask Allah to keep her for me forever.

My all heartful thanks to my loving daughters, Rozy, Jory, Noreen and my dear son, Omar who suffered more due to my research.

Many thanks to my dear sister, Eman and her husband for their great encouragement and support.

Finally, I can't forget to impart my deep thanks to my wife's family for their endless encouragement and support.

Sameh Abdelmoneem Mohammed Ali

Nagoya University

July, 2022